NOAA
Professional Paper 6

U.S. DEPARTMENT OF COMMERCE / National Oceanic and Atmospheric Administration

# Ionospheric Disturbances
## PRODUCED BY SEVERE THUNDERSTORMS

NOAA

**Professional Paper 6**

# Ionospheric Disturbances

## PRODUCED BY SEVERE THUNDERSTORMS

KENNETH DAVIES AND JOHN E. JONES
*Space Environment Laboratory,*
*Environmental Research Laboratories,*
*Boulder, Colo.*



UNITED STATES DEPARTMENT OF COMMERCE, Peter G. Peterson, *Secretary*
NATIONAL OCEANIC AND ATMOSPHERIC ADMINISTRATION, Robert M. White, *Administrator*
Rockville, Md., December 1972

For sale by the Superintendent of Documents, U.S. Government Printing Office, Washington, D.C. 20402
Price 80 cents domestic postpaid or 55 cents GPO Bookstore Stock Number 0317-00096

UDC 621.391.812.632 : 551.515.4 : 551.510.535 : 551.501.81

| | |
|---|---|
| 551.5 | Meteorology |
| .501.81 | Weather radar |
| .510.535 | Ionosphere |
| .515.4 | Thunderstorms |
| 621.391.81 | Radio propagation |
| .812.632 | Ionospheric disturbances to radio propagation |


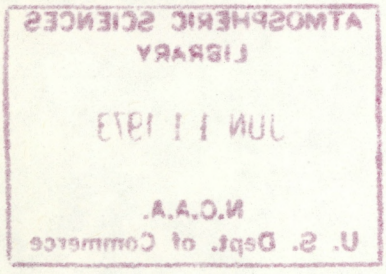

# Contents

## TABLES



## FIGURES

# Ionospheric Disturbances Produced by Severe Thunderstorms

KENNETH DAVIES AND JOHN E. JONES
*Space Environment Laboratory, Environmental Research Laboratories, Boulder, Colo.*

ABSTRACT. Radio observations near Oklahoma City during the spring of 1970 have shown ionospheric effects that occur within a radius of 200 km from severe thunderstorms having cloud tops above 12 km (40,000 ft). These effects frequently take the form of acoustic-gravity waves that appear to originate in the thunderstorm cells and propagate to F-region heights. The power in the waves usually has peaks at periods near 3.5 and 4.5 min, although periods between 7 and 10 min have been observed occasionally. Three-dimensional velocity vectors have been calculated for several ionospheric disturbances; and by means of acoustic wave ray-tracing, particular groups of thunderstorm cells have been identified as their sources. For the 7- to 10-min waves, an apparent inconsistency between the period and the velocity gives evidence of neutral winds with speeds of at least 70 m/s in the F region. We estimate that the power required to produce waves of the type observed is about 50 MW, one-millionth of the power generated by a large storm.

## 1. INTRODUCTION

We discuss certain types of wavelike disturbances observed on ionospheric radio echoes. We show that these disturbances are closely associated with the occurrence of severe thunderstorms within a horizontal distance of about 200 km from the ionospheric reflection point. The evidence suggests that the observed phenomena result from the interaction between ionospheric charged particles and the motion of neutral molecules caused by the passage of acoustic type waves with periods between 3 and 5 min.

In section 2, we discuss the evidence in the literature for ionospheric effects thought to be associated with tropospheric weather. Section 3 contains some basic radio propagation theory required for understanding the probing technique with spaced transmitters and also contains the description of the method of data analysis. Some physical theory of the propagation of acoustic gravity waves is presented in section 4 together with the results of ray tracing in the 1962 U.S. Standard Atmosphere [COESA(U.S. Committee on Extension to the Standard Atmosphere) 1962] with and without horizontal winds. In section 5 are the results obtained in Oklahoma during April through July 1970. The measured velocities of the disturbances are compared with radar summaries and radar photographs. Spectra of the recorded waveforms are also presented. We discuss disturbances that produce S-shaped records and have periods in the acoustic domain, but have speeds appropriate to gravity waves. These disturbances suggest the presence of neutral winds in the F region. The approximate source power required for the acoustic disturbances detected in the ionosphere is discussed in section 6 along with the effects of the geomagnetic field on the detectability of the waves. A microbarograph was installed in Oklahoma to see whether waves with periods such as those detected in the ionosphere were present near the surface. The (negative) results of the latter

experiment are discussed in section 7. Some statistical data on the occurrence of ionospheric disturbances, the characteristics of the spectra, the influence of geomagnetic disturbances, solar activity, etc., are presented in section 8. Finally, in section 9, we consider some of the possible causes of the disturbances, such as convective turbulence, shock waves from lightning, ionospheric absorption of sferics, and acoustic and buoyancy oscillations.

## 2. HISTORY

The idea that tropospheric weather affects the ionosphere began in the 1920s when Wilson (1925) was one of the first to suggest that the electric field of a thundercloud may cause ionization in the ionosphere. Other workers noted that reception of ionospheric radio echoes appeared to correlate with weather conditions. The appendix is a partial bibliography of publications in this field from 1925 through 1971.

Evidence for associations between weather and the ionosphere came from many parts of the world including the United States, the United Kingdom, Italy, and Australia. Regarding thunderstorms, it is interesting to recall the words of Watson-Watt (1933) in a discussion at the Royal Society of London.

"I think it is clearly established by this series of observations that the sudden appearance of these bursts of abnormal ionization (in the E region) just precedes the arrival of thunderstorms in the area within 50 km of the recording station."

Some of the correlations were misleading as, for example, the observation by Appleton et al. (1936) that ". . . abnormal E layer reflections occur most frequently in summer when local thunderstorms are at a maximum. . . ." We now know that this association results from two independent seasonal patterns. Associations between sporadic E increases and thunderstorms have also been found in India (Kesava Murthy 1963).

Extensive studies were conducted in Australia by Martyn (1934) and his collaborators who found that day-to-day changes in the F region were associated with meteorological changes at the ground. Healey's (1936) calculations showed that lightning radiation could not account for the magnitude of the ionospheric changes.

After World War II, there were renewed attempts to establish correlations between ionospheric variations and tropospheric weather, but with mixed success. Beynon and Brown (1951) inferred that the effects in both regions of the atmosphere were probably caused by solar activity. Evidence has been presented (e.g., Bauer 1958) for ionospheric effects of hurricanes.

One of the main difficulties encountered in this work has been the inability of independent workers to verify the results. Indeed, in several cases, on the basis of more complete data, scientists have withdrawn earlier claims.

That disturbances with acoustic periods in the lower atmosphere can couple into the ionosphere has been confirmed by observations of manmade explosions (Barry et al. 1966; Baker and Davies 1968) and earthquakes (Davies and Baker 1965; Yuen et al. 1969). In November 1965, ionospheric wavelike disturbances with periods near 3 min were observed for several days over Boulder, Colo., and were thought to be associated with tropospheric phenomena (Davies 1966). Georges (1967) suggested that the relatively narrow spectrum of these disturbances was the result of the atmosphere filtering acoustic-gravity waves. Georges (1969) observed these 3-min disturbances in the F region over the south-central part of the United States and made a major contribution by showing that they were associated with severe weather fronts passing through the observation area. Further studies of this phenomenon have been reported by Georges (1968) and by Baker and Davies (1969). They found that the following criteria must be fulfilled:

1. Cloud tops must be greater than about 40,000 ft (12 km).
2. Thunderstorm cells must lie within about 200–250 km from the point on the ground directly below the ionospheric reflection point.

Using the radar summary charts of the U.S. Weather Bureau (now the National Weather Service), Baker and Davies devised a severe weather index that ranged from 0 (no severe weather) to 5. They found that this index was always high (3 to 5) on days when disturbances were observed in the F2 region. However, on days of high severe weather index, ionospheric disturbances were not always observed. Similar observations of ionospheric disturbances associated with thunderstorms in Alabama have been made by Detert (1969).

## 3. IONOSPHERIC RADIO SOUNDING

### A. Magneto-Ionic Theory

To understand the radio sounding techniques used in this investigation, we shall briefly review the propagation of radio waves in a cold plasma containing a magnetic field. More detailed theory is given elsewhere (e.g., Ratcliffe 1959; Budden 1961; and Davies 1969). The interested reader should consult these books.

When a radio wave enters the ionosphere, it is split into two oppositely polarized waves. On radio frequencies above the electron cyclotron or gyrofrequency ($f_H \approx 1.4$ MHz), the left circular polarized wave (looking along the direction of the earth's magnetic field) is called the ordinary wave. The right circular polarized wave is called the extraordinary wave. On a single frequency, there are, in general, two radio echoes reflected from different heights. Because of collisions between electrons and neutral molecules, energy is absorbed from the wave. Most of the absorption occurs in the D region (60 to 90 km) where the collision frequency $\nu$ is high. The absorption of the extraordinary wave is usually greater than that of the ordinary wave; thus, the latter wave usually dominates the composite signal.

The maximum frequency reflected from a particular layer of the ionosphere is called the critical frequency of the layer. The ordinary wave critical frequency $f_o$ is related to the maximum electron density $N_m$ of the layer by the expression

$$N_m = 1.24 \times 10^{10} f_o^2 \, m^{-3} \tag{1}$$

where $f_o$ is in megahertz. The critical frequency of the extraordinary wave $f_x$ is related to $f_o$ by

$$f_o^2 = f_x^2 - f_x f_H. \tag{2}$$

Hence, $f_x > f_o$.

The complex refractive index of the ordinary (+) and extraordinary (−) waves of frequency $f$ are given by the Appleton equation

$$M^2 = (\mu - i\chi)^2 = 1 - X/D \tag{3}$$

where

$$D = 1 - iZ - [Y_T^2/2(1 - X - iZ)]$$

$$\pm \sqrt{[Y_T^4/4(1 - X - iZ)^2] + Y_L^2}$$

and

$$X = (f_N/f)^2$$

where

$f_N$ = plasma frequency,

$$Y = f_H/f, \qquad Y_L = Y \cos\theta, \qquad Y_T = Y \sin\theta,$$

$$Z = \nu/2\pi f,$$

and

$$i = \sqrt{-1}.$$

Here, $\theta$ is the angle between the direction of wave propagation and the geomagnetic field.

The important feature to notice in eq (3) is that the propagation depends on wave frequency (dispersion) and on direction of propagation (anisotropy). In dispersive propagation, the wave packet (energy) travels with the group speed that is, in general, different from the phase speed ($v$) with which the individual wave components travel. Hence, the individual waves tend to pass through the packet. In anisotropic propagation, the direction of motion of the packet (ray direction) differs from that of the phase normal. The component $u$ of the group velocity $\mathbf{V}_g$ in the direction of the wave normal ($k$) is given by

$$u = \mathbf{V}_g \sec\alpha = \frac{\partial\omega}{\partial k} = c\frac{\partial\omega}{\partial(\mu\omega)} \tag{4}$$

where $\omega$ is the angular wave frequency and $c$ is the free space speed; $\alpha$, the angle between the wave normal and the ray, is given by

$$\tan\alpha = \frac{1}{\mu}\frac{\partial\mu}{\partial\theta}. \tag{5}$$

It is important to bear these properties in mind because, as we shall see later, they apply also to the propagation of atmospheric waves.

Because of the anisotropy of the ionosphere, for a radio wave incident vertically on the ionosphere (in the Northern Hemisphere), the ordinary wave is reflected to the north of the point of entry; and the

474-478 O - 73 - 2

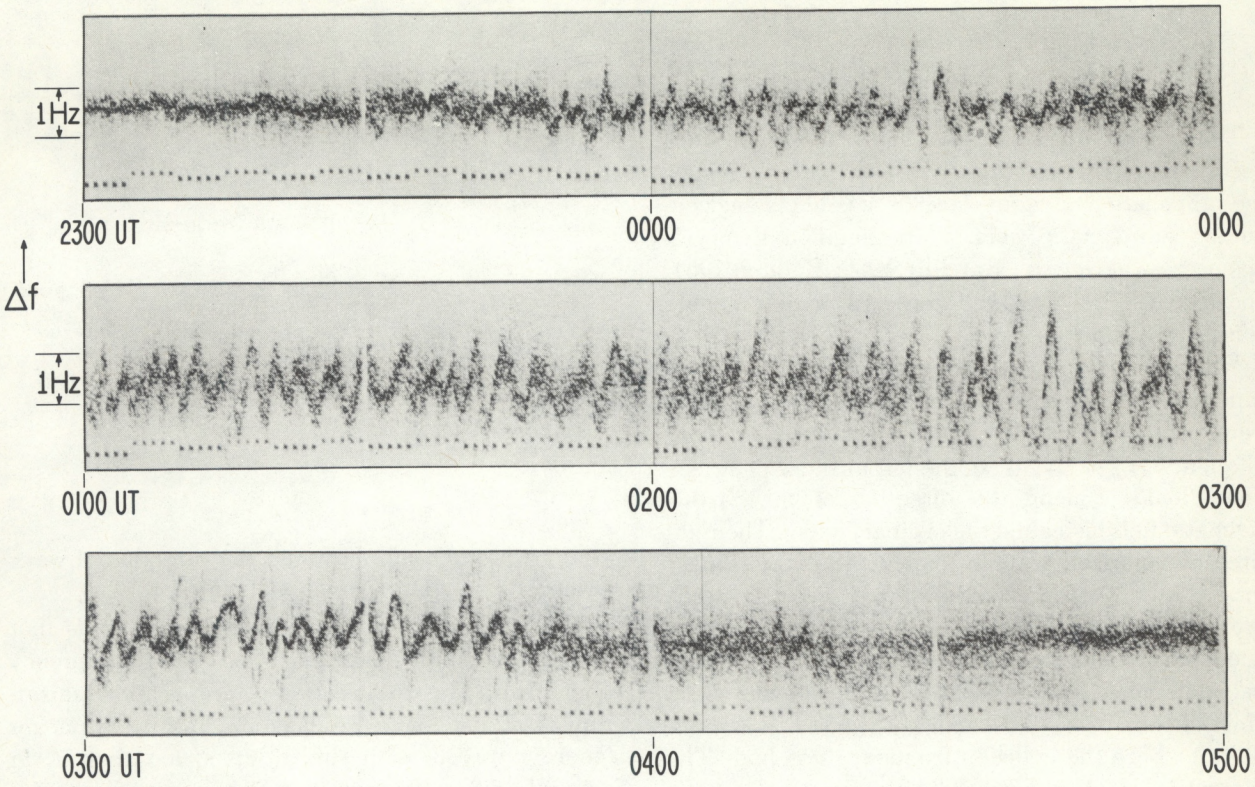


FIGURE 1.—Sample Doppler record (9.9 MHz, Havana, Ill., to Boulder, Colo., 13–14 June 1967)

extraordinary wave is reflected to the south. Hence, a disturbance traveling in the ionosphere will, in general, affect one wave before the other (Davies 1969, ch. 7).

The sweep frequency radar or ionosonde produces records of time delay (or virtual height) versus frequency for both ordinary and extraordinary waves. From these records, it is relatively easy to obtain the electron density profile up to the peak of the F2 layer (Wright and Smith 1967).

### B. Doppler Technique

When a change takes place in an electron density profile, the total phase path $P$ of a radio signal changes; and the instantaneous frequency shift $\Delta f$ of a radio echo of frequency $f$ is given by

$$\Delta f = -\frac{f}{c}\frac{dP}{dt} \tag{6}$$

where

$$P = \int_s \mu \cos\alpha \, ds. \tag{7}$$

Here, $ds$ is an element of the ray path $s$. As seen from eq (3) and (5), $\mu$ and $\alpha$ are rather complicated functions of frequency, direction, electron density, etc. In broad terms, however, two types of change predominate:

1. A change of path length $s$.
2. A change of refractive index at levels below reflection.

These two types of phase path change (provided we neglect collisions and the geomagnetic field) can be distinguished by observations on several close frequencies. In type 1,

$$\Delta f \propto f. \tag{8}$$

In type 2,

$$\Delta f \propto 1/f. \tag{9}$$

For the disturbances discussed in this paper, the Doppler shifts obey eq (8); henceforth, we shall assume that the observed shifts result from changing heights of reflection.

The continuous measurement of the Doppler shift is carried out by mixing the ionospheric echo

with a local offset reference signal and recording the beat frequency on magnetic tape moving 1 in./min. The frequency analysis is accomplished by fast playback of the tape, resulting in a frequency multiplication of about 1800. The audio signal thus produced is analyzed by conventional means (Davies 1969, sec. 9.3) and displayed on a facsimile chart. A sample record is shown in figure 1; from this, we see that the Doppler shifts are about 1 Hz. The smallest frequency shift that can be measured with this technique is about 0.1 Hz.

## C. Circuits

The radio paths used in this paper are shown in figure 2, together with the sounding frequencies used and the path midpoints. We dwell in detail on the spaced transmitter experiment in Oklahoma during the summer of 1970; we use the remaining data in an auxiliary role. Oklahoma was chosen for the observations because this State has the highest incidence of severe storms, especially tornadoes, per unit area of all States (National Weather Service 1970). Furthermore, weather radar data were available. The particular circuits shown in figure 2B were chosen partly because facilities were made available by NOAA's National Severe Storms Laboratory at Norman and by the Electrical Engineering Department of Oklahoma State University at Stillwater. A separation of about 50 km between ionospheric reflection points at the corners of an approximately equilateral triangle was selected because of the success of a somewhat similar experiment near Boulder (Davies and Jones 1971*a*). Ultimately, the distances selected were small because the horizontal trace velocities involved were about 1 km/s and the resulting time displacements less than a minute. Of course, if the separations are increased, the cross correlation between the various displaced Doppler curves is decreased. The choice of radio frequencies was restricted by ionospheric conditions to the range of frequencies that reaches, but does not penetrate, the F2 layer.

## D. Data Analysis

With the arrangement of spaced transmitters on 3.3, 4.0, and 5.1 MHz used in Oklahoma during April to July 1970, nine simultaneous $\Delta f(t)$ records were obtained. The beat frequencies were set about 1 Hz apart to distinguish the three traces on any one carrier. The velocity can be determined from

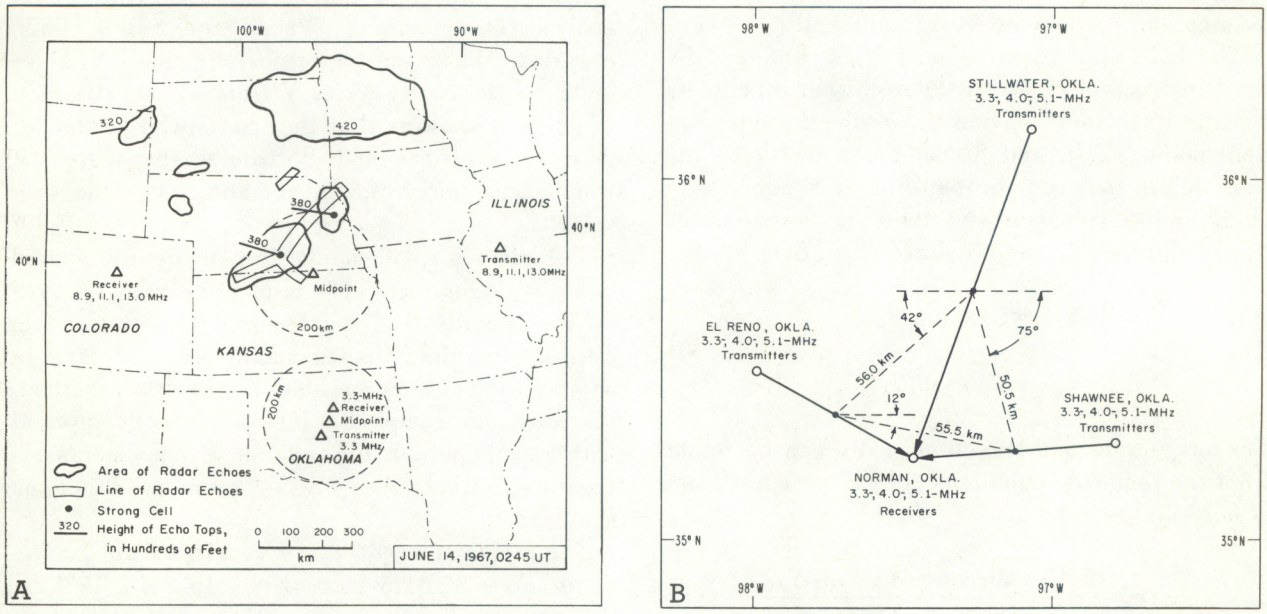


FIGURE 2. — (A) radar summary chart of the radio paths from Longbranch to Boulder and Norman to Stillwater; (B) spaced transmitters in Oklahoma

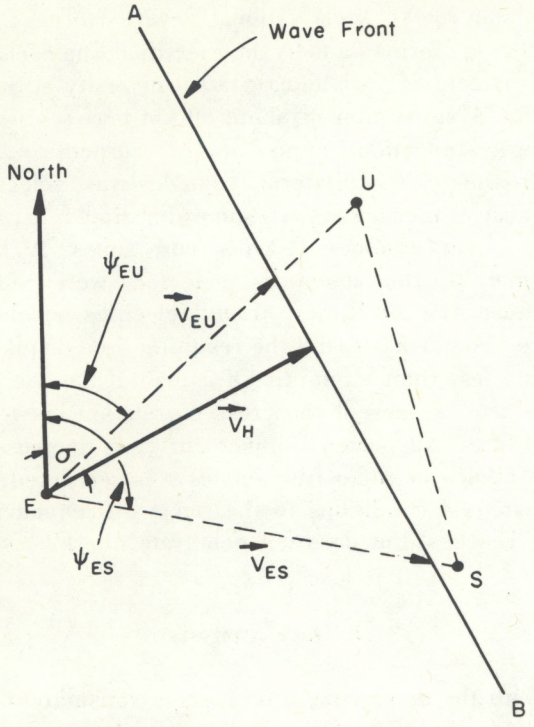


FIGURE 3.—Horizontal trace velocity $\mathbf{V}_H$ from time displacements

the time displacements by a procedure similar to that described by Davies and Jones (1971*a*), on the assumption that the disturbance is plane. This assumption is examined in subsection 4E.

The horizontal trace velocity $\mathbf{V}_H$ is obtained by the construction shown in figure 3 that represents a plane wave front moving across the three (reflection) points $E$, $U$, and $S$. Let $T_{EU}$ and $T_{ES}$ be the time delays between the patterns at $E$ and $U$ and at $E$ and $S$, respectively; then the apparent or trace velocities $\mathbf{V}_{EU}$ and $\mathbf{V}_{ES}$ are given by

$$\mathbf{V}_{EU}=56.0 \text{ km}/T_{EU}$$

and (10)

$$\mathbf{V}_{ES}=55.5 \text{ km}/T_{ES}.$$

The magnitude and direction of $\mathbf{V}_H$ can be found from the following equations. The direction $\sigma$ (east of north) is given by

$$\cot\sigma=-\frac{\mathbf{V}_{EU}\sin\psi_{EU}-\mathbf{V}_{ES}\sin\psi_{ES}}{\mathbf{V}_{EU}\cos\psi_{EU}-\mathbf{V}_{ES}\cos\psi_{ES}}; \quad (11)$$

the magnitude $V_H$ is given by

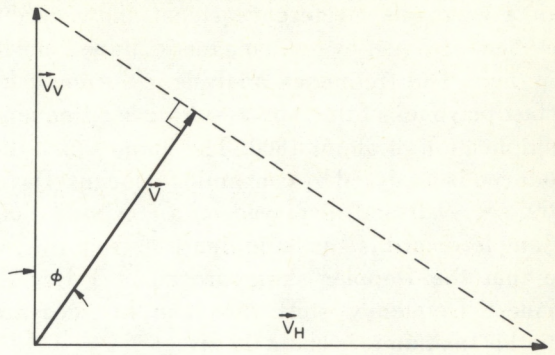


FIGURE 4.—Derivation of true velocity $\mathbf{V}$ from horizontal and vertical trace velocities $\mathbf{V}_H$ and $\mathbf{V}_V$

$$\frac{\sin^2(\psi_{ES}-\psi_{EU})}{V_H^2}=\frac{1}{V_{EU}^2}+\frac{1}{V_{ES}^2}-\frac{2\cos(\psi_{ES}-\psi_{EU})}{\mathbf{V}_{EU}\mathbf{V}_{ES}}. \quad (12)$$

Here, $\psi_{EU}$ and $\psi_{ES}$ are the angles between geographic north and the lines $EU$ and $ES$, respectively.

To obtain the true velocity $\mathbf{V}$, we also need the vertical trace velocity $\mathbf{V}_V$ found from the time displacements of the radio signals on different frequencies and the heights of reflection of the radio signals. The reflection points for a given transmitter and receiver location are assumed to lie on a vertical line. Errors introduced by this assumption are discussed in subsection 4E. The heights of reflection can be found by true height analysis of ionograms (Wright and Smith 1967). Knowing the trace velocities $\mathbf{V}_H$ and $\mathbf{V}_V$, we obtained the true velocity $\mathbf{V}$ from the construction in figure 4 showing that the true speed is smaller than the vertical and horizontal trace speeds, which are, therefore, not components of the true velocity.

The time displacements can be determined in two ways. One method is to locate similar features on the records (e.g., peaks, troughs, etc.) and to average the time displacements over as large a sample of cycles as possible. In the other method, the traces are sampled at intervals, short compared with a cycle period; and the time displacements are measured from the cross-correlation functions (Jones 1969).

The application of these two methods to the disturbance of 0425–0505 UT on June 11, 1970, is illustrated in figures 5 and 6. From the positions of the peaks and troughs, the average time displacements are $T_{ES}=35.8$ s and $T_{EU}=-23.3$ s. The

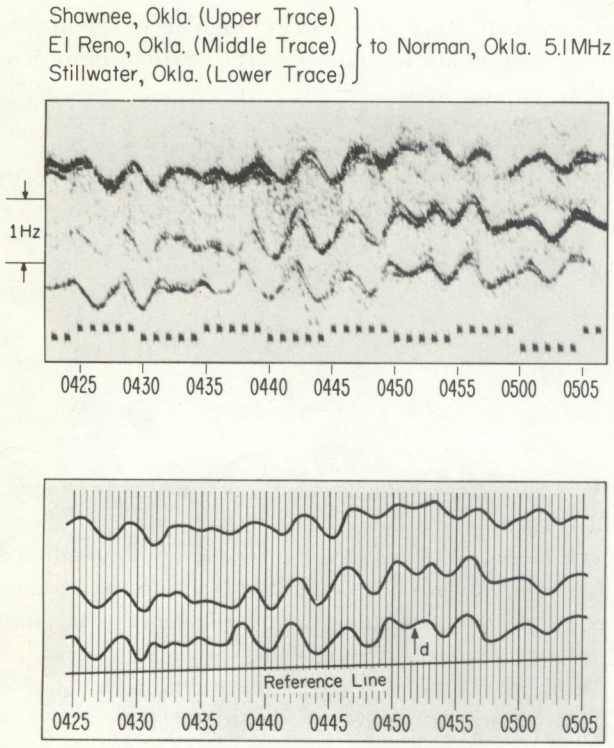


FIGURE 5.—Method of digitizing the Doppler records for the disturbance of June 11, 1970, at 0425–0505 UT

Doppler record has been carefully scaled every 30 s (fig. 5) to find the time displacement by cross correlation. The instantaneous Doppler frequency is represented by the distance $d$ on the record from the traces to the reference line. The reference line follows the long-period trends of the traces to eliminate their influence on the cross correlograms. The cross-correlation curves (fig. 6) give $T_{ES}=38$ s, $T_{EU}=-22$ s, and $T_{US}=58$ s. Similar analyses have been carried out for the disturbances of April 30 and May 13, 1970. The magnitude $V_H$ and azimuth $\sigma$ obtained by these two methods are given in table 1.

In general, the agreement is good except for the azimuth on April 30 when the trace velocity is large, which implies that the direction of propagation is nearly vertical.

## 4. ACCOUSTIC-GRAVITY WAVES

### A. Refractive Index and Parcel Orbits

Acoustic-gravity waves are oscillatory motions traveling in a stratified atmosphere in which the

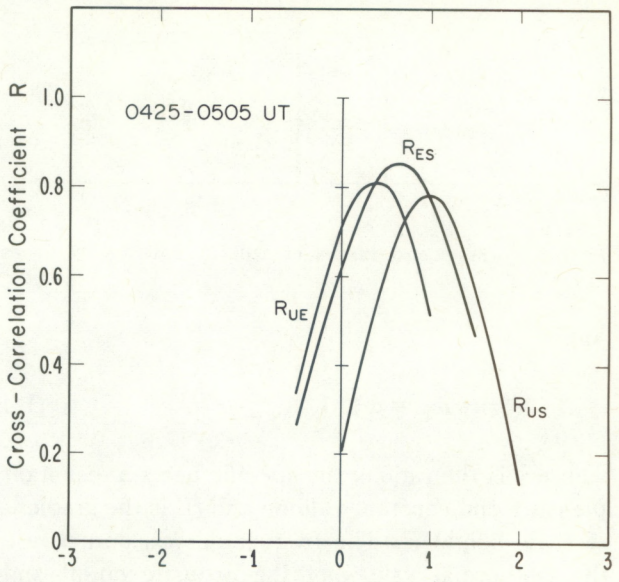


FIGURE 6.—Cross-correlation functions for the records from El Reno, Shawnee, and Stillwater on June 11, 1970

TABLE 1.—*Comparison of horizontal velocities obtained by similar features and cross correlation*

| Date (1970) | UT | | $V_H$ (m/s) | $\sigma$ (deg.) |
|---|---|---|---|---|
| June 11 | 0425–0505 | Peak and trough | 850 | 158 |
| | | cross correlation | 840 | 157 |
| Apr. 30 | 1025–1040 | Peak and trough | 2700 | 54 |
| | | cross correlation | 2600 | 78 |
| May 13 | 0345–0425 | Peak and trough | 900 | 172 |
| | | cross correlation | 880 | 176 |

forces of buoyancy are comparable to the compressional forces. Detailed studies of the propagation of these waves in nonuniform absorbing and windy atmospheres have been given by a number of authors (e.g., Hines 1960; Midgley and Liemohn 1966; and Pitteway and Hines 1963 and 1965).

The propagation of acoustic-gravity waves in a temperature and density stratified and flat atmosphere is dominated by certain characteristic frequencies. Neglecting the earth's rotation, there are two such frequencies: the acoustic cutoff frequency $\omega_A$ and the buoyancy (also called the Brunt-Väisälä) frequency $\omega_B$ given by

$$\omega_A = \omega_a \tag{13}$$

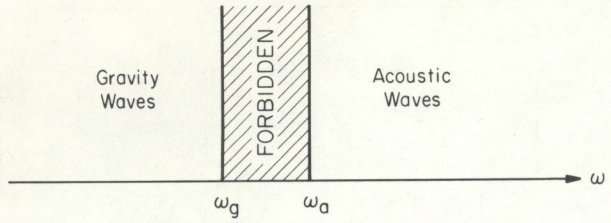


FIGURE 7.—Frequency ranges of acoustic and gravity waves

and

$$\omega_B^2 = \omega_g^2 \left(1 + \frac{\gamma}{\gamma - 1} H'\right) \tag{14}$$

where $\gamma$ is the ratio of the specific heats at constant pressure and constant volume and $H'$ is the gradient of scale height $H$. The frequencies $\omega_a$ and $\omega_g$ are the isothermal values of the acoustic cutoff and buoyancy frequencies given by

$$\omega_a = \frac{C}{2H} \tag{15}$$

and

$$\omega_g^2 = \frac{g}{H} \frac{\gamma - 1}{\gamma} . \tag{16}$$

Here,

$$C^2 = \gamma g H \tag{17}$$

is the square of the sound speed, and $g$ is the gravitational acceleration.

The physical significance of these two frequencies is as follows. If we squeeze the whole atmosphere vertically and then release it, the atmosphere will oscillate vertically about its equilibrium position at $\omega_a$. On the other hand, if we displace a parcel of the atmosphere vertically and then release it, the parcel will oscillate at $\omega_g$. The two frequencies are related by

$$\omega_a^2 \frac{4(\gamma - 1)}{\gamma^2} = \omega_g^2. \tag{18}$$

Hence for an atmosphere with diatomic molecules for which $\gamma \approx 1.4$,

$$\omega_g \approx 0.9\, \omega_a. \tag{19}$$

From Davies et al. (1969), the refractive index $\mu$ of an acoustic-gravity wave of angular frequency $\omega$ propagating at an angle $\phi$ to the vertical in an isothermal atmosphere is given by

$$\mu^2 = \frac{C^2}{V^2} = \frac{C^2 k^2}{\omega^2} = \frac{1 - X}{1 - Y^2 \sin^2 \phi} \tag{20}$$

where

$$X = \left(\frac{\omega_a}{\omega}\right)^2,$$

$$Y = \frac{\omega_g}{\omega},$$

**V** is the phase velocity, and $k$ is the wave propagation parameter.

Equation (20) reveals the frequency dependence (dispersion) and the angular dependence (anisotropy) of the propagation. It also shows that there are two families of waves that can propagate. One family has $X$ (and, hence, $Y$) less than unity. These high-frequency waves constitute the acoustic domain. The low-frequency waves have $X$ and $Y \sin \phi$ greater than unity and are called gravity waves. Thus, acoustic waves exist at frequencies greater than the acoustic cutoff frequency, whereas gravity waves exist at frequencies less than the buoyancy frequency. In between, there is a forbidden frequency range as sketched in figure 7. The $\mu(\phi)$ curves, parametric in $Y$, are shown in figure 8 for acoustic waves and figure 9 for gravity waves, together with the particle orbits given by

$$\frac{\xi}{\zeta} = \frac{\mu \sin \phi}{\mu^2 \sin^2 \phi - 1} \{-\mu \cos \phi + i(X - Y^2)^{1/2}\}. \tag{21}$$

Here, $\xi$ and $\zeta$ are the horizontal and vertical displacements (or velocities), respectively; and $i = \sqrt{-1}$. The orbits are ellipses that, under certain conditions, become circular or linear. For acoustic waves, the orbit is circular for horizontal propagation at a frequency $\omega_a \sqrt{2/\gamma}$. The orbits are linear with vertical propagation and almost the same at frequencies approaching the acoustic cutoff frequency for all directions of propagation. As the wave frequency departs farther from and above the acoustic cutoff frequency, the orbits become essentially longitudinal.

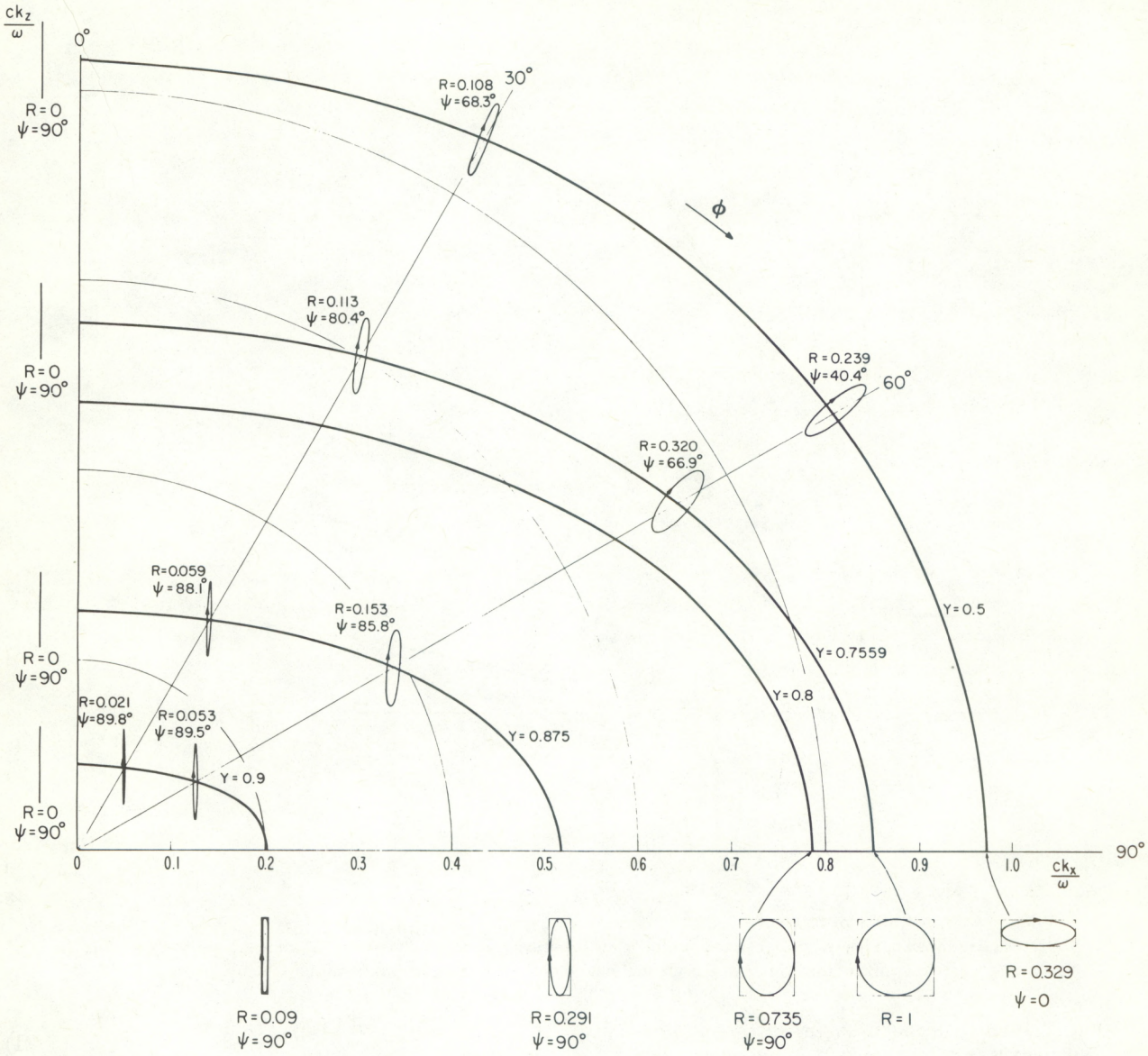


FIGURE 8.—Refractive index curves ($\mu$ surfaces) and parcel orbits for acoustic waves in an isothermal atmosphere ($\gamma=1.4$). $R$ is the axial ratio of the orbit, and $\psi$ is the inclination of the major axis from the horizontal.

For gravity waves, propagation is limited to certain directions. The minimum and maximum values of $\phi$ are

$$\phi_{min}=\sin^{-1}\left(\frac{\omega}{\omega_g}\right)$$

and (22)

$$\phi_{max}=\pi-\sin^{-1}\left(\frac{\omega}{\omega_g}\right)$$

The sense of rotation of the air parcels for gravity waves is the reverse of that for acoustic waves. The orbit is circular for horizontal propagation on a frequency $\omega=\sqrt{\gamma/2}\ \omega_g$. As $\phi$ approaches its asymptotic values, the parcel orbits become linear and transverse to the direction of propagation. Some of the properties of acoustic waves and gravity waves are compared and contrasted in table 2.

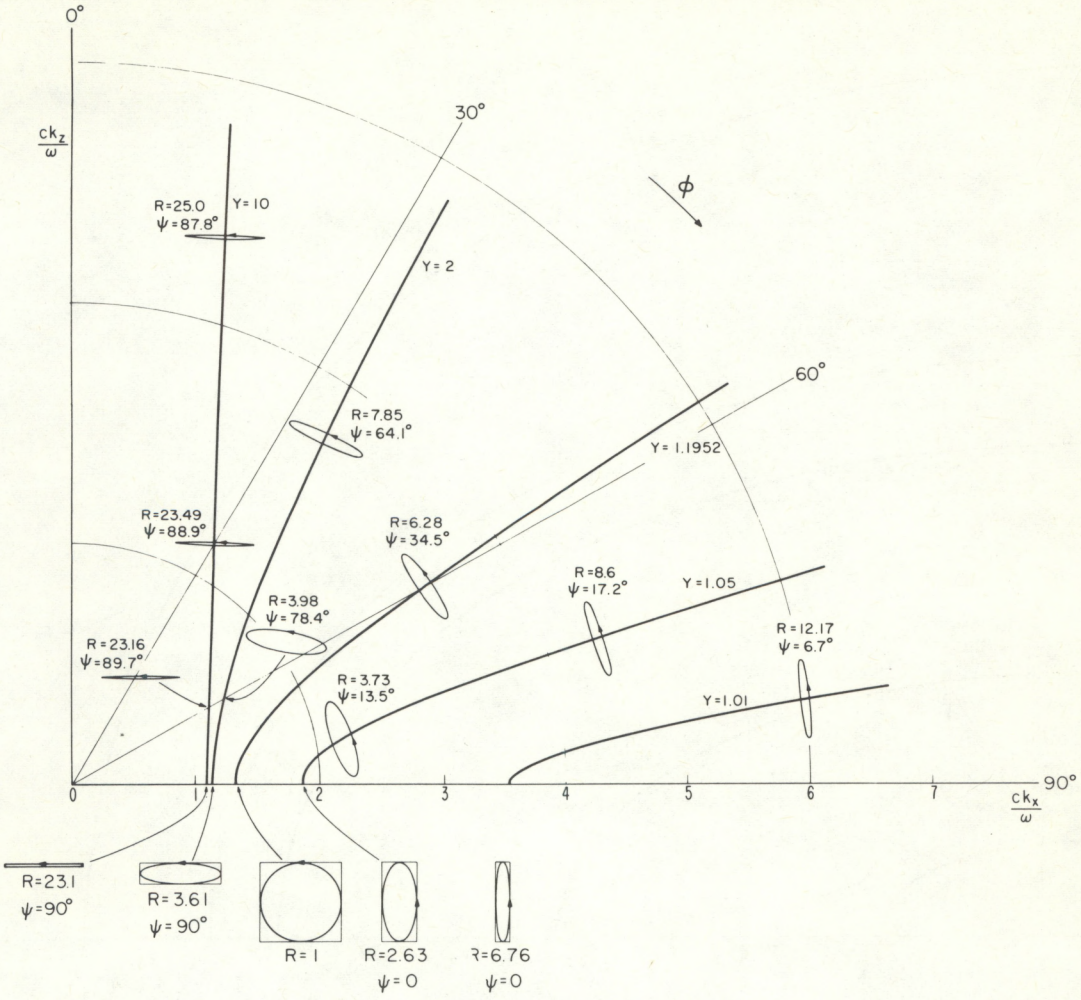


FIGURE 9.—Refractive index curves ($\mu$ surfaces) and parcel orbits for gravity waves in an isothermal atmosphere ($\gamma=1.4$). $R$ is the axial ratio of the orbit, and $\psi$ is the inclination of the major axis from the horizontal.

TABLE 2.—*Some properties of acoustic and gravity waves in an isothermal atmosphere*

| Parameter | Acoustic waves | Gravity waves |
|---|---|---|
| $X=(\omega_a/\omega)^2$ | $X<1$ | $X>1$ |
| $Y=\omega_g/\omega$ | $Y<1$ | $Y\sin\phi>1$ |
| Refractive index | $\mu<1$ | $\mu>1$ |
| Phase speed | $v>C$ | $v<C$ |
| Propagation angle | $0\leq\phi\leq 2\pi$ | $\pi-\sin^{-1}(1/Y)>\phi$ $>\sin^{-1}(1/Y)$ |
| Air parcel rotation | Clockwise | Anticlockwise |
| Energy vector **S** | Same quadrant as propagation | Energy flows up when phase travels down and vice versa. |

## B. Ray Tracing

We have seen that the propagation of acoustic-gravity waves is dispersive and anisotropic. As mentioned in subsection 3A, the flow of energy differs in both direction and speed from the flow of phase. The component $u$ of group velocity $\mathbf{V}_g$ in the direction of wave propagation is obtained by substituting eq (20) into eq (4). This gives

$$u=\mathbf{V}_g\cos\alpha=\frac{\mathbf{V}(\omega^2-\omega_a^2)}{\omega^2-\mu^2\omega_g^2\sin^2\phi}=\frac{\mathbf{V}(1-X)}{1-\mu^2Y^2\sin^2\phi}. \tag{23}$$

The angle $\alpha$ between the wave normal and the ray is

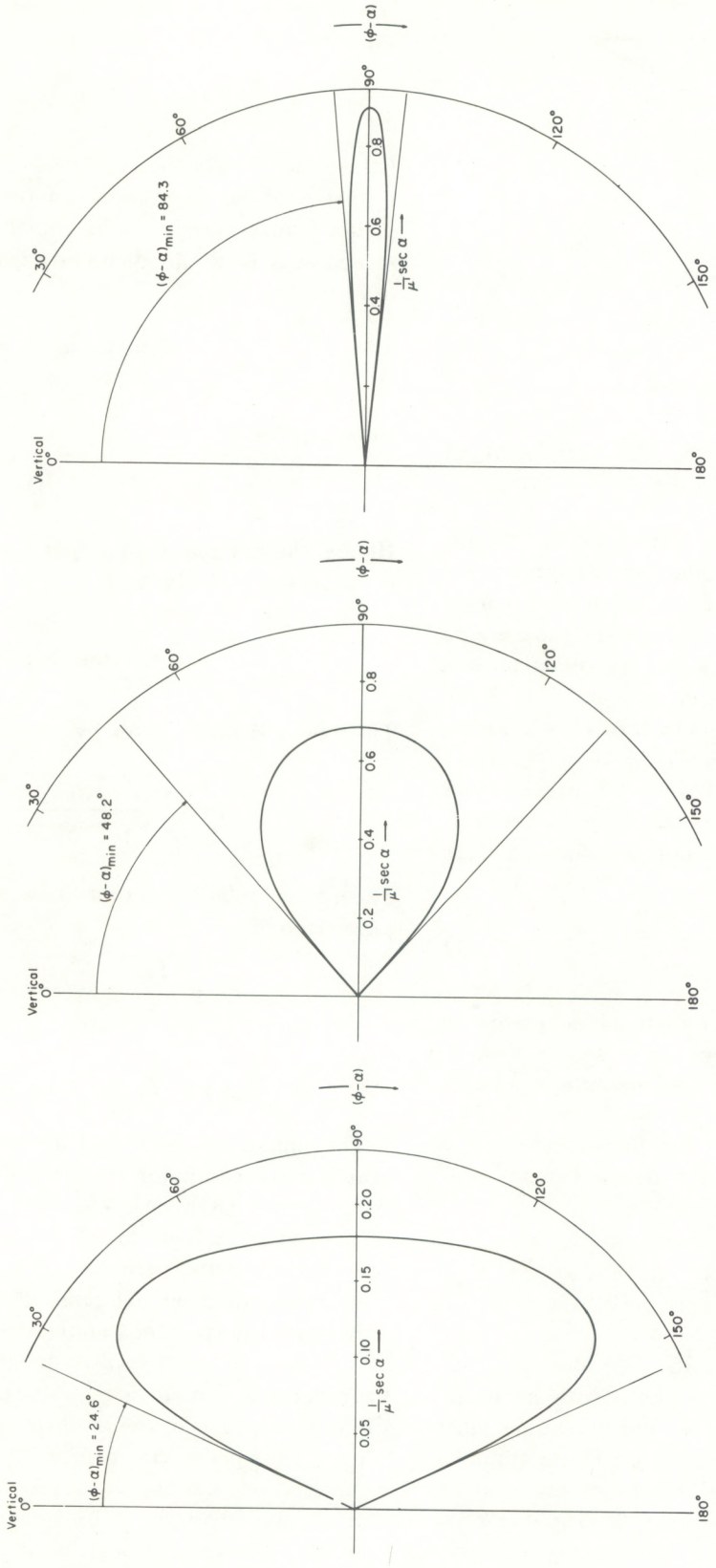


FIGURE 10.—Ray surfaces for an atmospheric gravity wave (energy surface reached by a gravity-wave packet, in unit time, showing the beaming property)

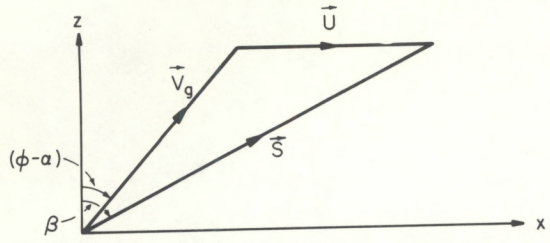


FIGURE 11.—Relative directions of group propagation without wind ($\mathbf{V}_g$) and with wind (S)

likewise obtained from eq (2) and (5):

$$\tan \alpha = \frac{Y^2 \sin \phi \cos \phi}{1 - Y^2 \sin^2 \phi}. \tag{24}$$

Equation (24) shows that, for acoustic waves, $\alpha (> 0)$ lies in the same quadrant as $\phi$; but for gravity waves, $\alpha (< 0)$ is in a different quadrant from $\phi$. This means that, for upward progression of energy flow in a gravity wave, the phase normal points downward. Applying eq (23) and (24) to the propagation of gravity waves illustrates the beaming properties of the propagation. Figure 10 (p. 11) shows surfaces reached in unit time by gravity-wave packets radiated from a (hypothetical) point source. The limiting angles of the energy propagation are given by

$$\tan (\phi - \alpha)_{\substack{max \\ min}} = \mp \sqrt{Y^2 - 1}. \tag{25}$$

Let us now derive the equations necessary to trace acoustic-gravity waves in a slowly varying atmosphere in the presence of a horizontal wind **U** in the plane of propagation.

The refraction condition for these waves in a windy atmosphere is expressed by the constancy of the horizontal trace velocity $\mathbf{V}_H$:

$$\frac{\mathbf{V}}{\sin \phi} + \mathbf{U} = \mathbf{V}_H \tag{26}$$

(see, e.g., Lamb 1960, sec. 75). We start at some reference level in the atmosphere with an initial value of $\phi$. To find $\mathbf{V}_H$ (for a known **U**), one must know **V**. This can, in principle, be found from eq (20); but the latter applies only to an observer at rest with respect to the medium. If $\omega$ is the wave frequency observed on the ground, the intrinsic frequency $\Omega$ as seen by the observer moving with the wind is

$$\Omega = \omega (1 - \mathbf{U}/\mathbf{V}_H) \tag{27}$$

(Hines and Reddy 1967); $\Omega$ must be used in eq (20) in place of $\omega$. Combining eq (20), (26), and (27) yields a quartic that can be solved for $\mathbf{V}_H$. The ray direction $\beta$ is obtained directly from the geometry of figure 11:

$$\tan \beta = \frac{\mathbf{U} + \mathbf{V}_g \sin (\phi - \alpha)}{\mathbf{V}_g \cos (\phi - \alpha)}. \tag{28}$$

From eq (23),

$$\tan (\phi - \alpha) = (1 - \omega_g^2/\Omega^2) \tan \phi. \tag{29}$$

Hence, the horizontal coordinate $x$ of a point on the ray at a height $z$ is given by

$$x = \int_{z_0}^{z} \tan \beta \, dz. \tag{30}$$

The time of flight $t$ is given by

$$t = \int_{z_0}^{z} \frac{dz}{\mathbf{V}_g \cos (\phi - \alpha)}. \tag{31}$$

The phase, relative to that at the reference height $z_0$, is given by

$$\Phi = \int_{z_0}^{z} \frac{\Omega \mu}{C} \cos \alpha \sec \beta \, dz. \tag{32}$$

### C. Ray Paths in Model Atmosphere

The equations developed above have been integrated by a computer for the 1962 U.S. Standard Atmosphere (COESA 1962). The height variations of molecular temperature $T_M$, sound speed $C$, and the characteristic periods $\tau_g$, $\tau_B$, and $\tau_a$ for this atmosphere are given in figures 12, 13, and 14.

Because the speed of sound increases above about 90 km, acoustic-gravity waves are refracted (and may be reflected). For acoustic waves, there exists an iris in this region of the atmosphere through which waves can penetrate to the F region. Gravity waves, which cannot propagate at angles to the vertical less than the critical angle $\phi_c$, can only reach the F region through an annulus. This latter

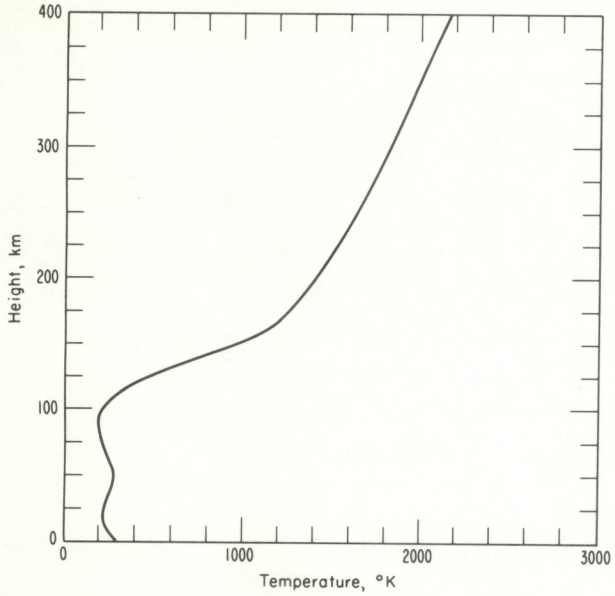


FIGURE 12.—Height variation of molecular temperature $T_M$ for the 1962 U.S. Standard Atmosphere

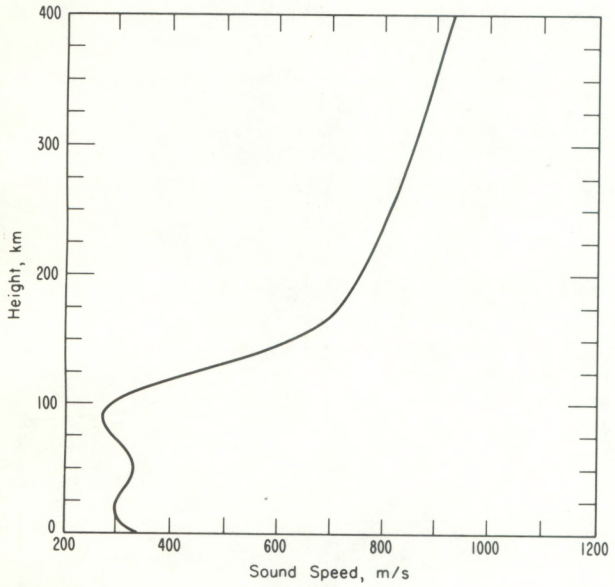


FIGURE 13.—Height variation of sound speed $C$ for the 1962 U.S. Standard Atmosphere

property results in an angular filtering of gravity waves propagating into the F region from sources in the lower atmosphere. Hence, F-region traveling disturbances originating in the lower atmosphere will propagate only at angles near the asymptotic value. This is illustrated in figure 15. Recall that,

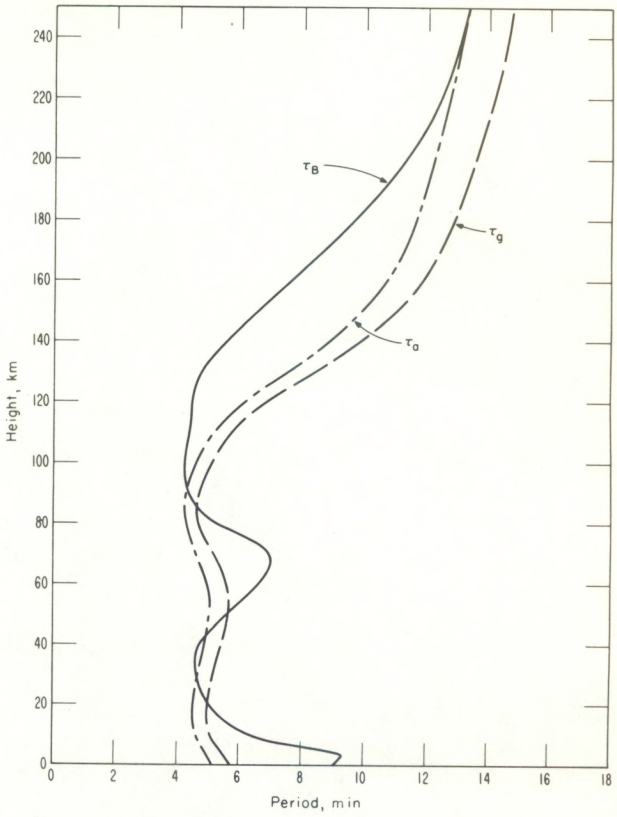


FIGURE 14.—Height variations of acoustic cutoff and buoyancy periods for the 1962 U.S. Standard Atmosphere

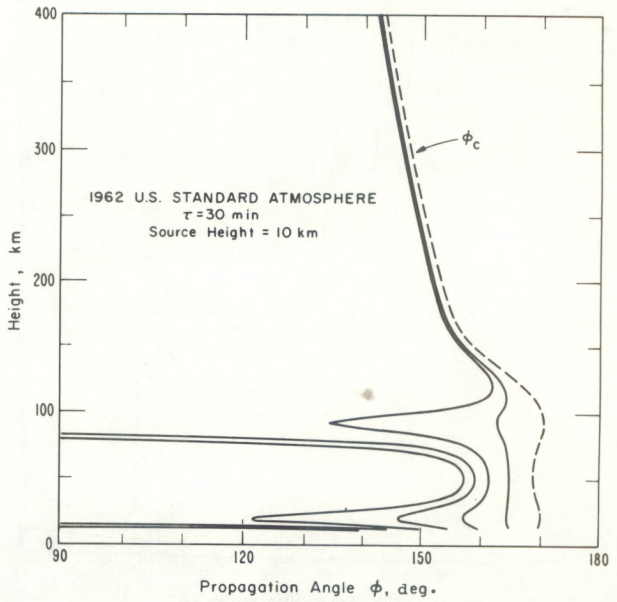


FIGURE 15.—Height variations of the propagation angles of 30-min gravity waves from a point source at 10 km (from Chang 1969)

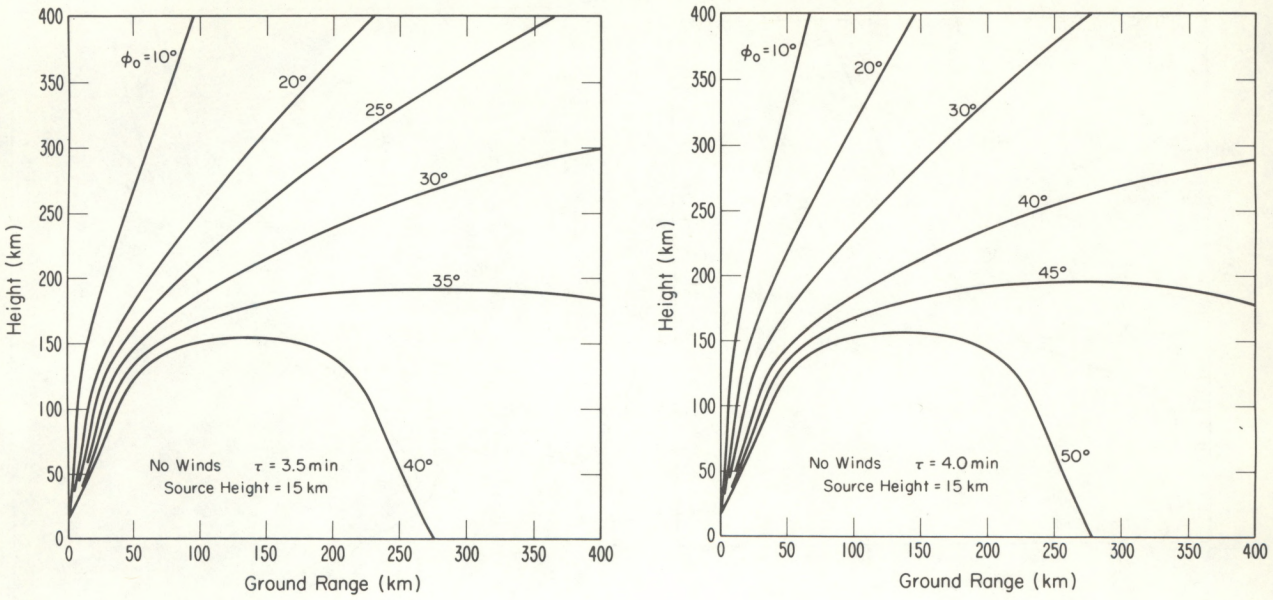


FIGURE 16.—Acoustic ray paths in the 1962 U.S. Standard Atmosphere from a source at 15 km and with periods of 3.5 and 4.0 min

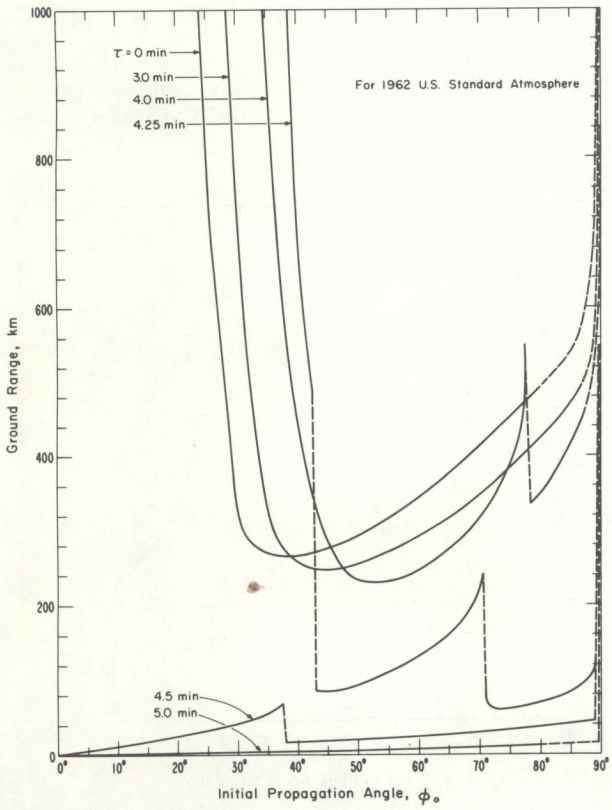


FIGURE 17.—Variation of ground range with the initial propagation angle

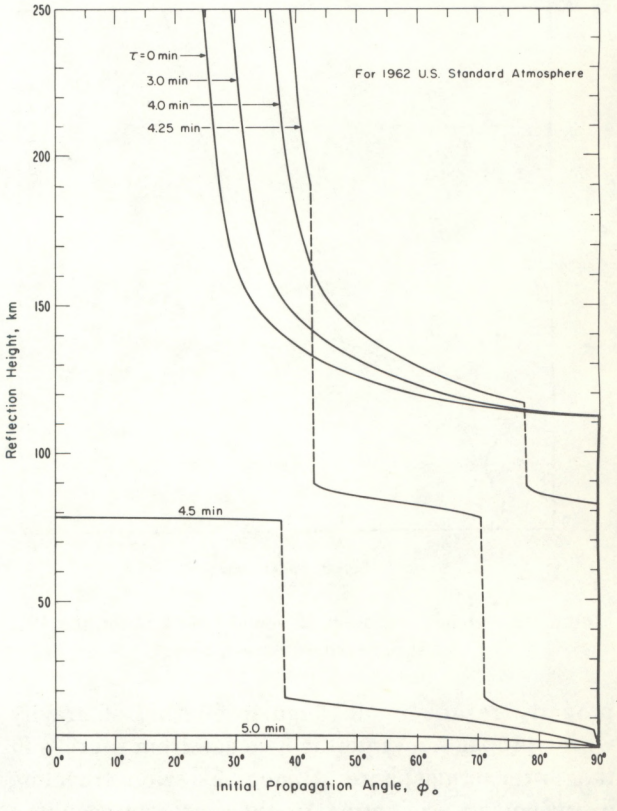


FIGURE 18.—Variation of reflection height with the initial propagation angle

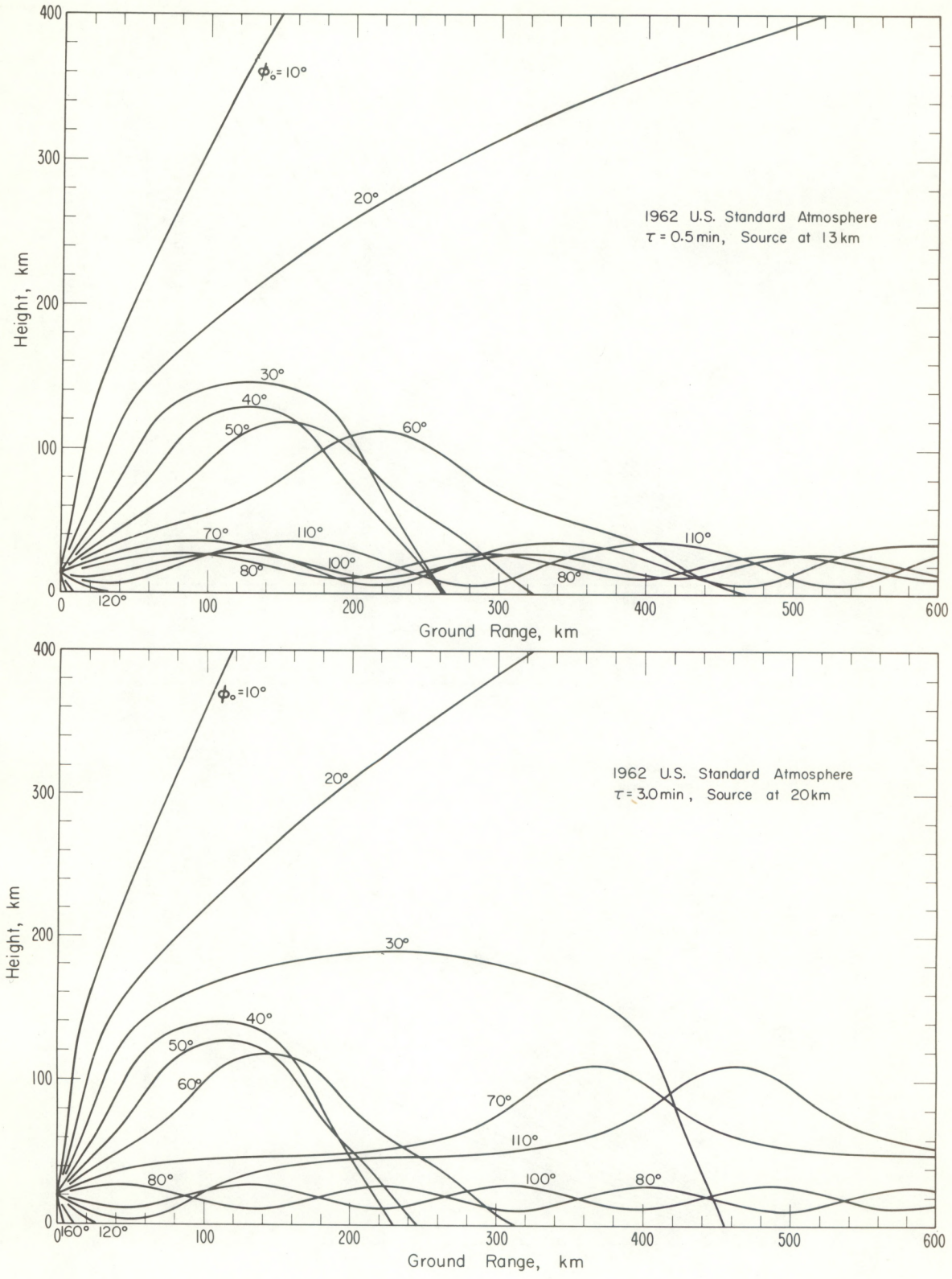


FIGURE 19.—Acoustic ray paths (from an elevated source) showing ducts

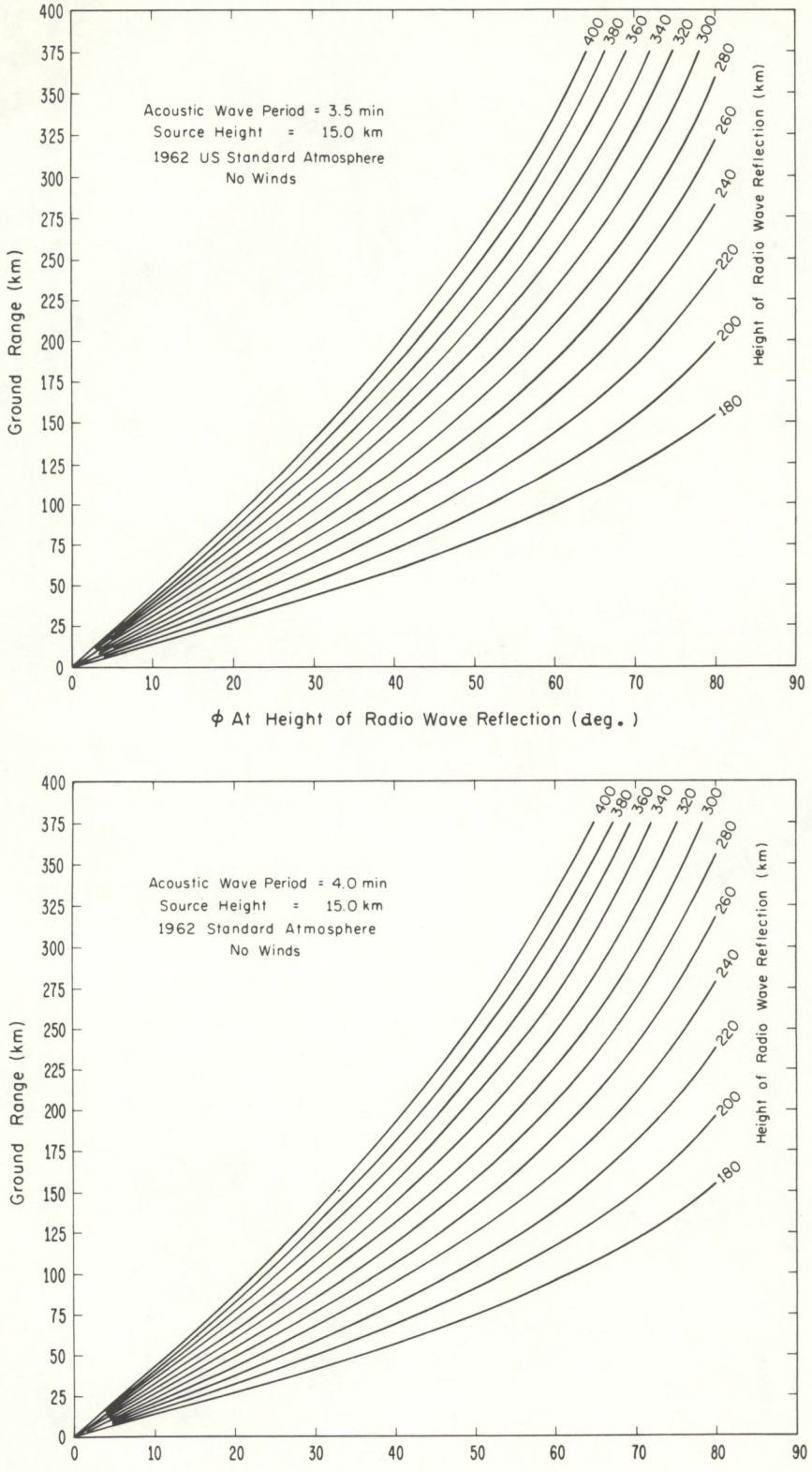


FIGURE 20.—Variation of ground range with the propagation angle $\phi$, measured at the level of radio reflection, for a source at a 15-km height and with periods of 3.5 and 4.0 min

for upward energy propagation, the propagation vector is directed downward.

The equations in subsection 4B have been integrated to give ray paths of acoustic waves with periods of 3.5 min and 4.0 min for no winds and for a source height of 15 km. These paths (fig. 16, p. 15) show that, above 100 km, the iris changes with wave period. Figure 16 shows that, for a given height in the atmosphere (e.g., 100 km), the aperture through which the waves flow for a given initial angle $\phi_0$ decreases with increase of wave period. However, when the wave period exceeds the minimum value of the acoustic cutoff period (which usually occurs near 85 km), total internal reflection occurs at all angles. Under these conditions, energy can only "tunnel" through the barrier, and "full wave" theory must replace ray tracing. It is interesting to note that, near the 85-km level, the propagation angle $\phi$ for a given initial angle $\phi_0$ tends to increase because the period is approaching the acoustic cutoff period; but this may be more than offset by the decrease brought about by the slow sound speed.

Notice also that the initial propagation angle required for reflection at a given height (around 150 km) increases as the period increases. Figure 17 shows how the ground range varies with initial propagation angle for waves of different periods. For waves with periods less than about 4.0 min, there are two initial angles for a given range greater than a minimum range. This property is reminiscent of the oblique propagation of ionospheric radio waves (Davies 1969, ch. 12) in which the minimum distance is called the skip distance and the rays with the smaller and larger values of $\phi$ are called high-angle and low-angle rays, respectively (high refers to the elevation angle). For waves with periods between 4 and 5 min, there are discontinuities at the angles at which the wave penetrates a layer formed by the temperature variations shown in figure 12. The heights of reflection also change abruptly at these angles, as can be seen in figure 18. The reflected waves are trapped between the reflection levels (one of which may be at the ground) and propagate as in a waveguide (fig. 19).

As we shall see later, our main concern in this paper is with acoustic waves having periods in the approximate range of 2 to 10 min; these waves penetrate to the F region. Hence, we shall no longer concern ourselves with reflected waves.

In practice, we measure the magnitude and direction of the phase speed in the F2 region at the radio reflection levels. From a knowledge of the propagation angle and the height of reflection (from ionogram analysis), the ground range to the source can be calculated as a function of $\phi$ for various reflection heights. Families of curves are shown in figure 20 for waves with periods of 3.5 and 4.0 min giving the variation of ground range with angle in the ionosphere for various heights. Comparison of the two families of curves in figure 20 shows very little difference. This is important because, as we shall see, disturbances associated with thunderstorms contain a range of periods. The reason for the close similarities in the curves for the two periods is that most of the ray refraction occurs above 100 km where the acoustic cutoff and buoyancy periods are considerably greater than the wave periods (i.e., $X << 1$, $\mathbf{Y} << 1$); therefore, the propagation is essentially nondispersive. Hence, the major error in these ground range calculations is caused by uncertainties in the temperature model above 100 km.

Figure 21 shows curves of constant phase for waves of period 3.5 min emanating from a point

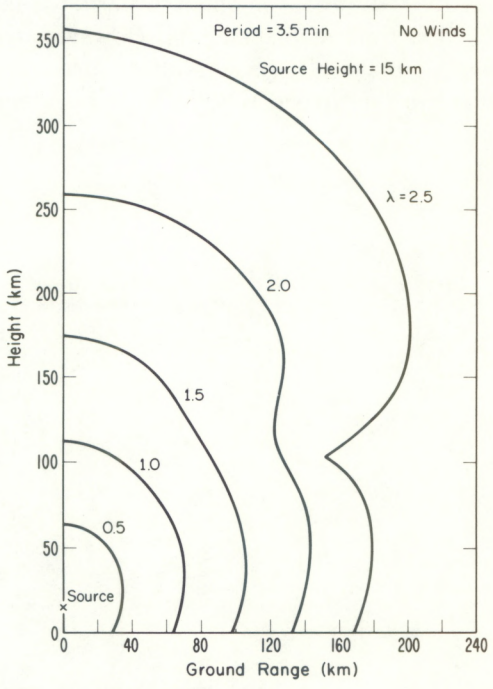


FIGURE 21.—Surfaces of constant phase in the 1962 U.S. Standard Atmosphere (no wind) for waves of period 3.5 min emanating from a source at 15 km

source 15 km above ground. The interesting feature to note here is that, for the heights of concern to us, there are only about two wavelengths between the source and the area of observation in the ionosphere. Under these conditions, it is clear that ray theory cannot be used to accurately determine the wave properties because the wavelengths are much larger than the scale heights of the medium.

### D. Determination of Velocity of Ionospheric Disturbances

The determination of the three-dimensional velocity of the ionospheric disturbance requires the horizontal and vertical trace velocities. The horizontal trace velocity is determined by the method described in subsection 3D. To find the vertical trace velocity, we need to know the locations of the reflection points of the radio waves of different frequencies and the appropriate time displacements. Unfortunately, in the present program, height information at the time of the measurements was not always available; in several cases, the amplitudes of the disturbances on the lower frequencies of 3.3 and 4.0 MHz were too small to permit measurement of the time displacements. However, we are satisfied that, for all waves with acoustic periods discussed in this paper, the phase propagation was upward.

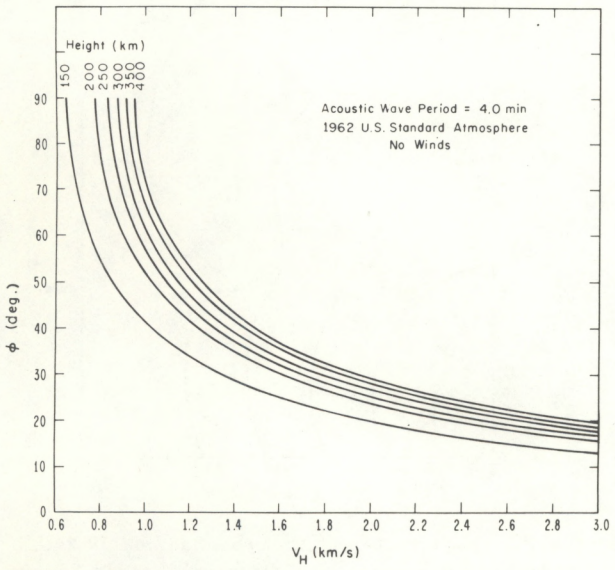


FIGURE 22.—Variation of propagation angle $\phi$ with horizontal trace velocity $\mathbf{V}_H$

To obtain the propagation angle $\phi$ at any height with no observations of the vertical trace velocity, we proceed as follows. From the model atmosphere given in figure 13, we have the sound speed $C$ and the characteristic periods $\tau_a$ and $\tau_g$. In the absence of winds, eq (26) gives

$$\sin\phi = \frac{\mathbf{V}}{\mathbf{V}_H}. \tag{33}$$

Substituting eq (33) into eq (20), we obtain

$$\frac{1}{V^2} = \frac{1-(\tau/\tau_a)^2}{C^2} + \frac{\tau^2}{\tau_g^2 V_H^2}. \tag{34}$$

Thus, for a given atmosphere, $\mathbf{V}$ and $\mathbf{V}_H$ are unique functions of $\phi$. The variation of $\phi$ with $\mathbf{V}_H$ is illustrated in figure 22.

### E. Some Possible Errors in the Velocities

It is now appropriate to discuss some errors that the assumptions introduce into the velocities. One of the important assumptions is that the wave front is plane, which will not be true for acoustic waves from severe thunderstorms. From observation, we know that the sources are about 300 to 500 km from the center of the triangle of sounding points. To get an idea of the error introduced by the curvature of the wave front, we assume a radius of curvature of 400 km and a 50-km equilateral triangle. The maximum error in direction occurs when propagation is parallel to a side of the triangle and amounts to 0.96°. There is no error in direction when propagation is parallel to a median. By contrast, the error in the magnitude of the velocity is a maximum for propagation along a median, 1.8% in this case.

Another assumption is that the reflection points for 3.3, 4.0, and 5.1 MHz are stacked vertically. The fact that they are not (because of magneto-ionic deviation) causes errors in the determination of the vertical trace velocity. Because the deviations, which lie in the magnetic meridians, differ for different frequencies, the triangles formed by the reflection points will be displaced and distorted. The midpoint triangles are shown in figure 23 for the concentric density profile shown in figure 24 (top). Electron density profiles were unavailable in Oklahoma, so we have used a Boulder, Colo., profile to illustrate these errors.

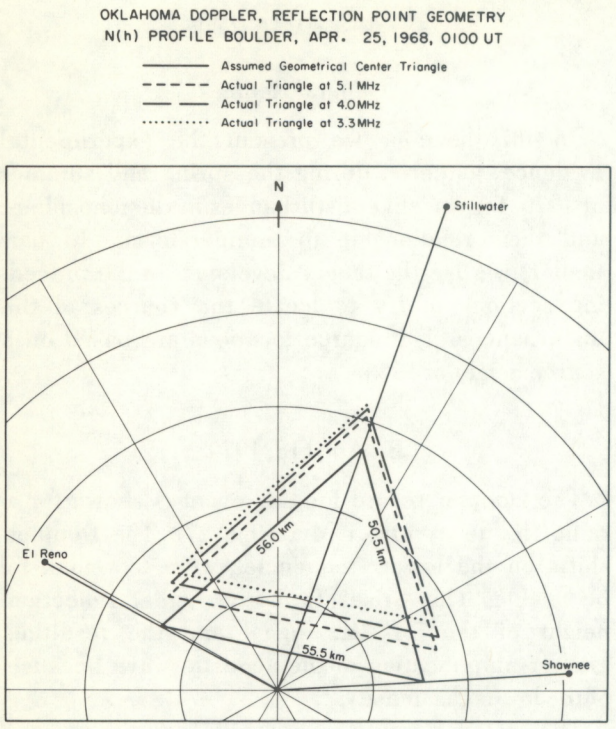


FIGURE 23.—Triangles formed by midpoints of radio paths and by the reflection points on 3.3, 4.0, and 5.0 MHz

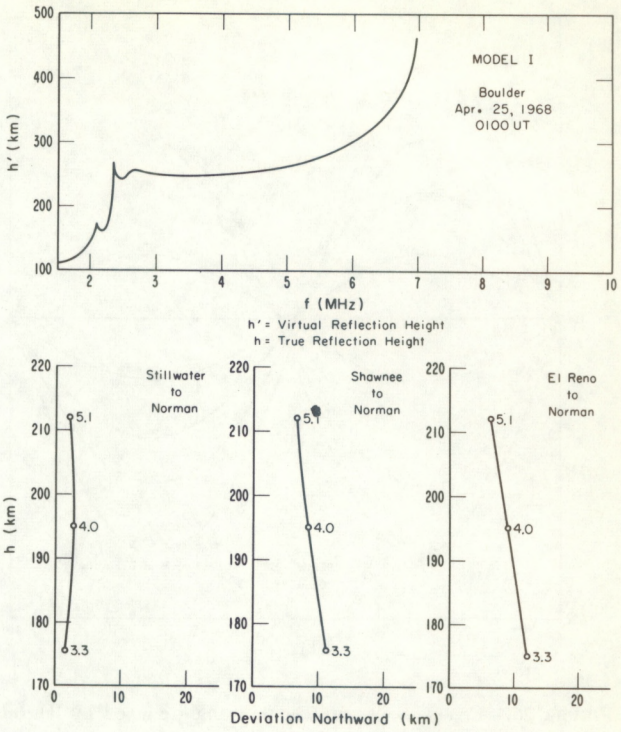


FIGURE 24.—Model I (M-I) ionogram (top) and the lateral deviations of the reflection points of the ordinary waves (bottom)

The neglect of the lateral deviations of the ordinary waves shown in figure 24 (bottom) can lead to appreciable errors in the vertical trace speed. This can easily be seen qualitatively by considering a vertical wave front moving south. It will affect the 3.3, 4.0, and 5.1 MHz successively. On the assumption of vertical stacking of the reflection points, it would be deduced that the wave has an upward component of velocity. The error in tilt of the propagation vector with respect to the vertical is shown in figure 25 for various azimuths $\sigma$. The maximum error of 9.3° occurs for meridional propagation and decreases to zero with propagation from west to east and east to west. The error in the true speed is shown in figure 26; note that the maximum errors of about 8.5% occur for propagation angles near 45° and near 135° with the vertical. However, as pointed out by Davies and Jones (1971*a*), the most important source of error is a mistake in distinguishing between an ordinary and an extraordinary trace.

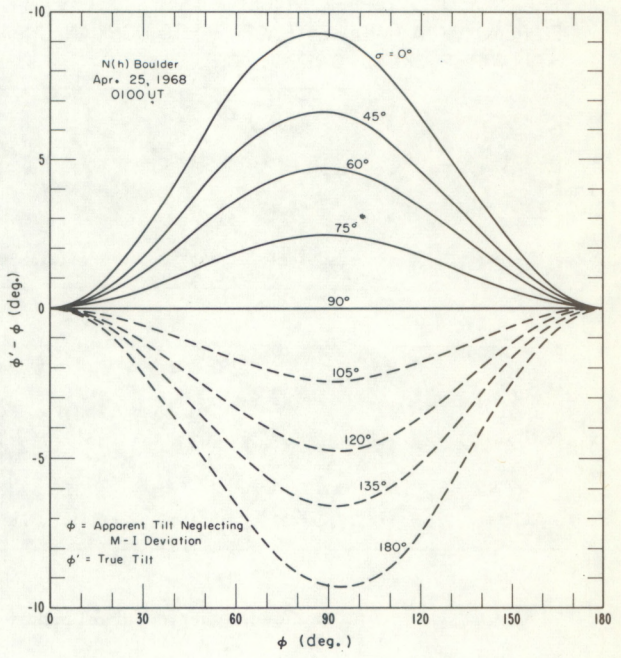


FIGURE 25.—Errors in speed (as function of propagation angle $\phi$ and azimuth $\sigma$) caused by lateral deviation

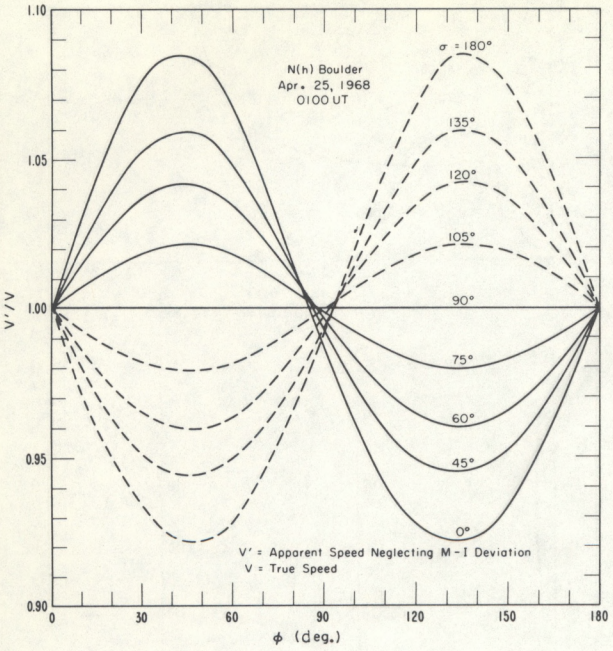


FIGURE 26.—Errors in the propagation angle caused by lateral deviation (as a function of the angle)

## 5. OBSERVATIONS

### A. General Remarks

In this section, we present the experimental evidence, gathered during the spring and summer of 1970, for wavelike disturbances in the ionosphere and their relationship to thunderstorms. In particular, we use the theory developed in the preceding sections to try to locate the sources of the disturbances. The source locations are based on a source height of 15 km.

### B. April 18, 1970

The Doppler record for this event is shown for a radio frequency of 5.1 MHz (fig. 27). The Doppler shifts on the lower frequencies were too small to be usable. This arises from the higher reflection height of the 5.1-MHz signal and the resulting greater amplification of the acoustic wave because of the lower gas density.

The Doppler traces in figure 27 have been separated by setting the three transmitters at frequencies about 1 Hz apart. The displaced lines of dots near the bottom of the record provide a time code.

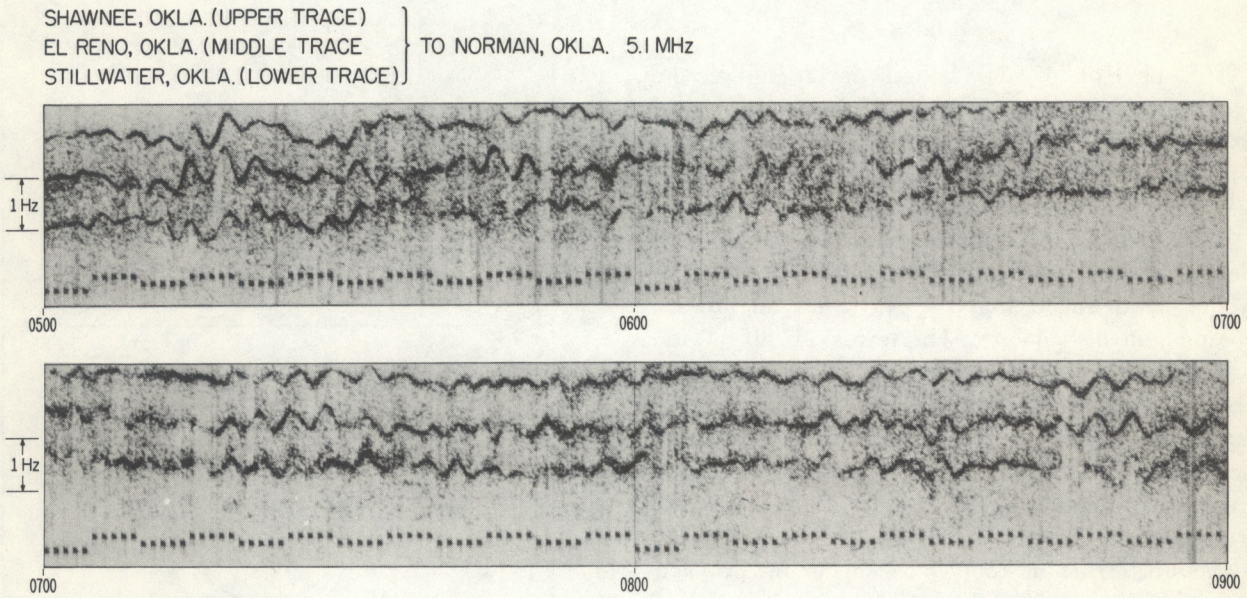


FIGURE 27.—Doppler record (5.1 MHz) for the disturbance of Apr. 18, 1970, at 0500–0900 UT

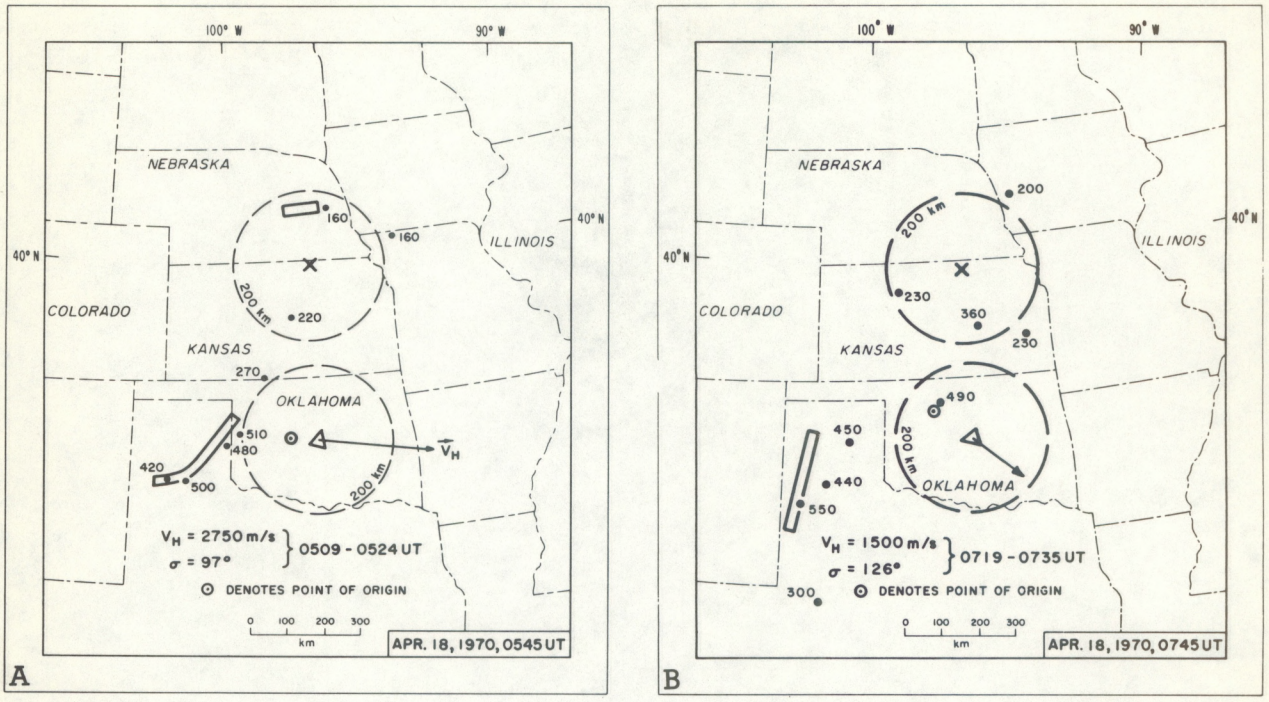


The locations and heights of the tops of the thunderstorm cells, as obtained from the National Weather Service's radar summary charts, are shown in figure 28. The horizontal trace velocities are shown by arrows, and the points of origin determined by ray tracing are shown by the symbol ⊙. Extrapolating in the direction opposite to $\mathbf{V}_H$ (fig. 28A), we come to the cells designated 480 and 510 (hundreds of ft). These thunder cells meet the criteria (established by Baker and Davies 1969 and by Davies and Jones 1971*b*) that the storm must lie within a radius of about 200 km of the sounder and have cloud tops higher than 40,000 ft. We conclude that one or both of these thunder cells is responsible for the acoustic wave effects detected in the ionosphere.

One of the more interesting features of this storm is that, from our ionospheric soundings, we could follow its movement to the northeast. This can be seen from the sequence of radar summaries in figure 28 and on the radar photographs of figure 29. We see that there is good overall agreement between the position of the storm and the direction of the trace velocity. The numerical data for this and the following disturbances are shown in table 3.

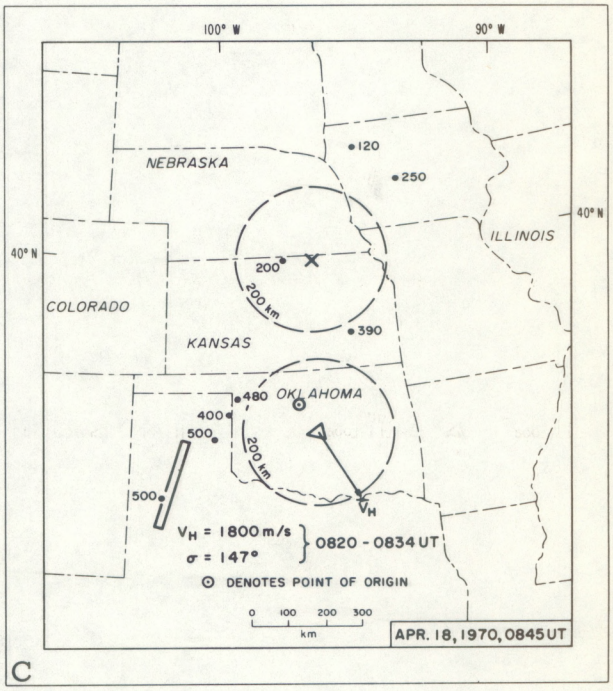


FIGURE 28.—Radar summary with horizontal trace velocity for the disturbance of Apr. 18, 1970

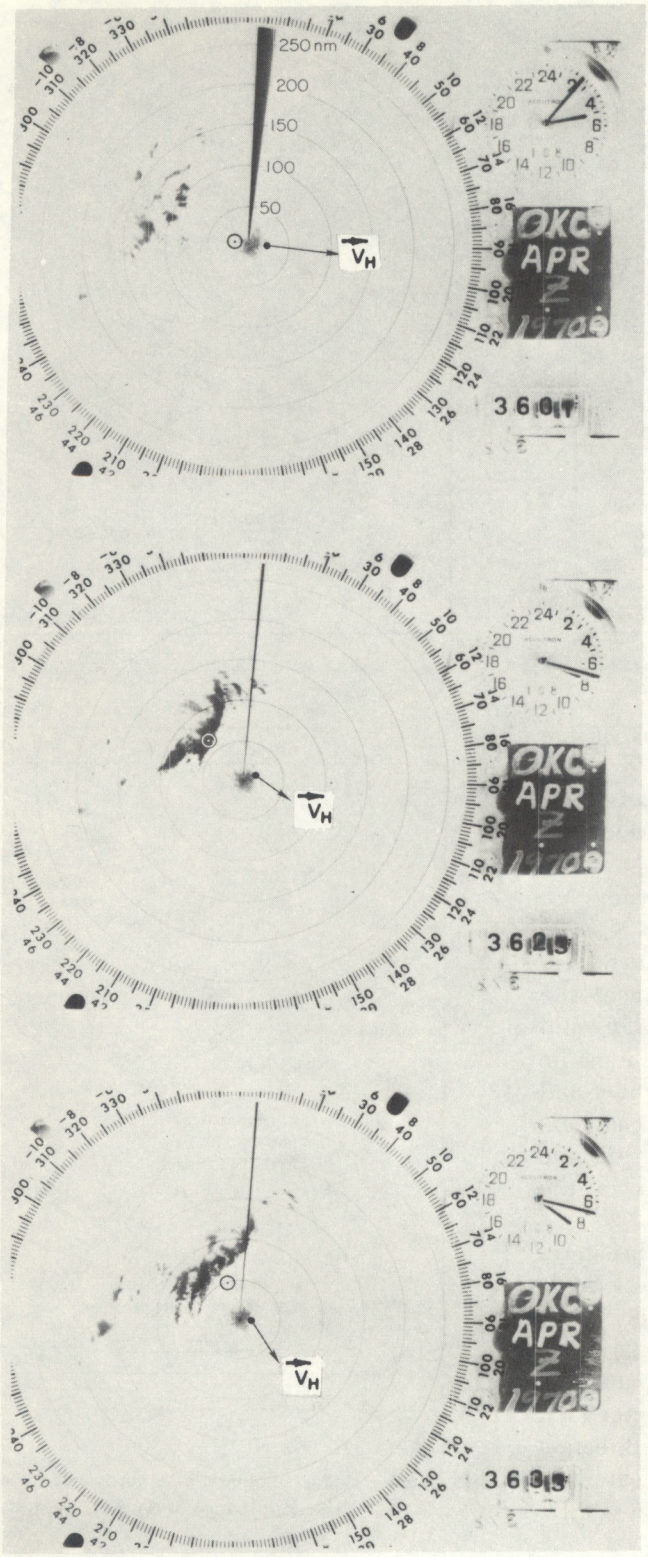


FIGURE 29.—Oklahoma City weather radar photographs (250-n.mi. range) of the storm of Apr. 18, 1970

TABLE 3.—*Summary of data from acoustic wave events of 1970*

| Date | UT | $V_H$ (m/s) | $\sigma$ (deg.) |
|---|---|---|---|
| Apr. 18 | 0509–0524 | 2750 | 97 |
| Apr. 18 | 0719–0735 | 1500 | 126 |
| Apr. 18 | 0820–0834 | 1800 | 147 |
| Apr. 30 | 1005–1017 | 850 | 206 |
| Apr. 30 | 1021–1036 | 2700 | 54 |
| May 13 | 0348–0426 | 900 | 172 |
| June 11 | 0425–0505 | 850 | 158 |

TABLE 4.—*True reflection heights (at the Oklahoma experimental site) estimated from White Sands, N. Mex., ionograms*

| Date (1970) | UT | True heights (km) | | |
|---|---|---|---|---|
| | | 3.3 MHz | 4.0 MHz | 5.1 MHz |
| Apr. 18 | 0800 | 299 | 312 | 352 |
| Apr. 25 | 1800 | 106 | 130 | 174 |
| Apr. 25 | 1900 | 112 | 131 | 183 |
| Apr. 29 | 2300 | 134 | 162 | 207 |
| Apr. 30 | 1100 | 333 | 352 | $f_o$<5.1 MHz |
| May 13 | 0000 | 144 | 174 | 212 |
| May 13 | 0200 | 230 | 236 | 249 |
| May 13 | 0500 | 306 | 326 | 373 |
| June 11 | 0500 | 256 | 266 | 284 |

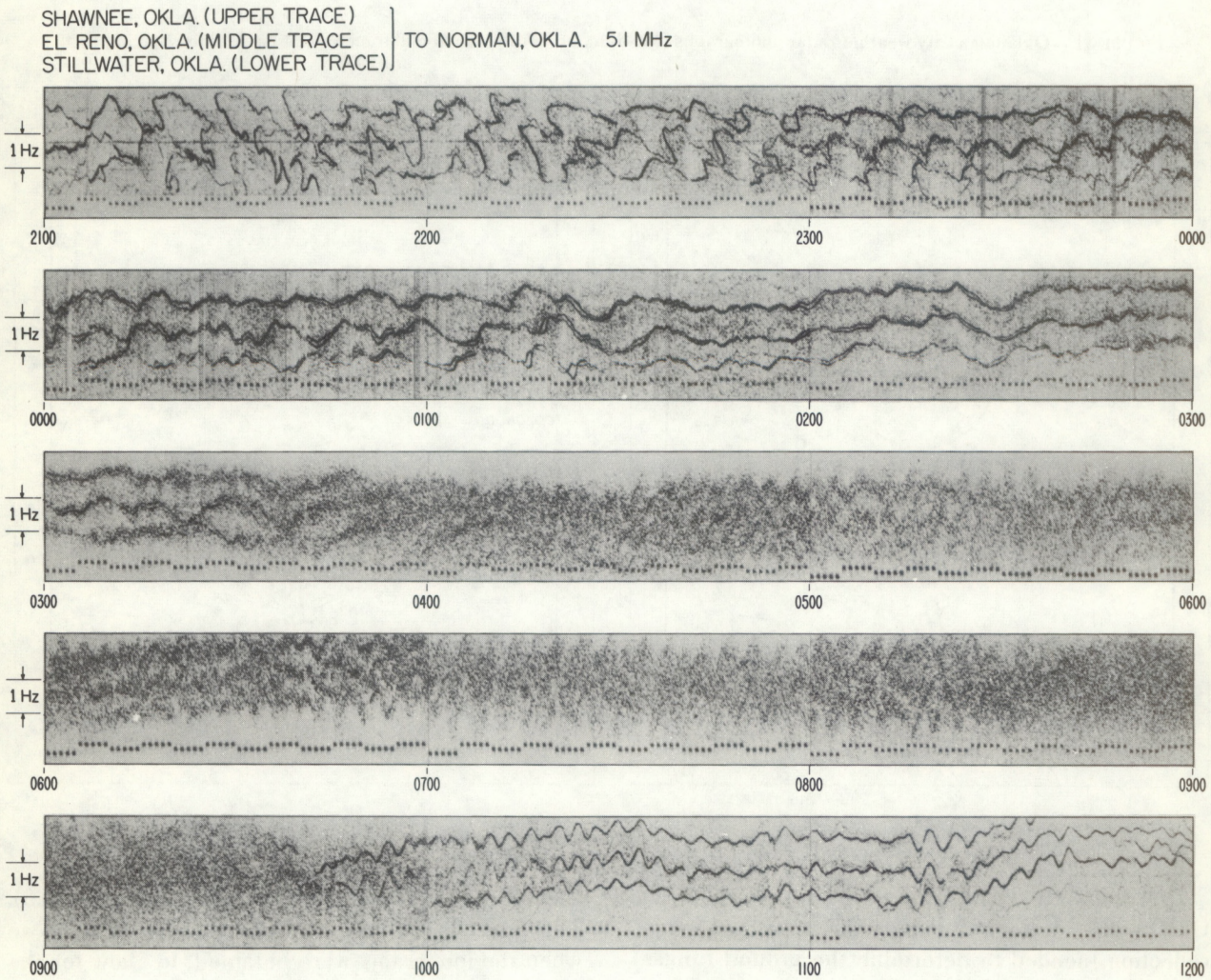


FIGURE 30.—Doppler record for Apr. 29, 1970, 2100 UT to Apr. 30, 1970, 1200 UT

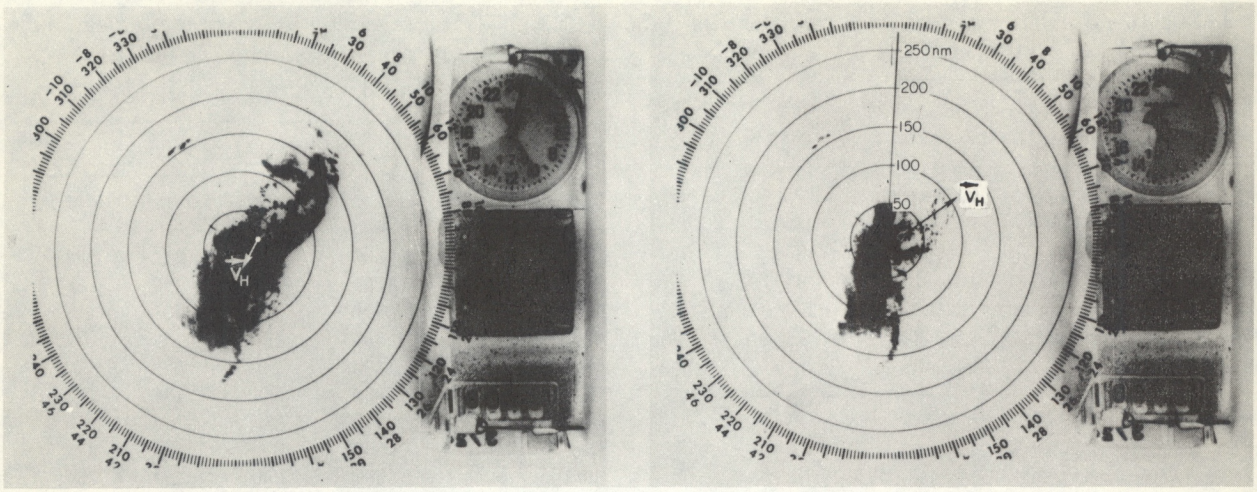


FIGURE 31.—Oklahoma City weather radar photographs (250-n.mi. range) and horizontal trace velocities ($V_H$) for Apr. 30, 1970

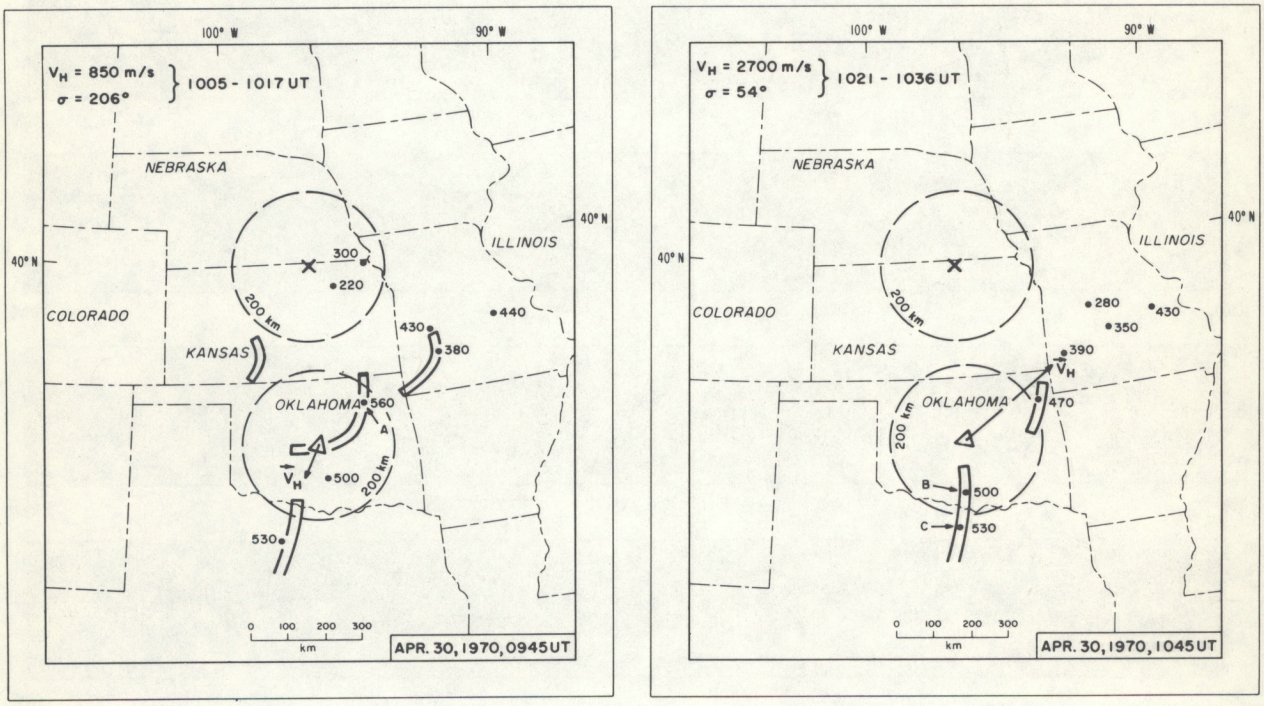


FIGURE 32.—Radar summaries with horizontal trace velocities for Apr. 30, 1970

Unfortunately, ionograms were not available from Oklahoma. In lieu of these, the true heights of reflection (needed to determine the ground ranges) were obtained by analysis of ionograms from White Sands, N. Mex., about 800 km west of Oklahoma City. The results are summarized in table 4 (p. 23). The times listed here are 0.5 hr earlier than those when the ionograms were obtained, to allow for the difference in local times.

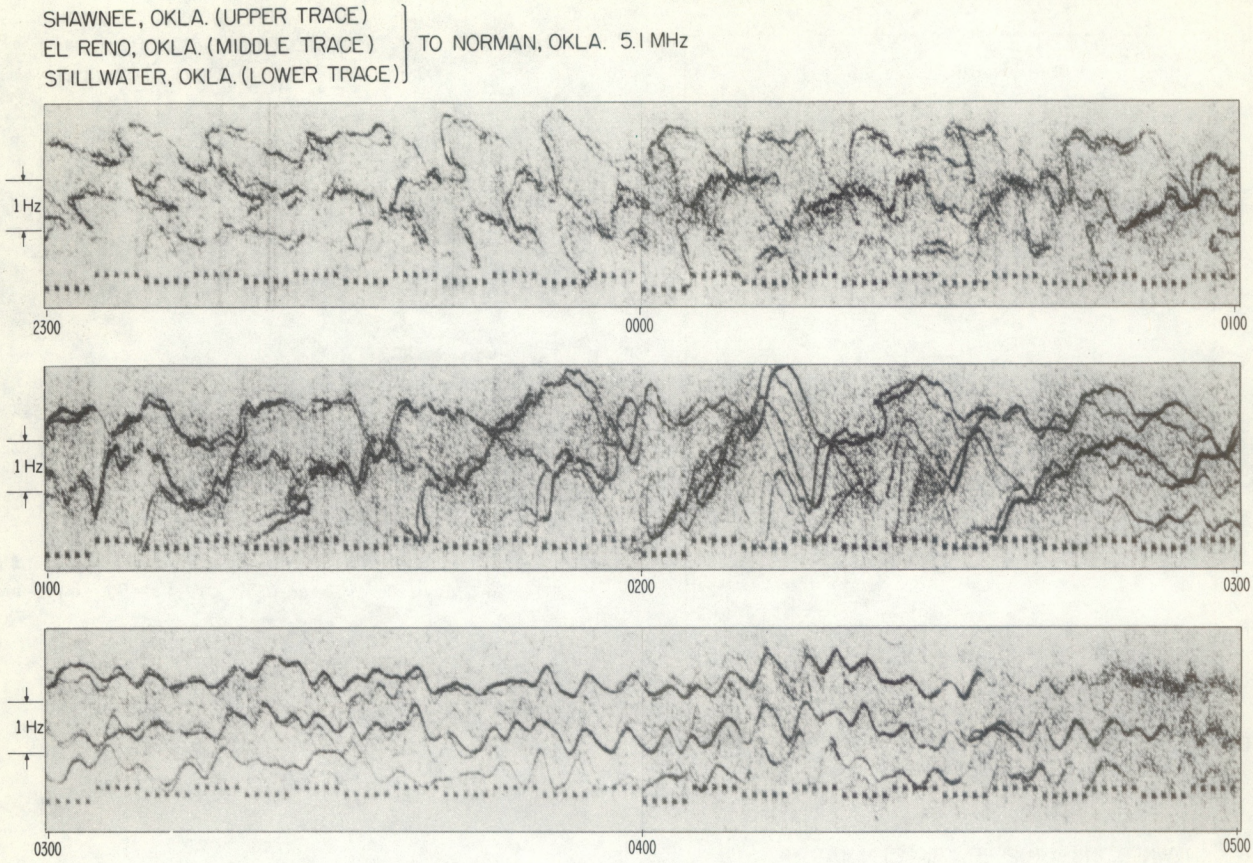


FIGURE 33. — Doppler record for May 12, 1970, 2300 UT to May 13, 1970, 0500 UT

## C. April 29–30, 1970

This disturbance shown in figure 30 (p. 23) is of particular interest because, near 0830 UT, a tornado accompanying it passed through the triangle formed by our transmitters. During the afternoon of April 29, a disturbance producing an S-shaped record occurred, which is discussed in subsection 5G. Evidence of shorter (3- to 5-min period) waves appears near 0030 UT but does not become prominent until about 0430 UT. At this time, unfortunately, the ionospheric signals are spread because of reflections from small ionospheric irregularities associated with enhanced geomagnetic activity. Hence, the record is unsuitable for detailed analysis until shortly before 1000 UT. Velocities, calculated from time differences near 1000 and near 1030 UT, are superimposed on the radar films in figure 31. There is an indication, which we believe to be real, that the source of the disturbance changes (rather abruptly) from one source within the storm system to another, as shown in the radar summaries of figure 32. Near 0945 UT, the primary source is probably that marked A in the left radar summary in figure 32. By 1045 UT, the primary source was either B or C (or possibly both) in the right summary. All these cells have the properties necessary for producing observable ionospheric disturbances.

## D. May 12–13, 1970

The Doppler record (fig. 33) shows an S-shaped disturbance followed by a 3- to 5-min wave. The splitting of the traces is caused by ordinary and extraordinary waves having different reflection points. The radar summary in figure 34 shows no activity over Oklahoma near 0245 UT, but there are two small cells in northern Texas associated with tornadoes and two large cells over northeastern

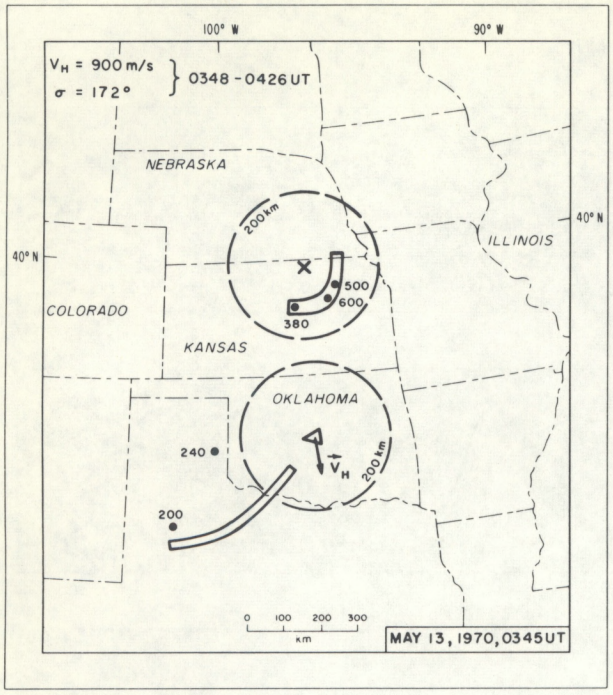


FIGURE 34.—Radar summary with horizontal trace velocity for May 13, 1970

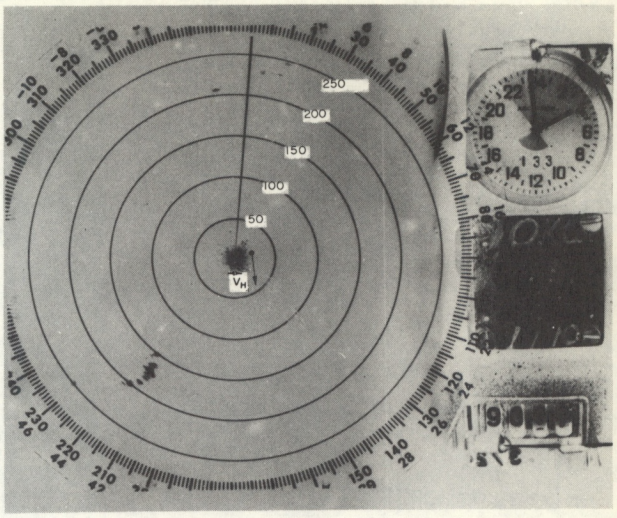


FIGURE 35.—Oklahoma City weather radar photograph (250-n.mi. range) on May 13, 1970 at 0359 UT. $V_H$=900 m/s, and $\sigma$=172°.

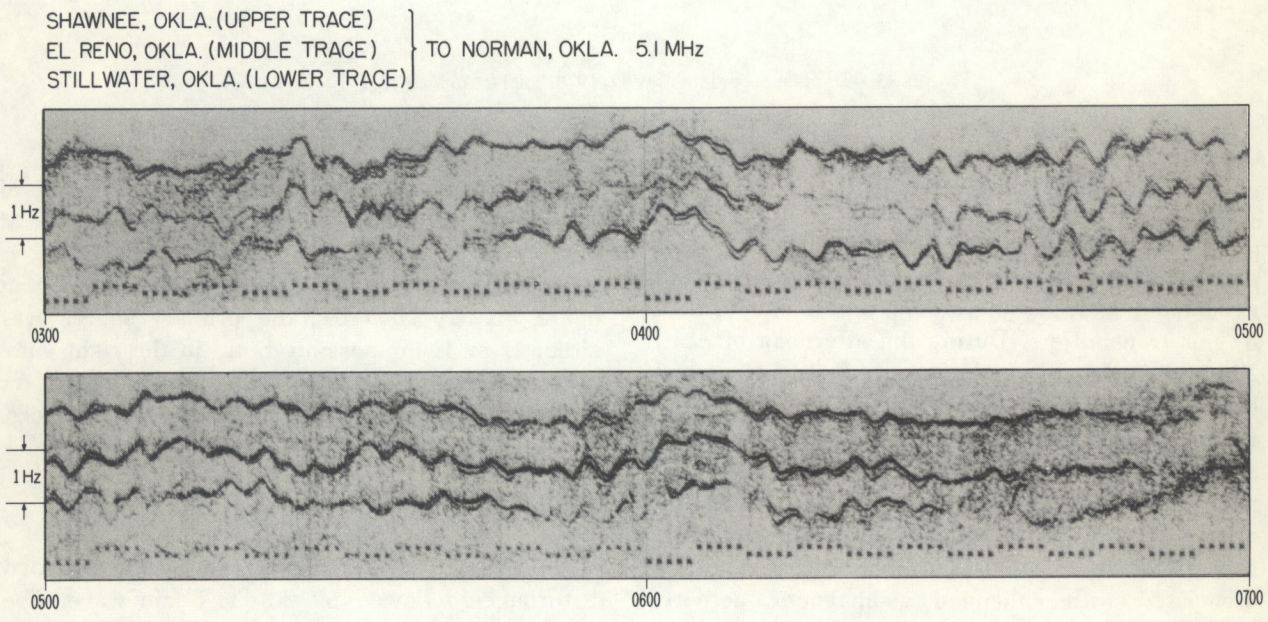


FIGURE 36.—Doppler record for June 11, 1970, at 0300–0700 UT

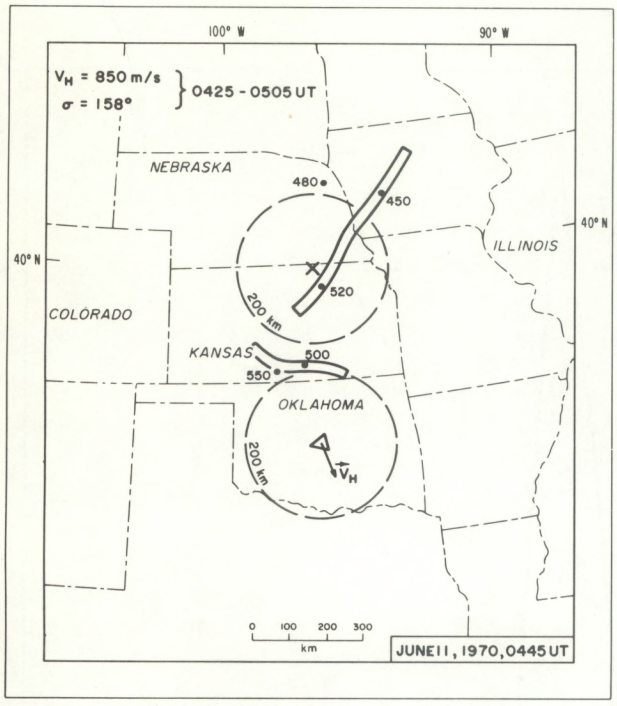


FIGURE 37.—Radar summary for June 11, 1970

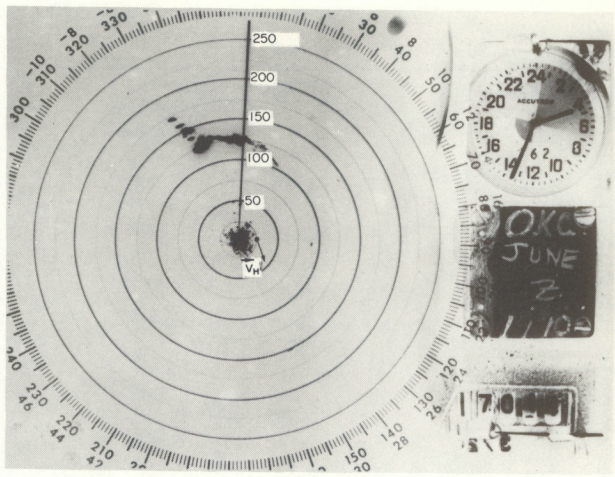


FIGURE 38.—Oklahoma City weather radar photograph (250-n.mi. range) with the horizontal trace velocity for the disturbance of June 11, 1970, at 0434 UT. $V_H$=850 m/s

Kansas. The horizontal trace velocity suggests that the source (or sources) of the ionospheric disturbance is in the Kansas storm. Of course, the waves may be coming from several sources; and this may well be the reason for the "ragged" appearance of the disturbance. The radar photograph in figure 35 shows the two centers of activity but is not nearly as impressive as the radar summaries. This event is one of the rare exceptions to the rule that the thunderstorm must lie within a radius of about 200–250 km of the sounding area to produce a detectable ionospheric disturbance.

## E. June 11, 1970

The Doppler record for this event is shown in figure 36. The radar data (figs. 37 and 38) show a single storm in the region; the direction of the velocity vector agrees well with the weather data.

## F. Power Spectra of Acoustic Disturbances

From a physical viewpoint, an important characteristic of these ionospheric disturbances is the power spectrum. The "power" in the Doppler record is proportional to the mean squared Doppler shift and is therefore porportional to the mean squared velocity of the air parcels excited by the acoustic wave. Thus, the power spectrum of the Doppler record is also a power spectrum of the wave itself. The records were scaled every minute, and the spectra were obtained by a program written by Lewis (1969) based on the method of Welch (1967). Before discussing the actual spectra obtained, we consider some tests we made to satisfy ourselves that the main features of the spectra are not introduced by data processing.

Since the data were obtained by sampling the records at 1-min intervals, the shortest period that can be included in the spectra is 2 min. Before sampling the traces, we smoothed them to eliminate any periods shorter than 2 min to avoid aliasing. No appreciable alteration was involved, however, since the amplitudes of components in the 2 min and shorter range are small compared with those with longer periods.

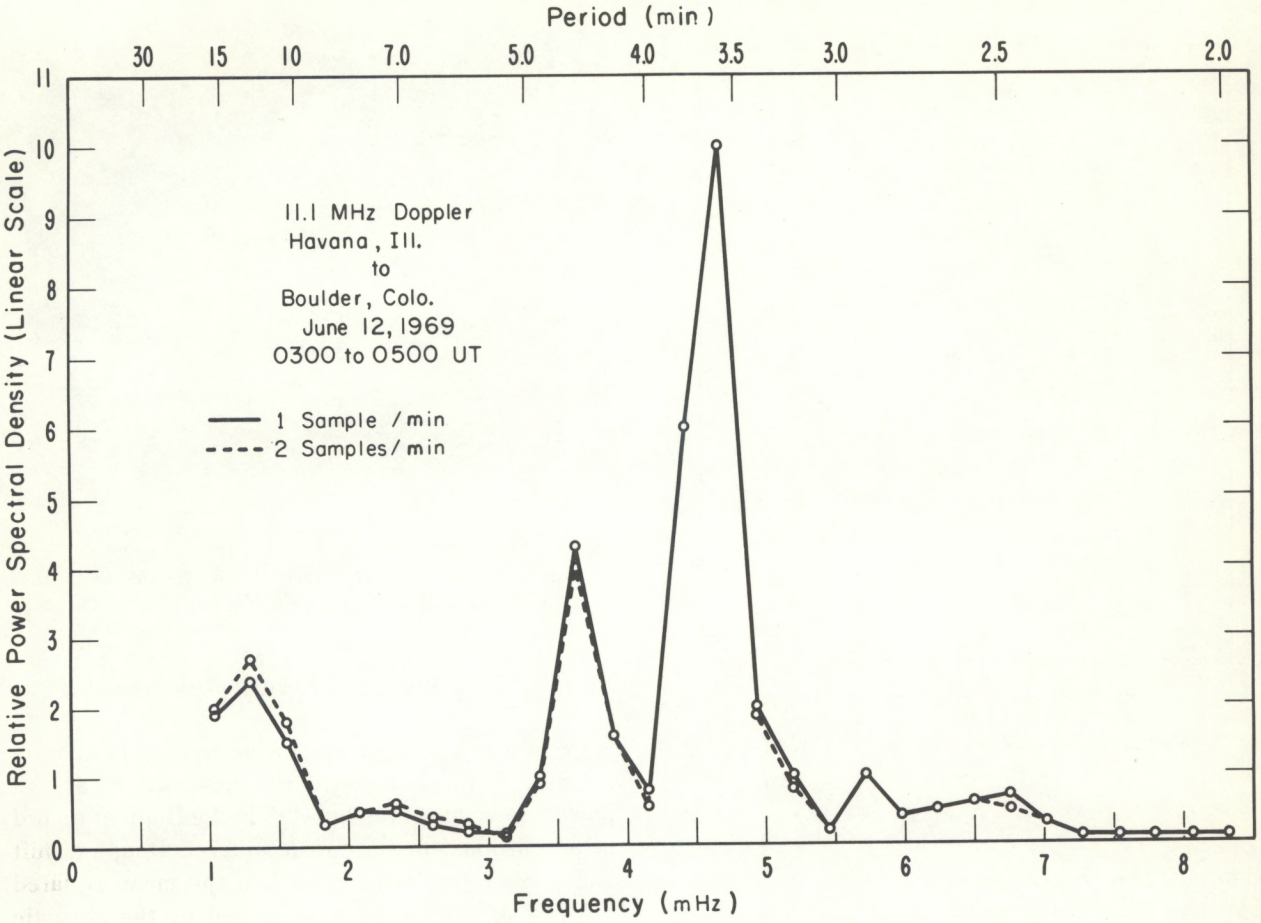


FIGURE 39.—Spectra of the ionospheric disturbance of June 12, 1969, computed with 30-s scalings and 1.0-min scalings, showing that the spectra are not appreciably affected by scaling every 1.0 min

To see whether the spectra were appreciably affected by choosing a sampling interval of 1 min, we scaled at 30-s intervals the disturbance of June 12, 1969, recorded at Boulder. The spectrum analysis was carried out using (1) all scaled points and (2) alternate values (1-min intervals). The resulting spectra are plotted in figure 39, showing that no advantage is gained by making the sampling interval less than 1 min.

Gravity wave components with periods longer than about 30 min were also eliminated from the data. These are not of interest here and, being of relatively large amplitude, tend to obscure the acoustic wave components by compressing them into the bottoms of the graphs. Hence, the spectra are cut off arbitrarily at a period of about 15 min.

A further test was carried out to see whether spurious components are generated by the computer program. The analytical function

$$y = 20 + 10 \sin\left(\frac{2\pi}{3} t\right) + \sin\left(\frac{2\pi}{4} t\right) \qquad (35)$$

was used to generate data for a composite signal containing 3- and 4-min waves. The resulting spectrum (fig. 40) indicates no spurious spectral components. The line broadening in figure 40 results from the finite duration of the function being analyzed.

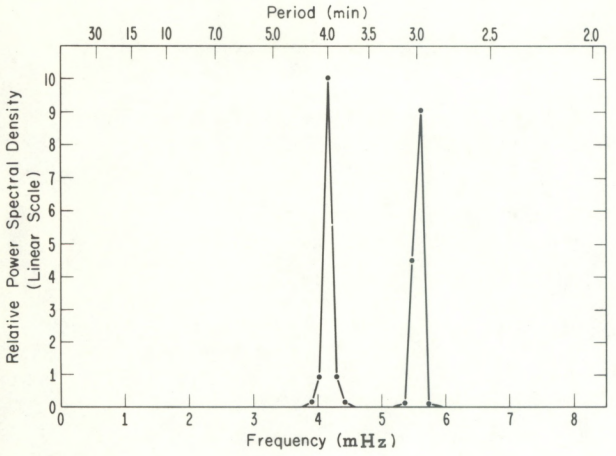


FIGURE 40.—Spectrum of the function $y=20+10\{\sin(2\pi/3)t+\sin(2\pi/4)t\}$ to test the computer program for spurious responses

Having established that no serious errors are introduced in the process of spectrum analysis, we now examine the extent that the spectrum changes during the disturbance. This is done for the disturbance of April 18 in figure 41, which shows the spectra for each of the 4 hr from 0500 to 0900 UT. The evidence suggests that the spectral content does change during the disturbance.

Spectra for the four events described in section 5 are shown in figures 42, 43, 44, and 45. The following features are common to all four:

1. Most of the acoustic wave energy lies between periods of about 2.5 min and about 5 min. This is what would be expected for a source in the lower atmosphere because the longest period is determined by the acoustic cutoff period in the lower parts of the atmosphere while the shorter periods are suppressed by viscosity (Georges 1969).

2. There is a range of periods between about 5 min and about 10 min with relatively little power. This range corresponds to the forbidden region of figure 7. The shorter period limit is the minimum acoustic cutoff period in the atmosphere; and the longer limit is the maximum buoyancy period that, in this case, is at the level of radio reflection. The increase of power for periods greater than about 10 min is due to background gravity waves nearly always present.

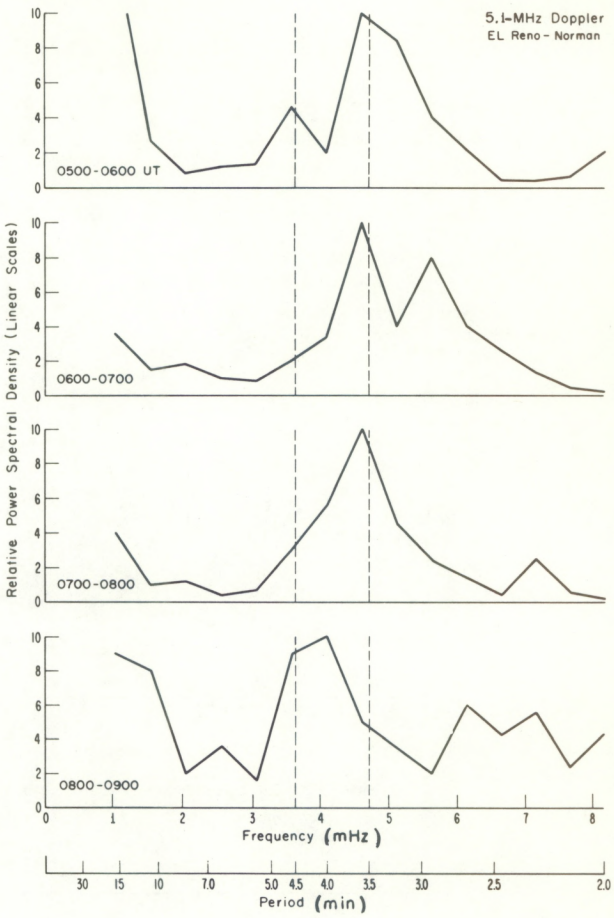


FIGURE 41.—Spectral analyses of subintervals for the ionospheric disturbance of Apr. 18, 1970, indicating that the spectrum changes during the life of the disturbance

3. The acoustic range is dominated by two power peaks, one near 3.5 min and the other near 4.5 min. The power scale is normalized so that the higher of these two peaks is 10.

The spectral peaks at 3.5 and 4.5 min never appear on the Doppler records with sufficient strength to be detected by visual inspection when there are no thunderstorms within several hundred kilometers. To see if these peaks exist but are too small to be seen directly in the normal fluctuations that occur every day, we analyzed 3 days that were free of severe weather (viz, April 11, May 7, and June 19, 1970). The peaks were not present on any of these days; therefore, there is no evidence that their source is anything other than thunderstorms.

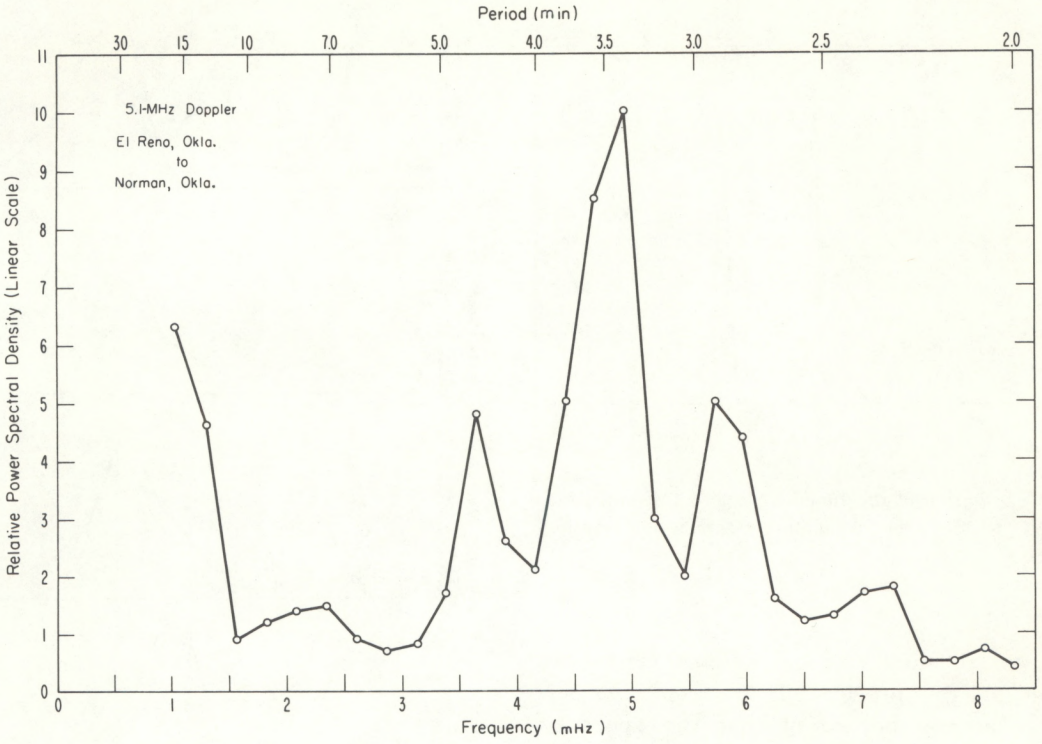


FIGURE 42. — Spectrum of the ionospheric disturbance of Apr. 18, 1970, at 0500–0900 UT

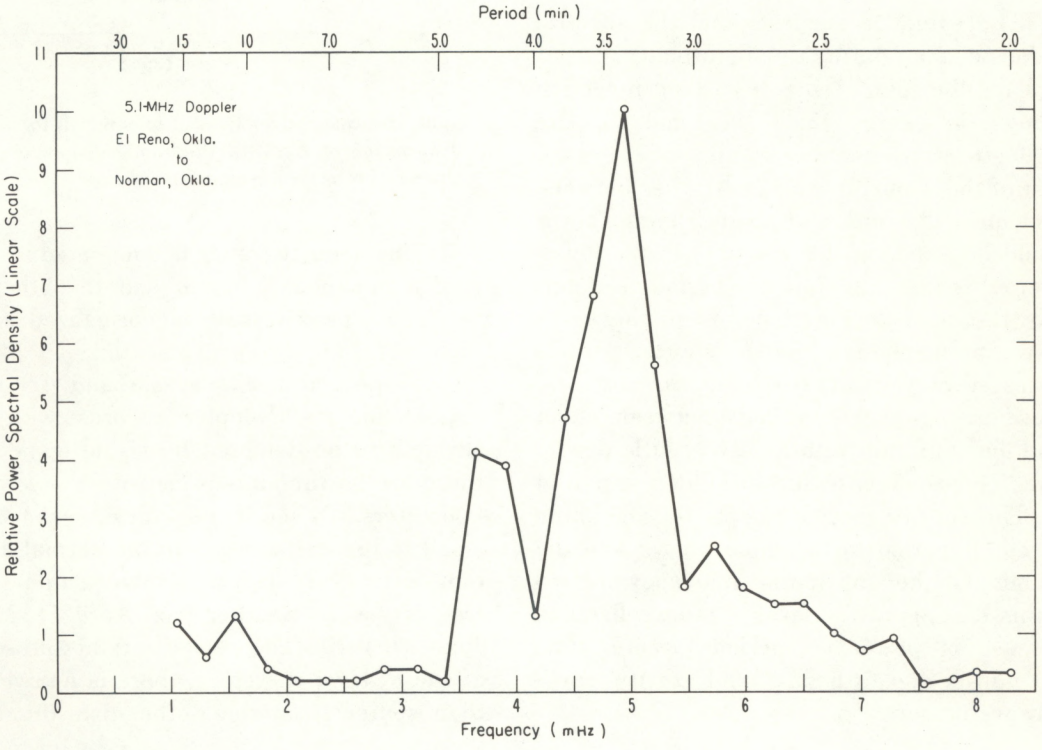


FIGURE 43. — Spectrum of the ionospheric disturbance of Apr. 30, 1970, at 1000–1200 UT

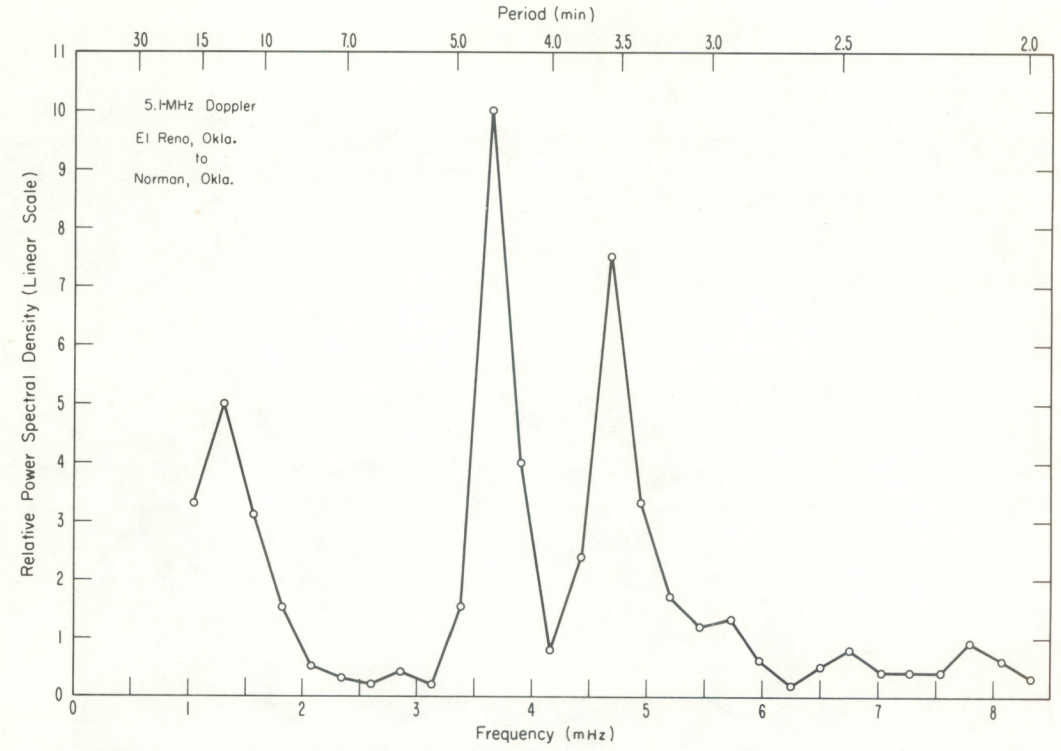


FIGURE 44. – Spectrum of the ionospheric disturbance of May 13, 1970, at 0300–0500 UT

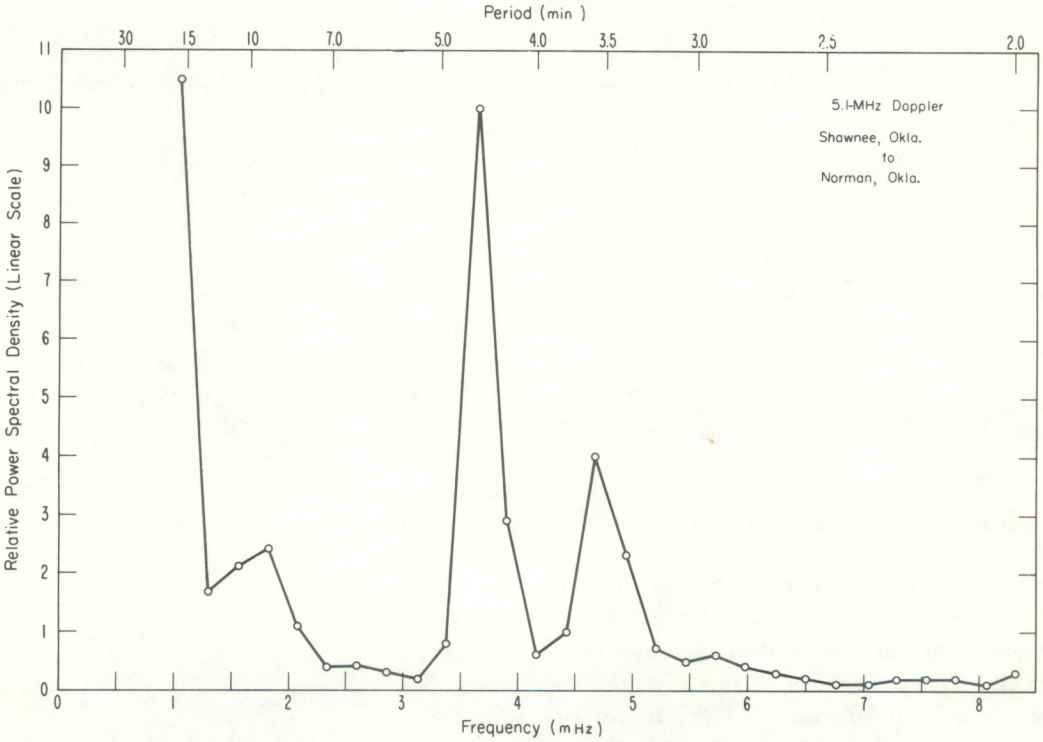


FIGURE 45. – Spectrum of the ionospheric disturbance of June 11, 1970, at 0300–0700 UT

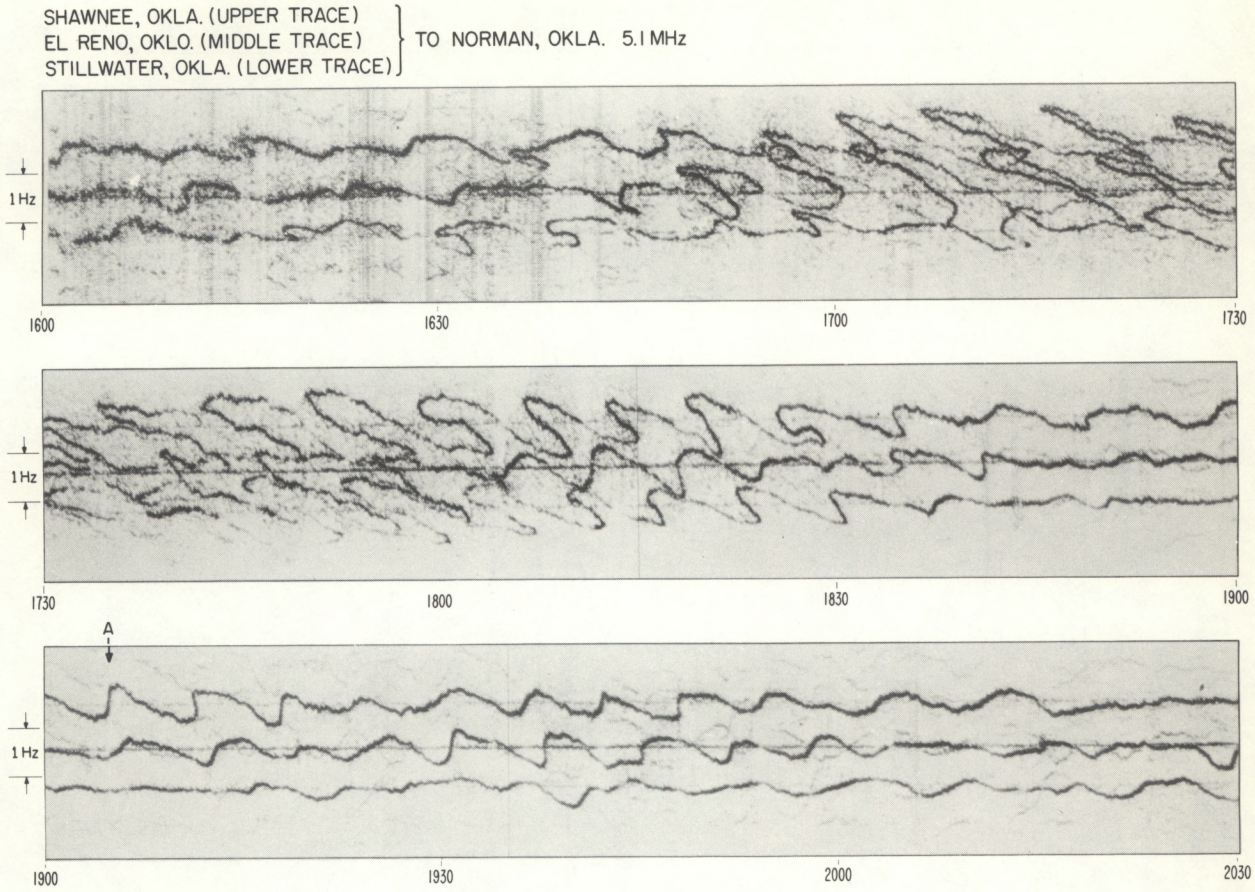


FIGURE 46.—S-shaped Doppler record of the ionospheric disturbance observed on Apr. 25, 1970, at 1600–2030 UT

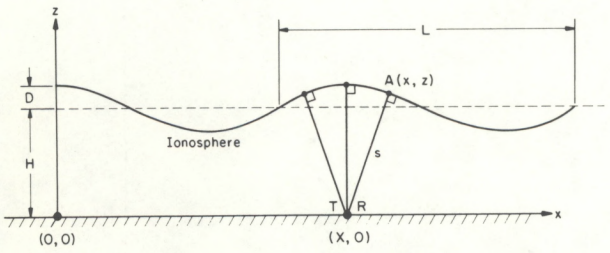


FIGURE 47.—Reflections from a sinusoidal surface

## G. Disturbances Producing S-shaped Records

The ionospheric disturbance observed on Apr. 25, 1970, is shown in figure 46; the disturbance is quite different from those described in subsections 5B through 5E. The periodicity of this disturbance lies in the range 7 to 10 min, and the waveform of the Doppler record is highly distorted in an S-shaped fashion. As we have seen in figures 30 and

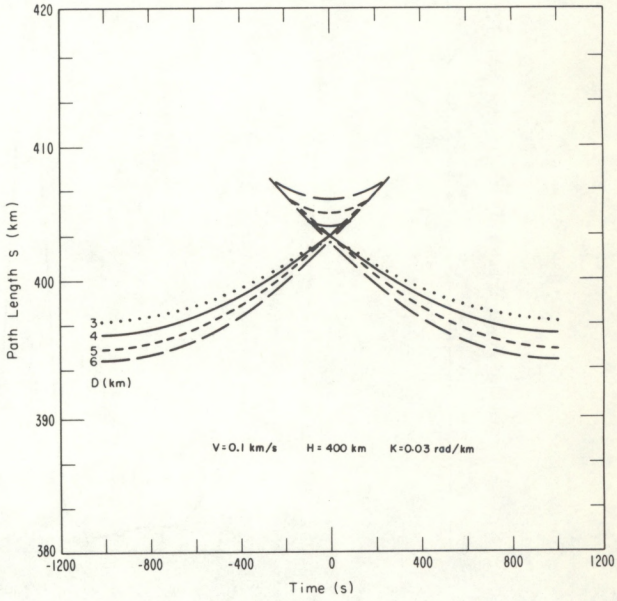


FIGURE 48.—Variation of path length with time

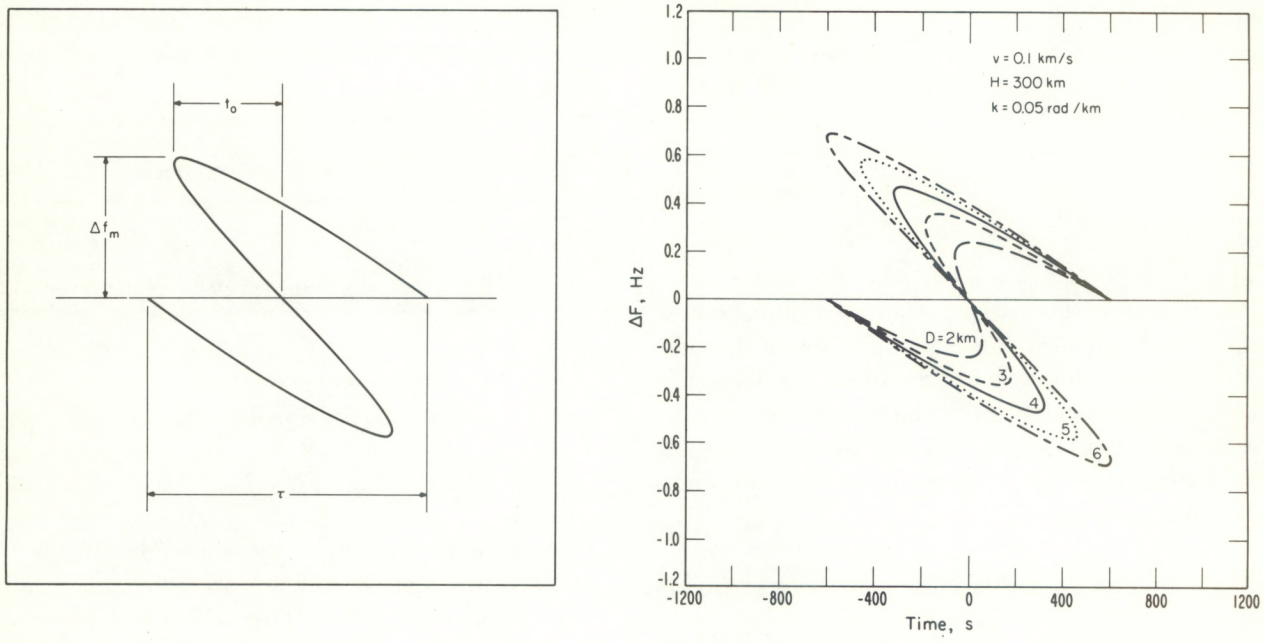


FIGURE 49.—Variation of Doppler shift with time

33, this type of disturbance precedes some of the 3-min thunderstorm events. We feel that some description of this type of disturbance is appropriate.

The S-shaped records can be explained in terms of a corrugated reflecting surface that moves horizontally with constant speed. We can make a simplified analysis of the problem by postulating a sine wave shape to the reflecting surface at a mean height $H$ with wavelength $L$ and amplitude $D$ (fig. 47). For our analysis, we assume that the transmitter and receiver ($T$ and $R$) coincide and move with a speed $V$ while the ionosphere is stationary. The former is not quite true in this case, but the difference is immaterial. Let the reflecting surface be

$$z = H + D\cos kx \tag{36}$$

where $k = 2\pi/L$. When the transmitter is at $(X, O)$ (fig. 47), the path $(s)$ up to the point of perpendicular reflection is given by

$$s^2 = (x - X)^2 + z^2 \tag{37}$$

where

$$X = Vt = \frac{\theta}{k} - kD(H + D\cos\theta)\sin\theta \tag{38}$$

and $\theta = kx$. Thus,

$$s = (H + D\cos\theta)\{1 + k^2D^2\sin\theta\}^{1/2}. \tag{39}$$

Substituting eq (39) into eq (6) (with $P = 2s$) gives

$$\Delta f = \frac{2fDkV}{c}\,\frac{\sin\theta}{\sqrt{1 + k^2D^2\sin^2\theta}} \tag{40}$$

for the instantaneous Doppler shift.

Equations (39) and (40) have been solved numerically, and typical results for the time variations of path length $(s)$ and Doppler shift $(\Delta f)$ are shown in figures 48 and 49. We see that, for a certain time range and for $D > 1$ (approximately), there are three paths with different lengths and three echoes with different frequency shifts. From the S-shaped curves, it is possible to get some information about the dimensions of the ionospheric disturbance, provided that we know the reflection height $H$ (e.g., from ionogram analysis) and make several approximations. First, let us consider what features of the S curves can be measured to a reasonable degree of accuracy. These are (1) average period $\tau$, (2) maximum frequency deviation $f_{max}$, and (3) the time $T_0$ from the zero crossing to the turning point of the $\Delta f(t)$ curve—see figure 49 (left). Since $\sin\theta \approx 1$, we have

$$\Delta f_{max} \simeq \frac{2fDkV}{c\sqrt{1+k^2D^2}} \tag{41}$$

from eq (40); and since $k^2D^2 \ll 1$,

$$D \approx \frac{c\tau}{4\pi f}\Delta f_{max} \tag{42}$$

where $\tau(=2\pi/kV)$ is the period of the disturbance. Equation (42) tells us that, to a first approximation, the peak frequency shift is independent of the sideway motion of the ray path; therefore, the amplitude of the disturbance $D$ can be estimated. A little more information can be gleaned from this analysis by noting that the approximate condition for a switchback to occur is that

$$HDk^2 \geq 1. \tag{43}$$

The critical condition exists around the period marked A (at 1905 UT) in figure 46. At this time, $\Delta f_{max} \approx 0.34$ Hz; hence, $D=0.69$ km. From table 5, the reflection height $H$ is 179 km that, on substitution into eq (46), gives $k=0.09$ km$^{-1}$, $L=70$ km, and

$$V_H = L/\tau = 166 \text{ m/s}. \tag{44}$$

We can also find $V_H$ from the time displacements between the traces in figure 46. In practice, both the period and shape of the traces vary from one cycle to another; this introduces difficulties in the measurement of period and time displacement. The zero Doppler frequency crossings, however, are essentially independent of the amplitude of the reflecting surface. Hence, we use these zero crossings to determine the average period and average time displacements during the approximate time interval 1800 to 1845 UT when the S-curves are most clearly defined. Cross correlograms of the zero crossings from El Reno (E), Shawnee (S), and Stillwater (U) are shown in figure 50. Because ambiguities occur in matching cycles, we consider the following possible time displacements (in s):

$$T_{ES} = +120 \text{ or } -250,$$
$$T_{EU} = +300 \text{ or } -100, \text{ and}$$
$$T_{SU} = +180 \text{ or } -240.$$

Acceptable combinations of time displacements must satisfy the relationship

$$T_{ES} + T_{SU} = T_{EU}. \tag{45}$$

Applying this criterion to the above data leads to the selection of a unique set (viz, $T_{ES}=120$, $T_{SU}=180$, and $T_{EU}=300$) that also corresponds to the highest peaks of the correlograms. Substituting these times into eq (12) gives $V_H=180$ m/s that agrees relatively well with eq (44). This selection of time displacements leads to an azimuth of 35° east of north. As shown in figure 51, this agrees excellently with the locations of severe thunderstorms.

Our next step is to estimate the vertical speed $V_V$. From these particular Doppler traces, it was impossible to determine $V_V$ for the same time interval as for $V_H$. During the approximate time interval 1700 to 1800 UT, the time displacements were determined for the different sounding frequencies. The true reflection heights were obtained from the White Sands ionograms. The combined data show two possibilities for $V_V$ (viz, +158 m/s and −247 m/s). If, as implied above, the disturbance originated in the thunderstorms shown in figure 51, phase propagation should be downward (see subsec. 4B); this leads to the choice of −247 m/s. From figure 15, we see that the direction of phase propagation is close to the critical value $\phi_c = \{\sin^{-1}(\tau_B/\tau_i)\}$ where

$$\phi_c = \tan^{-1}(V_H/V_V) = 126°. \tag{46}$$

This gives a value of 11.8 min for the intrinsic period $\tau_i$, corresponding to a buoyancy period of 9.5 min for the 1962 U.S. Standard Atmosphere. Thus, the intrinsic period is considerably greater than the observed period, which indicates the

TABLE 5.—*Approximate periods and heights of disturbances that produced S-shaped records during 1970*

| Date | Height (km) | Period (min) |
|---|---|---|
| Apr. 25 | 179 | 6.8 |
| Apr. 29 | 207 | 9.0 |
| May 12 | 230 | 10.5 |

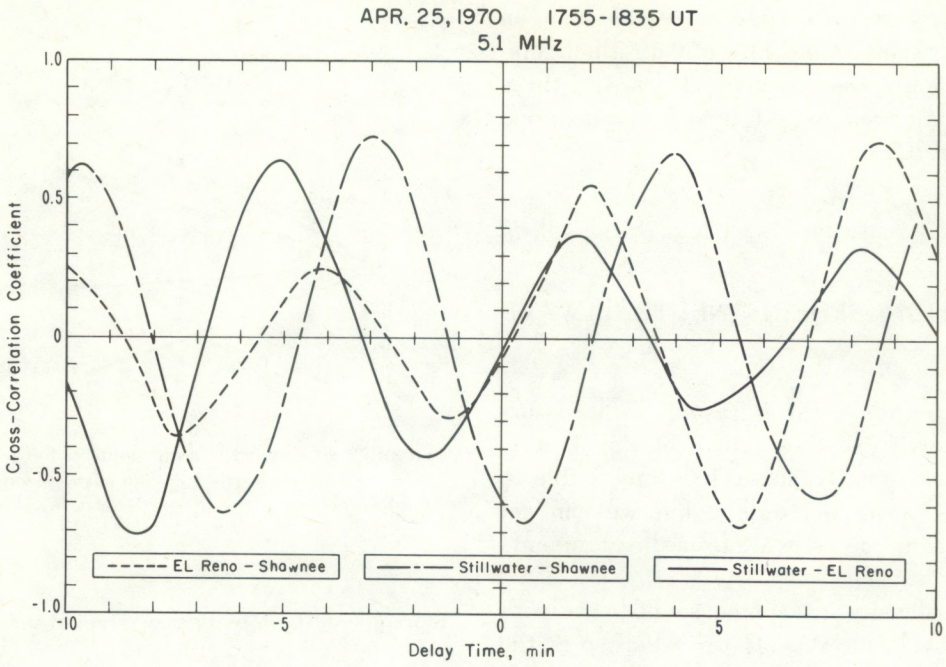


FIGURE 50.—Correlograms of zero crossings of S-shaped records

presence of a wind component $U$ given by

$$U = \frac{\tau_i - \tau}{\tau_i} V_H = 76 \text{ m/s} \qquad (47)$$

(see eq 27).

An alternative explanation is that there is no wind present but that the buoyancy period $\tau_B = \tau \sin \phi_c = 5.5$ min. Substituting this value into eq (14) gives

$$H = 7.22 + 25 H' \text{ km}. \qquad (48)$$

Near 180 km, we should expect $H'$ to be in the range 0.1 to 0.3, so that the scale height should be in the range 9.7 km to 15.7 km, corresponding to temperatures of 310°K to 500°K. Even the larger of these temperatures is very much less than the 1280°K given by the 1962 U.S. Standard Atmosphere. The Standard Atmosphere gives $H = 36.64$ at 180 km, which would require that $H' = 1.3$, an unrealistically large gradient.

Now, the measured speeds of the acoustic disturbances of section 5 are about 1 km/s and greater, suggesting a higher sound speed consistent with the U.S. Standard Atmosphere. Hence, we conclude that the S-shaped disturbances are evidence that the F region has neutral winds with speeds greater than about 70 m/s.

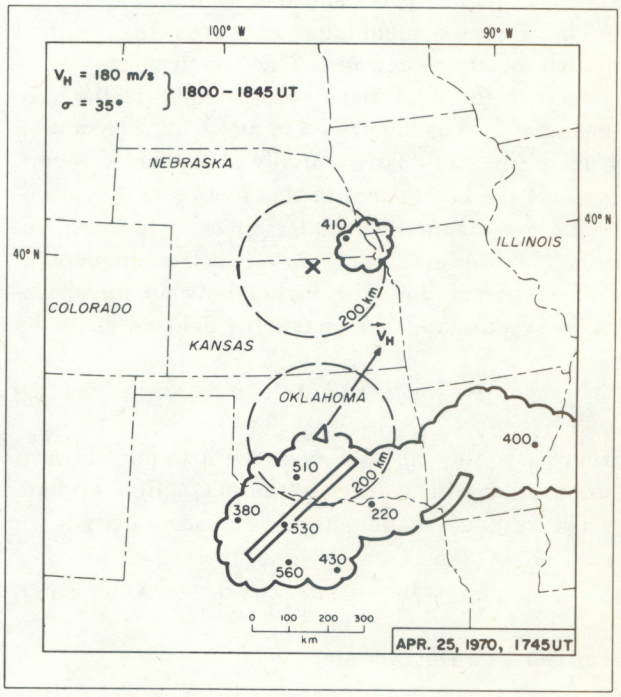


FIGURE 51.—Radar summary and horizontal trace velocity for Apr. 25, 1970

The S-shaped records were observed also on two other occasions (table 5), both of which preceded 3- to 5-min disturbances. From the three events, the indication is that the observed period increases with altitude.

## 6. POWER IN IONOSPHERIC (NEUTRAL) WAVE

The power output in the infrasonic range is important in identifying the nature of the source. With the information available, it is impossible to determine the power accurately, but we can get an order of magnitude estimate from the arguments presented below.

The energy density in a plane sound wave with peak particle velocity **v** is $^1/_2\ \rho v^2$ where $\rho$ is the mean density. Hence, the power flux density is $^1/_2\ \rho v^2\mathbf{u}$ where **u** is the group velocity. Now we have seen that, in the F region, the acoustic cutoff period and the buoyancy period are much larger than the wave period ($\leq$ 4.5 min). Therefore, the waves are essentially longitudinal, and the group speed is very nearly the speed of sound.

The Doppler technique measures the vertical motion of the electrons. This vertical motion is related to the neutral particle motion via the geomagnetic field as illustrated in figure 52. The motion $V$ of the neutrals is essentially along the **k** vector, but only the component of this motion that is parallel to the magnetic field is imparted to the electrons. We observe $\mathbf{V}_1$, the vertical component of this electron motion. The angle $\beta$ between the propagation vector and the magnetic field is given by

$$\cos\beta = \sin\phi\,\cos I\,\cos\psi + \cos\phi\,\sin I \qquad (49)$$

where $I$ is the dip and $\psi$ is the azimuth of wave propagation with respect to the magnetic meridian.

The vertical component of electron velocity is

$$V_V = V\sin I\cos\beta \qquad (50)$$

that causes a Doppler shift:

$$\Delta f = \frac{2f}{c}V_V = \frac{2f}{c}V\sin I\cos\beta. \qquad (51)$$

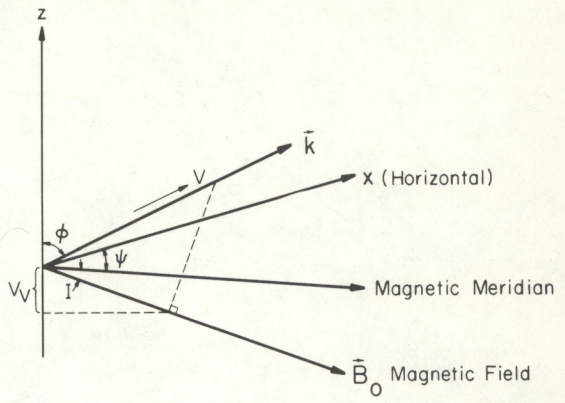


FIGURE 52.—Geometry relating motion of the neutral atmosphere to the vertical motion of the electrons

The power density flux is given by

$$S \approx \frac{1}{2}\rho C\left(\frac{c\Delta f}{2f\sin I\cos\beta}\right)^2. \qquad (52)$$

Let us further assume that we have a point source near the ground which radiates isotropically over a hemisphere. If our ionospheric observations are made at an effective distance $r$ from the source, the total radiated power $P$ is then given by

$$P = 2\pi r^2 S = \frac{\pi r^2\rho C c^2\Delta f^2}{4f^2\sin^2 I(\sin\phi\cos I\cos\psi+\cos\phi\sin I)^2}$$

$$= \frac{P_0}{\sin^2 I(\sin\phi\cos I\cos\psi+\cos\phi\sin I)^2} \qquad (53)$$

where $P_0$ is the source power that a vertically traveling wave must have to produce the same $\Delta f$ at the same height where the magnetic field is vertical.

To obtain an idea of the magnitude of $P_0$, we use the following atmospheric model:

$$\rho = 10^{-10}\ \mathrm{kg\cdot m^{-3}},$$
$$C = 800\ \mathrm{m/s},$$
$$\Delta f = 1\ \mathrm{Hz},$$
$$f = 5\cdot 10^6\ \mathrm{Hz}, \text{ and}$$
$$c = 3\cdot 10^8\ \mathrm{m\cdot s^{-1}}.$$

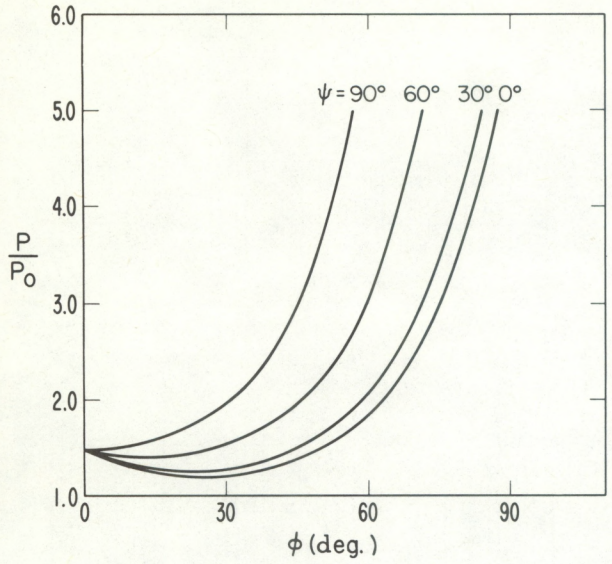


FIGURE 53.—Variation of ionospheric response with the direction of the ray path for $I = 65°$

Since the average height is about 250 km and the area of observation lies between horizontal ranges of 0 and 200 km from the source, a reasonable value of $r$ is 300 km. These values give

$$S_0 = 35 \cdot 10^{-6}\,\mathrm{W} \cdot \mathrm{m}^{-2}$$

and

$$P_0 = 20.4 \cdot 10^{6}\,\mathrm{W}.$$

The ratio $P/P_0$ calculated from eq (53) is near 1.5 for a vertically traveling acoustic wave (fig. 53) and reaches infinity for $\phi = 90°$ and $\psi = 90°$. The latter condition means that the wave propagates horizontally and perpendicularly to the magnetic field (magnetic east-west propagation); and under these conditions, there will be no electron motion. A typical value of $P/P_0$ is 2.5, so that the power in an acoustic wave source giving rise to an ionospheric disturbance is about $5 \times 10^6$ W. The smaller Doppler shifts detected by our Doppler system are about 0.1 Hz, which requires a source power of about $0.5 \times 10^6$ W.

Figure 53 shows that the ionospheric response is sensitive to the position of the source relative to the point of observation. The importance of this is illustrated in figure 54 for sources in the troposphere when the source and observing point lie in the magnetic meridian. With the source to the south of the ionospheric sounding point, as in

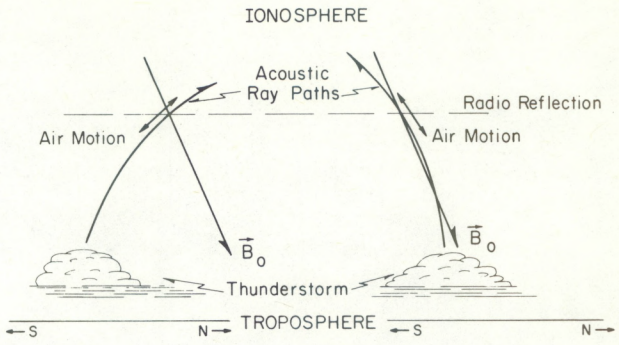


FIGURE 54.—Effect of the geomagnetic field on the sensitivity of the ionosphere to the location of the source

figure 54 (left), there will be only a small ionospheric disturbance because the acoustic wave tries to move the electrons across the magnetic field. With the source to the north, as in figure 54 (right), the electrons will move more easily along the magnetic field. Hence, the ionospheric response to a given source will be greater when it lies to the north of the sounding point than when it is to the south. Chang (1969) tested this ionospheric sensitivity to source position by using radio data for the path from Long Branch, Ill., to Boulder. With the path midpoint as the center, Chang divided the circle with 250-km radius into a northern semicircle and a southern semicircle. For the 14 disturbances he studied, all showed thunderstorm activity in the northern semicircle; and in 10 of these, the predominant activity was in the northern semicircle. In general, very few thunderstorms will lie in the magnetic meridian and at such locations that the acoustic ray path at the radio reflection point is perpendicular to the geomagnetic field. Also, the motion of the neutral air parcels is slightly elliptical (fig. 8) so that there is always some component of motion parallel to the geomagnetic field. Hence, very large thunderstorms at any location within a radius of about 200 km may produce ionospheric disturbances.

## 7. MICROBAROGRAPH OBSERVATIONS

If the infrasonic disturbances are indeed produced by thunderstorms, we might expect evidence of these waves near the ground. To investigate this, we installed a microbarograph at the National Severe Storms Laboratory in Norman for the period

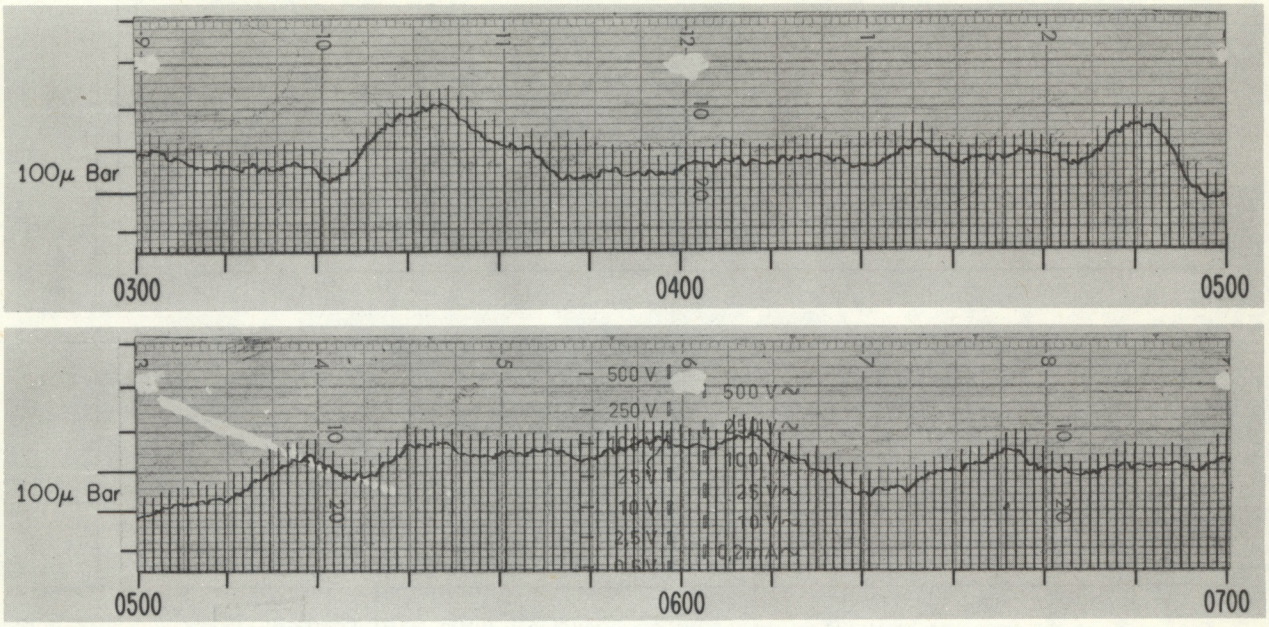


FIGURE 55.—Sample microbarograph records (Norman, Okla., on June 11, 1970, at 0300–0700 UT) showing scaling procedure

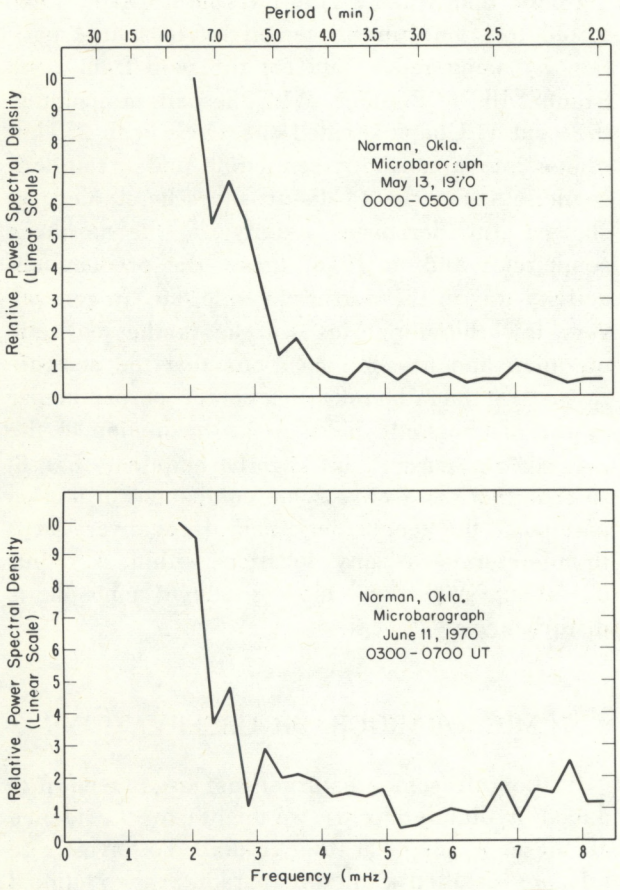


FIGURE 56.—Microbarograph spectra

April–July 1970. The microbarograph was loaned by Dr. H. Montes of Teledyne Isotopes, Westwood, N.J.

Sample microbarograph records are shown in figure 55. Several records have been spectrum analyzed by the technique described in section 6, and the spectra are presented in figure 56. In general, we do not find convincing evidence for the presence of strong signals with periods near 3.5 and 4.5 min. This does not mean that signals with these periods were not present. It is quite possible that they were swamped by the background. Much of this background is filtered out of the ionospheric disturbance by the propagation characteristics of the atmosphere.

Evidence that infrasonic waves originate in some of the thunderstorms associated with ionospheric disturbances has been provided by Vernon Goerke of NOAA. Using spaced microphones at Boulder, Goerke and Woodward (1966) monitored the direction of arrival of infrasound with periods between 20 and 50 s. Figure 57 shows radar summaries coinciding with two ionospheric events in 1969 and the azimuths of arrival of infrasound at Boulder. Hence, despite the negative results in the microbarograph recordings, there is reason to believe that infrasound is generated by thunderstorms that produce ionospheric disturbances.

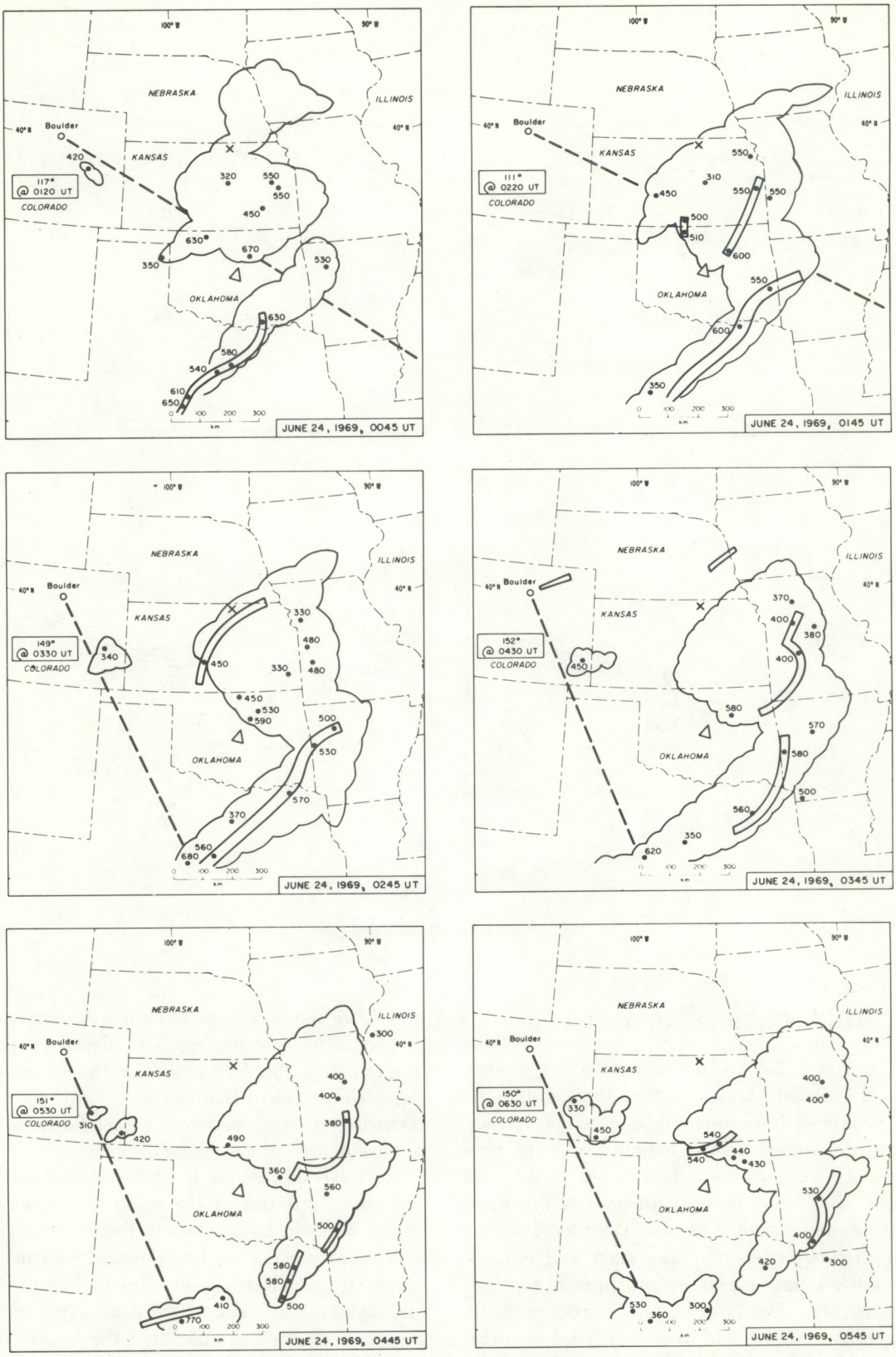


FIGURE 57.—Radar summaries and azimuths of infrasound received at Boulder (con. on p. 40).

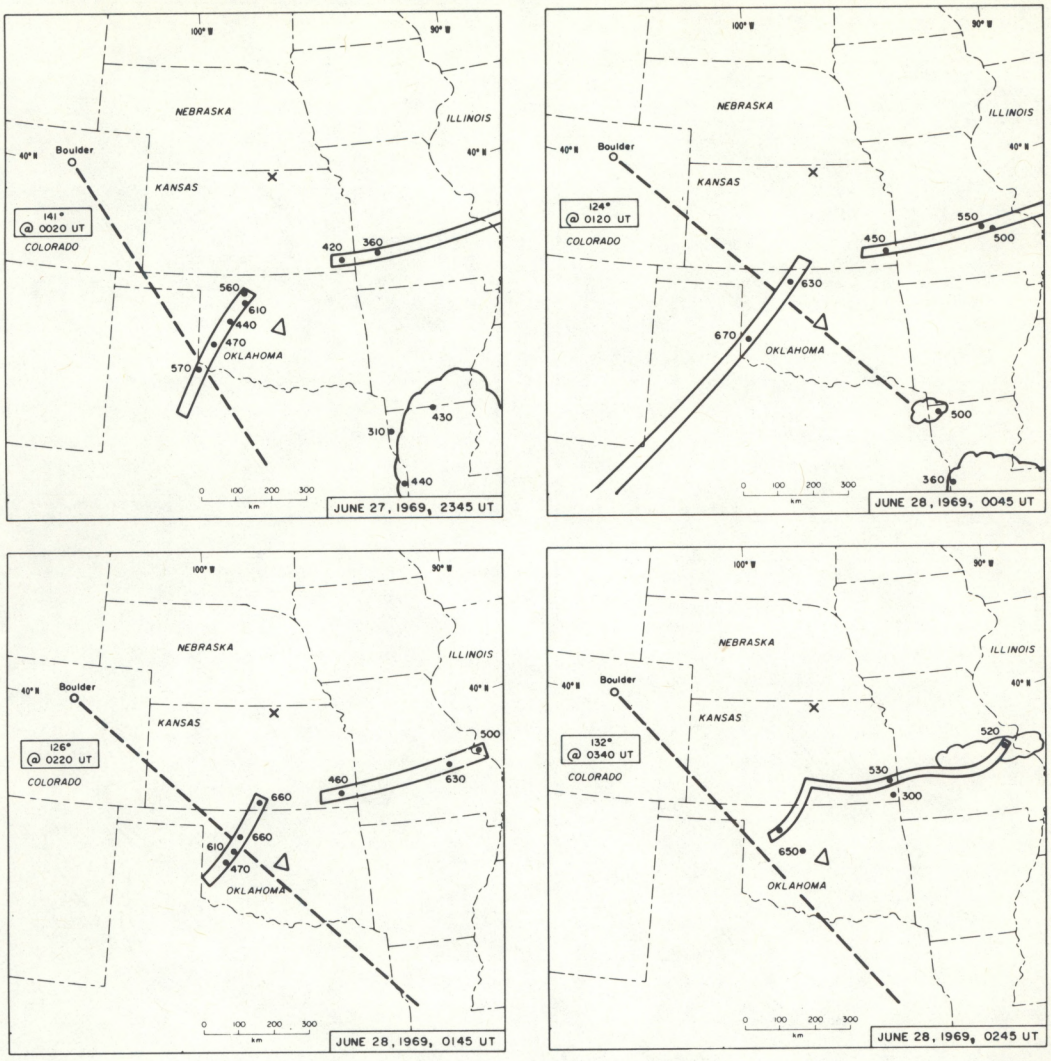


FIGURE 57. – Concluded

## 8. SOME STATISTICAL ASPECTS

Tables 6 and 7 list all the acoustic wave events detected at Norman, Okla., during 1969 and 1970. The disturbances have been designated as minor and major, depending on the magnitude of the rms Doppler shift – minor $< 0.1$ Hz, major $> 0.1$ Hz. The tables show that most disturbances are near the limit of detectability of our Doppler system. Some of the major events may start and end as minor events. Other major events appear to start rather abruptly. The sferics were recorded at Norman through April and May of 1970. From the daily geomagnetic and solar data listed in tables 6 and 7, we see little or no evidence of correlation with the occurrence of the acoustic disturbances. An examination of the $K_p$ values for the hours covering the observed disturbances and 5 quiet days and 5 disturbed days of the months have likewise failed to yield any sign of geomagnetic influence.

We have also sought to find temporal variations in the characteristics of the spectra. For example in figure 58, we have plotted the frequencies with maximum powers as functions of season and universal time. There is no convincing evidence of any systematic change in these frequencies. In figure 58 (bottom), notice that the lower frequency points show little dispersion. This is confined by

TABLE 6.—*Acoustic wave events during May 9–Sept. 25, 1969 ($f = 3.3$ MHz)*

| Date | Minor Begin (UT) | Minor End (UT) | Major Begin (UT) | Major End (UT) | Magnetic ($A_p$) | 2800-MHz flux |
|---|---|---|---|---|---|---|
| May 15 | 02 | 10 | | | 131 | 159 |
| May 22 | 02 | 08 | | | 11 | 177 |
| June 1 | 07 | 09 | | | 5 | 113 |
| June 12 | 00 | 08 | 03 | 06 | 18 | 237 |
| June 13 | 04 | 07 | | | 15 | 229 |
| June 18 | 02 | 08 | | | 4 | 154 |
| June 20 | 10 | 13 | | | 10 | 145 |
| June 22 | 00 | 08 | | | 2 | 133 |
| June 23 | 00 | 03 | | | 5 | 132 |
| June 24 | 00 | 12 | 01 | 06 | 12 | 129 |
| June 25 | 11 | 14 | | | 10 | 120 |
| June 27 | 03 | 08 | | | 5 | 114 |
| June 28 | 00 | 04 | 00 | 03 | 4 | 118 |
| | No records July 18–August 15 | | | | | |
| Aug. 27 | 12 | 14 | | | 21 | 168 |

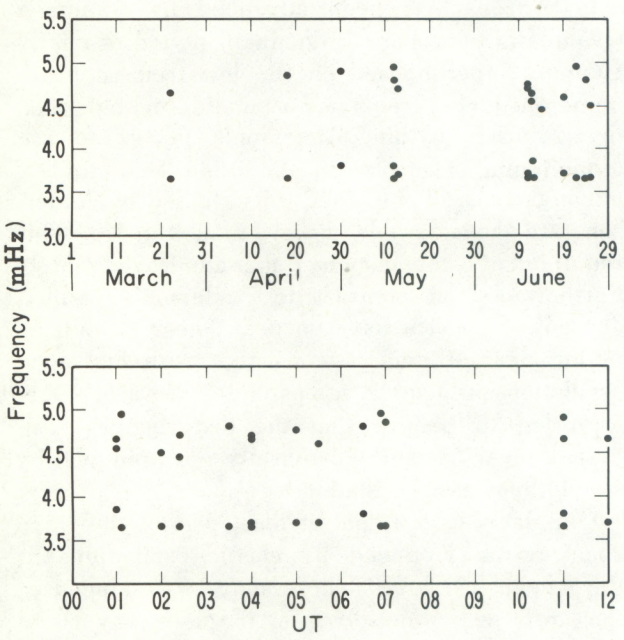


FIGURE 58.—Seasonal and diurnal variations of the power spectra peaks

TABLE 7.—*Acoustic wave events during Mar. 4–July 30, 1970 ($f = 5.1$ MHz)*

| Date | Minor Begin (UT) | Minor End (UT) | Major Begin (UT) | Major End (UT) | Sferics | Magnetic ($A_p$) | 2800-MHz flux |
|---|---|---|---|---|---|---|---|
| Apr. | | | | | | | |
| 17 | 04 | 08 | | | * | 29 | 148 |
| 18 | 04 | 16 | 05 | 09 | * | 18 | 142 |
| 19 | 11 | 16 | | | * | 21 | 136 |
| 21 | 20 | 24 | | | | 90 | 126 |
| 23 | 15 | 20 | | | * | 14 | 128 |
| 24 | 10 | 12 | | | | 16 | 130 |
| | 16 | 18 | | | | | |
| 27 | 08 | 12 | | | * | 17 | 135 |
| | 03 | 05 | | | | 10 | 138 |
| 30 | 02 | 05 | 04 | 12 | * | 18 | 153 |
| May | | | | | | | |
| 10 | 02 | 09 | | | | 2 | 163 |
| 11 | 01 | 03 | | | | 3 | 176 |
| | 09 | 11 | | | | | |
| 12 | 09 | 12 | | | | 15 | 180 |
| 13 | 03 | 12 | 03 | 05 | | 6 | 193 |
| | 03 | 12 | 09 | 11 | | | |
| | 22 | 23 | | | | | |
| 15 | 02 | 08 | | | | 10 | 206 |
| 28 | 05 | 09 | | | | 45 | 154 |
| | 14 | 16 | | | | | |
| 29 | 11 | 14 | | | * | 13 | 159 |
| 30 | 00 | 04 | | | * | 11 | 164 |
| June | | | | | | | |
| 10 | 00 | 12 | | | | 6 | 146 |
| | 22 | 07 | 03 | 07 | | | |
| 12 | 00 | 02 | 00 | 02 | | 5 | 172 |
| 13 | 04 | 06 | 04 | 06 | | 10 | 200 |
| 14 | 06 | 12 | | | | 8 | 207 |
| 15 | 09 | 15 | | | | 13 | 209 |
| 19 | 04 | 08 | 04 | 07 | | 8 | 175 |
| 21 | 02 | 06 | | | | 17 | 161 |
| 25 | 00 | 04 | 00 | 04 | | 6 | 149 |
| | 08 | 12 | | | | | |
| 27 | 05 | 08 | | | | 35 | 160 |
| | 15 | 17 | | | | | |
| July | | | | | | | |
| 2 | 14 | 16 | | | | 11 | 189 |
| 11 | 14 | 16 | | | | 10 | 138 |
| 12 | 01 | 05 | | | | 14 | 135 |
| 15 | 05 | 07 | 01 | 05 | | 5 | 122 |
| | 05 | 07 | 05 | 07 | | | |

*Events that coincided with high rates of electromagnetic pulsations caused by lightning discharges from thunderstorms within a radius of several hundred kilometers of Norman, Okla. (Taylor 1971)

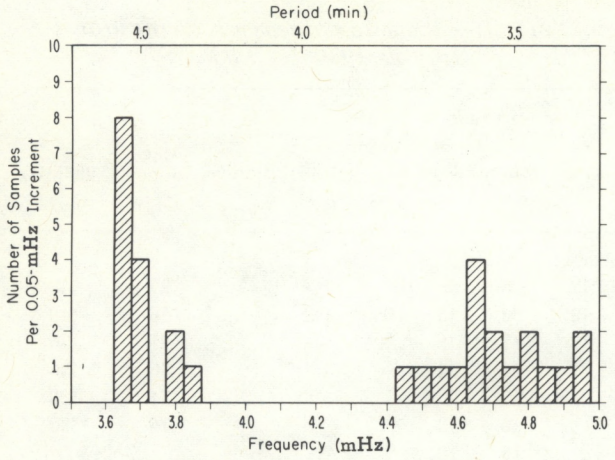


FIGURE 59.—Histogram showing the distributions of the peaks in the spectra of ionospheric disturbances

the histogram in figure 59 showing that most of the observed values are at 3.65 mHz ($\tau \approx 4.6$ min); there are no events with smaller values. On the other hand, the high-frequency peak ($\approx 4.7$ mHz) is more variable. These facts reflect the general properties of the spectra (viz, that the peak near 4.6 min is narrow, whereas the peak near 3.5 min is broad). There seems to be no fixed relationship between the two frequencies.

## 9. DISCUSSION

The experiments carried out in Oklahoma prove that ionospheric disturbances with periods in the range of 2 to 5 min are indeed generated by thunderstorms. In fact, during the thunderstorm season, the ionospheric radio data and the radar summaries were often collected independently; and by inspecting one set of data, we could predict the properties of the other.

The interesting questions to ask are (1) "How is the acoustic wave produced?" and (2) "How does it propagate from the source to the ionosphere?" In the treatment here, we have assumed that the disturbance is generated by the motion of the thunderstorm and propagates to the ionosphere as an acoustic wave. However, other possibilities should be considered, for example, (1) the disturbance could arise from a shock wave caused by the heating effect of lightning and filtered by dispersive propagation or (2) Herman (1970) has suggested that high frequency radio noise pulses (sferics) emitted by lightning discharges propagate to the *F* region where they are absorbed. Utlaut (1970) and his collaborators have shown that a certain type of ionospheric disturbance (spread F) can be produced by heating the F layer with a powerful radio transmitter.

Before discussing the various possibilities, let us summarize the facts that any theory must explain.

1. Disturbances occur only when severe thunderstorms are in the vicinity ($\simeq$ 200 km).

2. Not all thunderstorms with tops higher than 40,000 ft and within a radius of 200 km produce detectable disturbances.

3. The spectra of the disturbances have two peaks, one (near 4.5 min) that is narrow and frequency stable and the other (near 3.5 min) that is broader than the first and tends to vary somewhat in frequency from one event to another.

4. The direction of propagation of the ionospheric disturbance may change abruptly during a long-lived event.

A likely source of these waves lies in the mechanical motions of the air mass that constitutes a thunderstorm cell. Based on photographs of clouds, evidence for oscillatory motions in thunderclouds over Arizona has been advanced by Anderson (1960). His data show a dominant period of nearly 10 min. Superimposed on the low frequency are numerous higher frequency oscillations with periods near 2 min. If anything, Anderson's spectra indicate a minimum of energy in the 3- to 4-min range, although most of the cloud tops studied by Anderson are considerably lower than the 40,000-ft requirement established by Baker and Davies (1969). Furthermore, in contrast to Anderson's results, our power spectra have no peaks near 10 min. A period near 10 min is consistent with buoyancy oscillations in a moist atmosphere. We are, therefore, led to believe that the disturbances with periods near 3.5 and 4.5 min are not produced by simple buoyancy oscillations.

Our data suggest that at least part of the wave spectrum is produced by elastic oscillations at the tropopause level. These may be produced in the storm cells themselves, or the cells may excite natural oscillations in the surrounding gas at the tropopause.

The temperature gradient at the tropopause is zero; hence, the acoustic cutoff period is related to

the temperature by

$$\tau_a = \frac{4\pi C}{\gamma_g} = 18.39\ \sqrt{T} \tag{54}$$

where $\tau_a$ is in seconds and $T$ is in degrees Kelvin. The mean temperature over Oklahoma in 1969 at the 200-mb level, which is approximately the tropopause height, was −55°C or 218°K. This corresponds to an acoustic cutoff period of 4.52 min, which is very close to one of the peaks in the observed spectra. The sensitivity of $\tau_a$ to the temperature fluctuation $\Delta T$ is given by

$$\Delta\tau_a = -9.2\, T^{-1/2}\, \Delta T. \tag{55}$$

The 200-mb temperature extremes over Oklahoma are $-55° \pm 10$°C so that $\Delta\tau = \mp 0.1$ min. This would explain the observed stability in the 4.5-min peak.

At this point, it is of interest to calculate the pressure perturbation $(p'/p_0)$ in the ionosphere:

$$\frac{p'}{p_0} = \frac{\gamma V_H}{C^2}\,\mathbf{u} \tag{56}$$

where **u** is the horizontal velocity of the air parcels. Taking $V_H = 1$ km/s, $C = 0.8$ km/s, and $u = 10$ m/s, we find that

$$\frac{p'}{p_0} = 0.022 = 2.2\%. \tag{57}$$

Remember that the power in the acoustic wave is only one-millionth of the power generated by a big storm.

Another possible cause of these disturbances lies in the shock waves generated by lightning discharges (Few 1969). Estimates of the power generated by lightning in a severe thunderstorm vary over a wide range from about $10^6$ to about $10^{12}$ kW (Loeb 1954 and Vonnegut 1960). Taking a value of $10^9$ kW, we see that there is adequate power available even when allowing for a highly inefficient conversion process. Nevertheless, it is difficult to see how such a process can produce the spectrum observed in the ionosphere.

Our data suggest that the sources of the ionospheric disturbances are the individual thunderstorm cells rather than the storm system as a whole. Evidence for this is provided by the sudden change in direction of the horizontal trace velocity on April 30. It appears that the waves from one source die away while those from another source build up and eventually dominate. Further support for this hypothesis comes from the ground-based infrasonic recordings. These observations of distant thunderstorms show rather abrupt changes of azimuth indicating changes of sources. This generally agrees with the meteorological classification that divides the life of a cell into a buildup stage, a mature stage, and a decay stage (Palmén and Newton 1969, ch. 13). The average life of such cells is about 0.5 hr with large "super cells" persisting for several hours. These lifetimes are consistent with the durations of ionospheric disturbances.

## 10. CONTINUING OBSERVATIONS

During 1971, the recording of ionospheric disturbances has continued with observations made in Florida. A single 5.2-MHz transmitter was set up at a National Weather Service field site near Lakeland, with the receiver located at the University of Florida campus in Gainesville. We intended to look for ionospheric disturbances associated with hurricanes and to see if coastal thunderstorms produce effects that are different from those produced inland, such as in Oklahoma.

Records obtained from April through August 1971 do not show nearly as much acoustic wave activity as records of 1970 in Oklahoma. In fact, there was not even one ionospheric disturbance that would have been classified as a major event, or one that had a long-enough duration for spectrum analysis. Although the data have not yet been thoroughly analyzed, the difference may be because the tropopause over Florida is higher (about 16 km) than that over Oklahoma (about 12 km). Therefore, if penetration of the tropopause is necessary to produce disturbances, higher cloud tops would be required in Florida; and the 40,000-ft criterion would not apply.

### ACKNOWLEDGMENTS

This work was partially supported by the Advanced Research Projects Agency, Nuclear Monitoring Research Office, under ARPA Order No. 1361.

We thank Dr. Edwin Kessler and his staff for facilities at the National Severe Storms Laboratory, NOAA, and Prof. W. Hughes of the Electrical Engineering Department, Oklahoma State University, for facilities at Stillwater.

## REFERENCES

Anderson, Charles E., "A Technique for Classifying Cumulus Clouds Based on Photogrammetry," *Cumulus Dynamics: Proceedings of the First Conference on Cumulus Convection, Portsmouth, N.H., May 19–22, 1959*, Pergamon Press, New York, N.Y., **1960**, pp. 50–59.

Appleton, Edward Victor, Naismith, R., and Ingram, L. J., "British Radio Observations During the Second International Polar Year 1932–1933," *Philosophical Transactions of the Royal Society of London*, Ser. A, No. 236, England, **1936**, pp. 191–259.

Baker, Donald M., and Davies, Kenneth, "Waves in the Ionosphere Produced by Nuclear Explosions," *Journal of Geophysical Research*, Vol. 73, No. 1, Jan. 1, **1968**, pp. 448–451.

Baker, Donald M., and Davies, Kenneth, "F2-Region Acoustic Waves From Severe Weather," *Journal of Atmospheric and Terrestrial Physics*, Vol. 31, No. 11, Oxford, England, Nov. **1969**, pp. 1345–1352.

Barry, G. H., Griffiths, L. J., and Taenzer, J. C., "HF Radio Measurements of High-Altitude Acoustic Waves From a Ground-Level Explosion," *Journal of Geophysical Research*, Vol. 71, No. 17, Sept. 1, **1966**, pp. 4173–4182.

Bauer, Siegfried J., "Correlations Between Tropospheric and Ionospheric Parameters," *Geofisica Pura e Applicata*, Vol. 40, Milan, Italy, **1958**, pp. 235–240.

Beynon, W. J. G., and Brown, G. M., "Geophysical and Meteorological Changes in the Period January–April 1949," *Nature*, Vol. 167, No. 4260, London, England, June 23, **1951**, pp. 1012–1014

Budden, K. G., *Radio Waves in the Ionosphere: the Mathematical Theory of the Reflection of Radio Waves From Stratified Ionised Layers*, Cambridge University Press, London, England, **1961**, 542 pp.

Chang, Norman J. F., "Acoustic Gravity Waves in the Ionosphere and Their Effects on High Frequency Radio Propagation," Ph. D. thesis, Electrical Engineering Dept., University of Colorado, Boulder, Colo., **1969**, 238 pp.

COESA, U.S. Committee on Extension to the Standard Atmosphere, *U.S. Standard Atmosphere, 1962*, Environmental Science Services Administration (ESSA), National Aeronautics and Space Administration (NASA), and United States Air Force (USAF), Washington, D.C., Dec. **1962**, 278 pp.

Davies, Kenneth, "Ionospheric Effects of an Earthquake and Other Geophysical Disturbances," *ESSA Symposium on Earthquake Prediction*, Environmental Science Services Administration, U.S. Dept. of Commerce, Washington, D.C., **1966**, pp. 146–152.

Davies, Kenneth, *Ionospheric Radio Waves*, Blaisdell Publishing Co., Waltham, Mass., **1969**, 460 pp.

Davies, Kenneth, and Baker, Donald M., "Ionospheric Effects Observed Around the Time of the Alaskan Earthquake of March 28, 1964," *Journal of Geophysical Research*, Vol. 70, No. 9, May 1, **1965**, pp. 2251–2253.

Davies, Kenneth, Baker, Donald M., and Chang, Norman J. F., "Comparison Between Formulas for Ionospheric Radio Propagation and Atmospheric Wave Propagation," *Radio Science*, Vol. 4, No. 3, Mar. **1969**, pp. 231–233.

Davies, Kenneth, and Jones, John E., "Three-Dimensional Observations of Traveling Ionospheric Disturbances," *Journal of Atmospheric and Terrestrial Physics*, Vol. 33, No. 1, Jan. **1971***a*, pp. 39–46.

Davies, Kenneth, and Jones, John E., "Ionospheric Disturbances in the F2 Region Associated With Severe Thunderstorms," *Journal of the Atmospheric Sciences*, Vol. 28, No. 2, Mar. **1971***b*, pp. 254–262.

Detert, D. G., "A Study of the Coupling of Acoustic Energy From the Troposphere to the Ionosphere," *Technical Report*, Contract No. NAS 8–21079, AVCO Corp., Lowell, Mass., Feb. 15, **1969**, 197 pp.

Few, A. A., "Power Spectrum of Thunder," *Journal of Geophysical Research*, Vol. 74, No. 28, Dec. 20, **1969**, pp. 6926–6934.

Georges, T. M., "Ionospheric Effects of Atmospheric Waves," *ESSA Technical Report* IER 57–ITSA 54, Institute for Telecommunication Sciences and Aeronomy, Institutes for Environmental Research, Environmental Science Services Administration, U.S. Dept. of Commerce, Boulder, Colo., Oct. **1967**, 341 pp.

Georges, T. M., "HF Doppler Studies of Traveling Ionospheric Disturbances," *Journal of Atmospheric and Terrestrial Physics*, Vol. 30, No. 5, Oxford, England, May **1968**, pp. 735–746.

Georges, T. M., "Short-Period Ionospheric Oscillations Associated With Severe Weather," *Proceedings of the Symposium on Acoustic-Gravity Waves in the Atmosphere, Boulder, Colorado, July 15–17, 1968*, Environmental Science Services Administration, U.S. Dept. of Commerce, and the Advanced Research Projects Agency, Washington, D.C., **1969**, pp. 171–178.

Goerke, Vernon H., and Woodward, M. W., "Infrasonic Observation of a Severe Weather System," *Monthly Weather Review*, Vol. 94, No. 6, June **1966**, pp. 395–398.

Healey, R. H., "The Influence of the Radiation Field From an Electrical Storm on the Ionization Density of the Ionosphere," *Philosophical Magazine*, Ser. 7, Vol. 21, London, England, **1936**, pp. 187–198.

Herman, J. R. (The Lowell Technological Institute, Mass.), "RF Heating of the Ionosphere by Lightning Discharges," **1970** (unpublished manuscript).

Hines, Colin O., "Internal Atmospheric Gravity Waves at Ionospheric Heights," *Canadian Journal of Physics*, Vol. 38, No. 11, Ottawa, Nov. **1960**, pp. 1441–1481.

Hines, Colin O., and Reddy, C. A., "On the Propagation of Atmospheric Gravity Waves Through Regions of Wind Shear," *Journal of Geophysical Research*, Vol. 72, No. 3, Feb. 1, **1967**, pp. 1015–1034.

Jones, John E., "Observation of Traveling Ionospheric Disturbances by the Doppler Technique With Spaced Transmitters," *ESSA Technical Report* ERL 142–SDL 11, Space Disturbances Laboratory, ESSA Research Laboratories, Environmental Science Services Administration, U.S. Dept. of Commerce, Boulder, Colo., Dec. **1969**, 54 pp.

Kesava Murthy, M. J., "Studies on Sporadic E-Relationship With Thunderstorms and Magnetic Disturbances," *Current Science*, Vol. 32, No. 5, Bangalore, India, May **1963**, p. 206.

Lamb, Horace, *The Dynamical Theory of Sound*, 2d edition, Dover Publications, Inc., New York, N.Y., **1960**, 307 pp.

Lewis, L. David (Space Environment Laboratory, Environmental Research Laboratories, National Oceanic and Atmospheric Administration, U.S. Dept. of Commerce, Boulder, Colo.), "PSPEC—A Package of FORTRAN Subroutines for the Estimation of the Power Spectrum of a Real Time Series," Apr. **1969**, 13 pp. (unpublished manuscript).

Loeb, Leonard B., "Thunderstorms and Lightning Strokes," *Modern Physics for the Engineer*, Ch. 13, McGraw-Hill Book Co., Inc., New York, N.Y., **1954**, pp. 330–357.

Martyn, David Forbes, "Atmospheric Pressure and the Ionization of the Kennelly-Heaviside Layer," *Nature*, Vol. 133, No. 3356, London, England, Feb. 24, **1934**, pp. 294–295.

Midgley, J. E., and Liemohn, H. B., "Gravity Waves in a Realistic Atmosphere," *Journal of Geophysical Research*, Vol. 71, No. 15, Aug. 1, **1966**, pp. 3729–3748.

National Weather Service, *Tornado*, NOAA/PI 70007, National Oceanic and Atmospheric Administration, U.S. Dept. of Commerce, Washington, D.C., **1970**, 15 pp.

Palmén, E., and Newton, C. W., *Atmospheric Circulation Systems: Their Structure and Physical Interpretation*, Academic Press, New York, N.Y., June **1969**, 603 pp.

Pitteway, M. L. V., and Hines, Colin O., "The Viscous Damping of Atmospheric Gravity Waves," *Canadian Journal of Physics*, Vol. 41, No. 12, Ottawa, Dec. **1963**, pp. 1935–1948.

Pitteway, M. L. V., and Hines, Colin O.,"The Reflection and Ducting of Atmospheric Acoustic-Gravity Waves," *Canadian Journal of Physics*, Vol. 43, No. 12, Ottawa, Dec. **1965**, pp. 2222–2243.

Ratcliffe, John Ashworth, *The Magneto-Ionic Theory and Its Applications to the Ionosphere*, Cambridge University Press, London, England, **1959**, 206 pp.

Taylor, William L., "Review of Electromagnetic Radiation Data From Severe Storms in Oklahoma During April 1970," *NOAA Technical Memorandum* ERL WPL–6, Wave Propagation Laboratory, Environmental Research Laboratories, National Oceanic and Atmospheric Administration, U.S. Dept. of Commerce, Boulder, Colo., June **1971**, 80 pp.

Utlaut, W. F., "Radio-Wave Modification of the Ionosphere: An Ionospheric Modification Experiment Using Very High Power, High Frequency Transmission," *Journal of Geophysical Research, Space Physics*, Vol. 75, No. 31, Nov. 1, **1970**, pp. 6402–6405.

Vonnegut, Bernard, "Electrical Theory of Tornadoes," *Journal of Geophysical Research*, Vol. 65, No. 1, Jan. **1960**, pp. 203–212.

Watson-Watt, Robert Alexander, "Discussion on the Ionosphere," *Proceedings of the Royal Society of London*, Ser. A, Vol. 141, No. 845, England, Sept. 1, **1933**, pp. 715–718.

Welch, P. D., "The Use of Fast Fourier Transform for the Estimation of Power Spectra," *IEEE Transactions on Audio and Electroacoustics*, AU–15, Institute of Electrical and Electronics Engineers, New York, N.Y., **1967**, pp. 70–73.

Wilson, C. T. R., "The Electric Field of a Thundercloud and Some of Its Effects," *Proceedings of the Physical Society of London*, Vol. 37, England, Dec. **1924**–Aug. **1925**, pp. 32D–37D.

Wright, J. W., and Smith, G. H., "A Review of Current Methods for Obtaining Electron-Density Profiles From Ionograms," *Radio Science*, Vol. 2, No. 10, Oct. **1967**, pp. 1119–1125.

Yuen, P. C., Weaver, P. F., Suzuki, R. K., and Furumoto, A. S., "Continuous, Traveling Coupling Between Seismic Waves and the Ionosphere Evident in May 1968 Japan Earthquake Data," *Journal of Geophysical Research, Space Physics*, Vol. 74, No. 9, May 1, **1969**, pp. 2256–2264.

## APPENDIX 1: Partial Bibliography of Ionospheric Effects With Tropospheric Weather

Anderson, Charles E., "A Technique for Classifying Cumulus Clouds Based on Photogrammetry," *Cumulus Dynamics: Proceedings of the First Conference on Cumulus Convection, Portsmouth, N.H., May 19–22, 1959*, Pergamon Press, New York, N.Y., 1960, pp. 50–59.

Appleton, Edward Victor, Naismith, R., and Ingram, L. J., "British Radio Observations During the Second International Polar Year 1932–1933," *Philosophical Transactions of the Royal Society of London*, Ser. A, No. 236, England, 1936, pp. 191–259.

Bhar, J. M., and Syam, P., "Effect of Thunderstorms and Magnetic Storms on the Ionization of the Kennelly-Heaviside Layer," *Philosophical Magazine*, Ser. 7, Vol. 23, London, England, 1937, pp. 513–528.

Baker, Donald M., "Observations of Acoustic Waves in the Ionosphere Following Nuclear Explosions," *ESSA Technical Report* ERL 89–SDL 5, Space Disturbances Laboratory, ESSA Research Laboratories, Environmental Science Services Administration, U.S. Dept. of Commerce, Boulder, Colo., Oct. 1968, 47 pp.

Baker, Donald M., and Davies, Kenneth, "Waves in the Ionosphere Produced by Nuclear Explosions," *Journal of Geophysical Research*, Vol. 73, No. 1, Jan. 1, 1968, pp. 448–451.

Bannon, John Kerman, Higgs, A. J., Martyn, David Forbes, and Munro, G. H., "The Association of Meteorological Changes With Variations of Ionization in the $F_2$ Region of the Ionosphere," *Proceedings of the Royal Society of London*, Ser. A, Vol. 174, No. 958, England, Feb. 21, 1940, pp. 298–309.

Barry, G. H., Griffiths, L. J., and Taenzer, J. C., "HF Radio Measurements of High-Altitude Acoustic Waves From a Ground-Level Explosion," *Journal of Geophysical Research*, Vol. 71, No. 17, Sept. 1, 1966, pp. 4173–4182.

Bauer, Siegfried J., "A Possible Troposphere-Ionosphere Relationship," *Journal of Geophysical Research*, Vol. 62, No. 3, Sept. 1957, pp. 425–430.

Bauer, Siegfried, J., "Correlations Between Tropospheric and Ionospheric Parameters," *Geofisica Pura e Applicata*, Vol. 40, Milan, Italy, 1958, pp. 235–240.

Bauer, Siegfried J., "An Apparent Ionospheric Response to the Passage of Hurricanes," *Journal of Geophysical Research*, Vol. 63, No. 1, Mar. 1958, pp. 265–269.

Best, J. E., Farmer, F. T., and Ratcliffe, John Ashworth, "Studies of Region E of the Ionosphere," *Proceedings of the Royal Society of London*, Ser. A, Vol. 164, No. 916, England, Jan. 7, 1938, pp. 96–116.

Beynon, W. J. G., and Brown, G. M., "Geophysical and Meteorological Changes in the Period January–April 1949," *Nature*, Vol. 167, No. 4260, London, England, June 23, 1951, pp. 1012–1014.

Bowman, G. G., and Shrestha, K. L., "Ionospheric Storms and Small Pressure Fluctuations at Ground Level," *Nature*, Vol. 210, No. 5040, London, England, June 4, 1966, pp. 1032–1034.

Colwell, R. C., "A Method of Weather Forecasting," *Physical Review*, Vol. 37, No. 4, American Physical Society, Minneapolis, Minn., Feb. 15, 1931, p. 464.

Colwell, R. C., "Atmospheric Conditions and the Kennelly-Heaviside Layer," *Nature*, Vol. 130, No. 3286, London, England, Oct. 22, 1932, pp. 627–628.

Colwell, R. C., "Effect of Thunderstorms Upon the Ionosphere," *Nature*, Vol. 133, No. 3373, London, England, June 23, 1934, p. 948.

Damon, Thomas D., "Interrelation of Ionospheric Sporadic E With Thunderstorms and Jet Streams," *U.S. Air Weather Service Technical Report* 204, Scott Air Force Base, Ill., May 1968, 22 pp.

Davies, Kenneth, and Baker, Donald M., "Ionospheric Effects Observed Around the Time of the Alaskan Earthquake of March 28, 1964," *Journal of Geophysical Research*, Vol. 70, No. 9, May 1, 1965, pp. 2251–2253.

Davies, Kenneth, and Baker, Donald M., "On Frequency Variations of Ionospherically Propagated HF Radio Signals," *Radio Science*, Vol. 1, No. 5, May 1966, pp. 545–556.

Georges, T. M., "Ionospheric Effects of Atmospheric Waves," *ESSA Technical Report* IER 57–ITSA 54, Institute for Telecommunication Sciences and Aeronomy, Institutes for Environmental Research, Environmental Science Services Administration, U.S. Dept. of Commerce, Boulder, Colo., Oct. 1967, 341 pp.

Georges, T. M., "HF Doppler Studies of Traveling Ionospheric Disturbances," *Journal of Atmospheric and Terrestrial Physics*, Vol. 30, No. 5, Oxford, England, May 1968, pp. 735–746.

Gherzi, Ernest, "Ionospheric Reflections and Weather Forecasting for Eastern China," *Bulletin of the American Meteorological Society*, Vol. 27, No. 3, Mar. 1946, pp. 114–116.

Gherzi, Ernest, "Ionosphere and Weather," *Nature*, Vol. 165, No. 4184, London, England, Jan. 7, 1950, pp. 38–39.

Haubert, A., "A Propos des Relations Entre les Phénomènes Atmosphériques et Ionosphériques" (Relationship Between Atmospheric and Ionospheric Phenomena), *Journal of Atmospheric and Terrestrial Physics*, Vol. 33, No. 1, Oxford, England, Jan. 1971, pp. 117–118.

Healy, R. H., "The Influence of the Radiation Field From an Electrical Storm on the Ionization Density of the Ionosphere," *Philosophical Magazine*, Ser. 7, Vol. 21, London, England, 1936, pp. 187–198.

Hoffman, William C., "The Current-Jet Hypothesis of Whisler Generation" (condensed version), *Planetary and Space Science*, Vol. 2, No. 1, Oct. 1959, pp. 72–73.

Hoffman, William C., "The Current-Jet Hypothesis of Whisler Generation," *Journal of Geophysical Research*, Vol. 65, No. 7, July 1960, pp. 2047–2054.

Iyengar, R. S., "An Aerodynamic-Acoustic Theory of High-Altitude Fluctuation Phenomena," *Journal of Sound Vibration*, Vol. 6, No. 2, London, England, Sept. 1967, pp. 199–208.

Jones, M. W., and Jones, J. G., "A Correlation Between Ionospheric Phenomena and Surface Pressure," *Physical Review*, Series 2, Vol. 77, No. 6, American Institute of Physics, Lancaster, Pa., Mar. 15, 1950, p. 845.

Kohl, H., and King, J. W., "Atmospheric Winds Between 100 and 700 Km and Their Effects on the Ionosphere," *Journal of Atmospheric and Terrestrial Physics*, Vol. 29, No. 9, Oxford, England, Sept. 1967, pp. 1045–1062.

Kundu, Mukul Ranjan, "Correlations Between Variations of Surface Pressure and Ionospheric Parameters," *Indian Journal of Physics*, Vol. 27, Calcutta, India, 1953, pp. 235–243.

MacDonald, Norman J., and Knecht, Robert W., "A Statistical Study of Lower Atmospheric-Ionospheric Coupling," *Journal of Geophysical Research*, Vol. 66, No. 10, Oct. 1961, pp. 3187–3190.

Martyn, David Formes, "Troposphere-Ionosphere Relations" *The Dynamic Characteristics of the Ionosphere, Geophysical Research Paper* No. 12, U.S. Air Force Cambridge Research Center, Mass., Apr. 1952, pp. 31–34.

Martyn, David Forbes, and Pulley, O. O., "The Temperatures and Constituents of the Upper Atmosphere," *Proceedings of the Royal Society of London*, Ser. A, Vol. 154, No. 882, England, Apr. 1, 1936, pp. 455–486.

Mihran, T. G., "A Note on a New Ionospheric-Meteorological Correlation," *Proceedings of the IRE*, Vol. 36, No. 9, Institute of Radio Engineers, New York, N.Y., Sept. 1948, pp. 1093–1095.

Mitra, Sisir Kumar, "Ionospheric Studies in India," *Nature*, Vol. 137, No. 3462, London, England, Mar. 7, 1936, pp. 503–504.

Mitra, Sisir Kumar, and Kundu, M. R., "Thunderstorms and Sporadic E Ionization of the Ionosphere," *Nature*, Vol. 174, No. 4434, London, England, Oct. 23, 1954, pp. 798–799.

Mook, Conrad Payne, "The Apparent Ionospheric Response to the Passage of Hurricane Diane (1955) at Washington, D.C." *Journal of Geophysical Research*, Vol. 63, No. 3, Sept. 1958, pp. 569–570.

Murty, R. C., and Curry, M. J., "Microbarographic Observation of Acoustic Gravity Waves," *Nature*, Vol. 224, No. 5215, London, England, Oct. 11, 1969, pp. 169–170.

Pierce, Allan D., and Coroniti, Samuel C., "A Mechanism for the Generation of Acoustic-Gravity Waves During Thunderstorm Formation," *Nature*, Vol. 210, No. 5042, London, England, June 18, 1966, pp. 1209–1210.

Ranzi, Ivo, "A Possible Connection Between the Troposphere and the Kennelly-Heaviside Layer," *Nature*, Vol. 130, No. 3279, London, England, Sept. 3, 1932, p. 368.

Rastogi, R. G., "Thunderstorms and Sporadic E Layer Ionisation," *Indian Journal of Meteorolog ıd Geophysics*, Vol. 8, No. 1, Delhi, Jan. 1957, pp. 43–54.

Rastogi, R. G., "Thunderstorms and Sporadic-E Layer Ionization Over Ottawa, Canada," *Journal of Atmospheric and Terrestrial Physics*, Vol. 24, London, England, June 1962, pp. 533–540.

Ratcliffe, John Ashworth, and White, E. L. C., "An Automatic Recording Method for Wireless Investigations Reflected From the Ionosphere," *Proceedings of the Physical Society of London*, Vol. 45, No. 248, England, May 1, 1933, pp. 399–410.

Ratcliffe, John Ashworth, and White, E. L. C., "Some Automatic Records of Wireless Waves Reflected From the Ionosphere," *Proceedings of the Physical Society of London*, Vol. 46, No. 252, England, Jan.–Nov. 1934, pp. 107–115.

Row, Ronald V., "Acoustic-Gravity Waves in the Upper Atmosphere Due To a Nuclear Detonation and an Earthquake," *Journal of Geophysical Research*, Vol. 72, No. 5, Mar. 1, 1967, pp. 1599–1610.

Shatkin, Kh. Z., "Ionospheric-Tropospheric Relationships," *Geomagnetism and Aeronomy*, Vol. 4, No. 4, Washington, D.C., Feb. 1965, pp. 623–625 (translation of "Ob Ionosferno-Troposfernykh Sviaziakh," *Geomagnetizm i Aeronomiia*, Vol. 4, No. 4, Moscow, U.S.S.R., July/Aug. 1964, pp. 800–802).

Stergis, C. G., Rein, G. C., and Kangas, T., "Electric Field Measurements Above Thunderstorms," *Journal of Atmospheric and Terrestrial Physics*, Vol. 11, No. 2, Oxford, England, 1957, pp. 83–90.

Tolstoy, Ivan, and Lau, Joseph, "Ground Level Pressure Fluctuations Connected With Ionospheric Disturbances," *Journal of the Atmospheric Sciences*, Vol. 27, No. 3, May 1970, pp. 494–503.

Venkateswarlu, P., and Satyanarayana, R., "Some Studies on Sporadic E," *Journal of Scientific and Industrial Research*, Sec. B, Vol. 20, No. 1, New Delhi, India, Jan. 1961, pp. 8–10.

Watson-Watt, Robert Alexander, "Discussion on the Ionosphere," *Proceedings of the Royal Society of London*, Ser. A, Vol. 141, No. 845, England, Sept. 1, 1933, pp. 715–718.

Wilson, C. T. R., "The Electric Field of a Thundercloud and Some of Its Effects," *Proceedings of the Physical Society of London*, Vol. 37, England, Dec. 1924–Aug. 1925, pp. 32D–37D.

U. S. GOVERNMENT PRINTING OFFICE : 1973 O - 474-478